

A REVIEW REPORT ON HIGH BURNUP SPENT NUCLEAR FUEL—DISPOSAL ISSUES

Prepared for

**U.S. Nuclear Regulatory Commission
Contract NRC-02-02-012**

Prepared by

**Center for Nuclear Waste Regulatory Analyses
San Antonio, Texas**



**A REVIEW REPORT ON HIGH BURNUP SPENT
NUCLEAR FUEL—DISPOSAL ISSUES**

Prepared for

**U.S. Nuclear Regulatory Commission
Contract NRC-02-02-012**

Prepared by

**V. Jain
G. Cragolino
L. Howard**

**Center for Nuclear Waste Regulatory Analyses
San Antonio, Texas**

September 2004

PREVIOUS REPORTS IN SERIES

Number	Name	Date Issued
CNWRA 91-004	A Review of Localized Corrosion of High-Level Nuclear Waste Container Materials—I	April 1991
CNWRA 91-008	Hydrogen Embrittlement of Candidate Container Materials	June 1991
CNWRA 92-021	A Review of Stress Corrosion Cracking of High-Level Nuclear Waste Container Materials—I	August 1992
CNWRA 93-003	Long-Term Stability of High-Level Nuclear Waste Container Materials: I—Thermal Stability of Alloy 825	February 1993
CNWRA 93-004	Experimental Investigations of Localized Corrosion of High-Level Nuclear Waste Container Materials	February 1993
CNWRA 93-006	Characteristics of Spent Nuclear Fuel and Cladding Relevant to High-Level Waste Source Term	May 1993
CNWRA 93-014	A Review of the Potential for Microbially Influenced Corrosion of High-Level Nuclear Waste Containers	June 1993
CNWRA 94-010	A Review of Degradation Modes of Alternate Container Designs and Materials	April 1994
CNWRA 94-028	Environmental Effects on Stress Corrosion Cracking of Type 316L Stainless Steel and Alloy 825 As High-Level Nuclear Waste Container Materials	October 1994
CNWRA 95-010	Experimental Investigations of Failure Processes of High-Level Radioactive Waste Container Materials	May 1995
CNWRA 95-020	Expert-Panel Review of the Integrated Waste Package Experiments Research Project	September 1995
CNWRA 96-004	Thermal Stability and Mechanical Properties of High-Level Radioactive Waste Container Materials: Assessment of Carbon and Low-Alloy Steels	May 1996
CNWRA 97-010	An Analysis of Galvanic Coupling Effects on the Performance of High-Level Nuclear Waste Container Materials	August 1997

PREVIOUS REPORTS IN SERIES (continued)

<u>Number</u>	<u>Name</u>	<u>Date Issued</u>
CNWRA 98-004	Effect of Galvanic Coupling Between Overpack Materials of High-Level Nuclear Waste Containers—Experimental and Modeling Results	March 1998
CNWRA 98-008	Effects of Environmental Factors on Container Life	July 1998
CNWRA 99-003	Assessment of Performance Issues Related to Alternate Engineered Barrier System Materials and Design Options	September 1999
CNWRA 99-004	Effects of Environmental Factors on the Aqueous Corrosion of High-Level Radioactive Waste Containers—Experimental Results and Models	September 1999
CNWRA 2000-06 Revision 1	Assessment of Methodologies to Confirm Container Performance Model Predictions	January 2001
CNWRA 2001-003	Effect of Environment on the Corrosion of Waste Package and Drip Shield Materials	September 2001
CNWRA 2002-01	Effect of In-Package Chemistry on the Degradation of Vitrified High-Level Radioactive Waste and Spent Nuclear Fuel Cladding	October 2001
CNWRA 2002-02	Evaluation of Analogs for the Performance Assessment of High-Level Waste Container Materials	March 2002
CNWRA 2003-01	Passive Dissolution of Container Materials—Modeling and Experiments	October 2002
CNWRA 2003-02	Stress Corrosion Cracking and Hydrogen Embrittlement of Container and Drip Shield Materials	October 2002
CNWRA 2003-05	Assessment of Mechanisms for Early Waste Package Failures	March 2003
CNWRA 2004-01	Effect of Fabrication Processes on Materials Stability—Characterization and Corrosion	October 2003
CNWRA 2004-02	Natural Analogs of High-Level Waste Container Materials—Experimental Evaluation of Josephinite	January 2004

ABSTRACT

During irradiation, UO_2 fuel undergoes significant changes in chemical composition, which includes generation and decay of fission products, and changes in microstructure, which includes formation of rim structure. Steep radial thermal gradient during irradiation results in pellet cracking that allows fission gases and volatile fission products to migrate to gap regions in the fuel rod. These changes become more prominent as burnup increases. In addition, significant microstructural changes, characterized by the formation of a porous structure and loss of optically definable grain structure, originate in the rim region for burnup exceeding 60 gigawatts day per metric ton of uranium (GWd/MTU). Based on 1998 projections, high burnup will constitute more than 70 percent of the total inventory of the spent nuclear fuel generated between 1998 and 2015. Spent nuclear fuel exceeding 45 GWd/MTU is classified as high burnup spent nuclear fuel. Projections show that the potential Yucca Mountain repository could receive 30 percent of the spent nuclear fuel that could be classified as high burnup. The spent nuclear fuel burnup from nuclear reactors in the United States is currently limited to 62-GWd/MTU average burnup for the fuel rod with maximum burnup. This report summarizes pertinent information and presents current understanding of the issues related to the disposal of the high burnup spent nuclear fuel. The inventory of radionuclides is important for several reasons. It will determine the amount of heat generated per unit mass of the waste form (decay heat) as well as the background radiation created by the waste form. The irradiation or burnup of the fuel and the initial enrichment and design of the fuel element determine the inventory of radionuclides that will be discharged from the reactor as spent nuclear fuel and at any time thereafter as the radionuclides decay. An analysis using a source term based on 100-percent high burnup fuel inventory shows it to be of low risk significance to repository performance. Similarly, the variation in decay heat load due to varying burnup also is of low risk significance. The release of radionuclides upon contact with water and the performance of spent nuclear fuel cladding are discussed in terms of the changes in the high burnup spent nuclear fuel and cladding microstructure. The importance of the key long-lived radionuclides, such as Cs-135, I-129, Cl-36, C-14, and Tc-99, to the repository safety is examined in relation to the burnup. A literature review indicates significant uncertainties in estimating the instant release fraction for burnup exceeding 50 GWd/MTU because of the unavailability of data and uncertainties of rim characteristics for burnups exceeding 60 GWd/MTU. Spent nuclear fuel dissolution, however, indicates no significant effect of burnup. The most important effect of high burnup on Zircaloy cladding is the increase in the thickness of the oxide layer as a result of the extended exposure to the reactor environment and the concurrent increase of the hydrogen content. Under disposal conditions, as a result of the higher hydrogen content at high burnups, it appears that hydride reorientation and embrittlement upon cooling could have a more adverse effect on the integrity of cladding than that expected for medium burnup fuel. Creep failure of high burnup fuel also requires further evaluation as well as the concurrent effect of the higher hydrogen content. As in the case of medium burnup fuel, localized corrosion and stress corrosion cracking may also cause cladding failure in the in-package aqueous environment. The negative consequences of corrosion and hydrogen pickup on fuel cladding performance are being attenuated, at least partially, by the use of newly developed zirconium alloys that are more corrosion resistant, exhibiting significantly lower corrosion rates. Nevertheless, further evaluation of the initial condition of high burnup fuel cladding prior to disposal may be needed, regardless of the cladding material.

CONTENTS

Section	Page
PREVIOUS REPORTS IN SERIES	ii
ABSTRACT	v
FIGURES	ix
TABLES	xi
ACKNOWLEDGMENTS	xiii
EXECUTIVE SUMMARY	xv
1 INTRODUCTION	1-1
1.1 Organization of the Report	1-1
2 HIGH BURNUP INVENTORY SOURCE TERM	2-1
2.1 Assessment of the Source Term	2-1
2.2 Assessment of the Thermal Load	2-3
2.3 Summary	2-6
3 HIGH BURNUP SPENT NUCLEAR FUEL STRUCTURE AND FISSION GAS RELEASE	3-1
3.1 Summary	3-8
4 INSTANT RELEASE FRACTION	4-1
4.1 Literature Review	4-1
4.1.1 Instant Release Fraction for I-129 and Cs-135	4-1
4.1.2 Instant Release Fraction for Chloride	4-3
4.1.3 Instant Release Fraction for C-14	4-4
4.1.4 Instant Release Fraction for Tc-99	4-5
4.1.5 Instant Release Fraction for Other Radionuclides	4-6
4.2 Review of DOE Approach	4-7
4.3 Discussion and Assessment of the NRC Approach for Instant Release Fraction	4-8
4.3.1 Justification for Extrapolation of Instant Release Fraction Data to High Burnups	4-8
4.3.2 Proposed Instant Release Fraction Distribution	4-11
4.4 Summary	4-11
5 HIGH BURNUP SPENT NUCLEAR FUEL DISSOLUTION RATE	5-1
5.1 Literature Review	5-1
5.2 Assessment of DOE Spent Nuclear Fuel Data	5-7
5.3 Assessment of NRC and CNWRA Approaches for High Burnup Spent Nuclear Fuel	5-8
5.4 Summary	5-9

CONTENTS (continued)

Section	Page
6	HIGH BURNUP SPENT NUCLEAR FUEL CLADDING 6-1
6.1	Cladding Degradation Processes Under Disposal Conditions 6-1
6.2	Effect of Burnup on Spent Fuel Cladding 6-4
6.3	Characteristics of Spent Fuel Cladding 6-5
6.3.1	General Corrosion and Oxide Thickness of Cladding 6-5
6.3.2	Hydrogen Content and Distribution 6-8
6.3.3	Other Factors Affecting Spent Fuel Cladding 6-10
6.3.3.1	Internal Fuel Rod Pressure and Hoop Stress 6-10
6.3.3.2	Fuel Pellet Swelling and Irradiation Growth 6-10
6.4	Assessment of High Burnup Fuel Cladding Disposal Performance 6-11
6.4.1	General Corrosion 6-11
6.4.2	Localized Corrosion 6-14
6.4.3	Stress Corrosion Cracking 6-16
6.4.4	Creep Failure 6-17
6.4.5	Hydride Embrittlement and Delayed Hydride Cracking 6-20
6.4.6	Fuel and Cladding Oxidation 6-24
6.4.7	Fuel Side Stress Corrosion Cracking 6-25
6.5	Assessment of the Effect of High Burnup on Spent Fuel Cladding Performance 6-26
7	CONCLUSIONS 7-1
8	REFERENCES 8-1
	APPENDIX A A-1

FIGURES

Figure		Page
2-1	Radionuclide Inventory and Decay—45 GWd/MTU Fuel	2-3
2-2	Radionuclide Inventory and Decay—65 GWd/MTU Fuel	2-4
2-3	High Burnup Fuel Decay Heat Comparison	2-5
3-1	Fission Gas Release for Boiling Water Reactor Fuel Rods with Dry Conversion Pellets and Pellet-Cladding Gap Variations	3-2
3-2	Pressurized Water Reactor Fuel Rod Fission Gas Release	3-3
3-3	Fractional Fission Gas Release of Pressurized Water Reactor Fuel Rods with Enrichments	3-3
3-4	Comparisons Between Predicted and Measured Local Xenon Concentrations As a Function of the Local Burnup	3-4
3-5	The Thickness of the High Burnup Structure (Rim Zone) As a Function of the Cross Section Average Burnup As Revealed by Xenon Measurements	3-5
3-6	Percentage of Fission Gas Released to the Rod-Free Volume	3-6
3-7	Micro Probe Analysis Concentration Profiles for the Radial Distribution of Xenon	3-6
4-1	Instant Release Fraction for I-129 As a Function of Burnup	4-2
4-2	Instant Release Fraction for Cs-135 As a Function of Burnup	4-2
4-3	Instant Release Fraction for Cl-36 As a Function of Burnup	4-4
4-4	Instant Release Fraction for Tc-99 As a Function of Burnup	4-6
5-1	Dissolution Rates Based on U-238 and Cs-137 for Different pH Under Oxidizing and Reducing Conditions	5-2
5-2	Average Fractional Release Rate	5-3
5-3	Spent Nuclear Fuel Dissolution Rate As a Function of Burnup Under Different Temperatures (T) and Molar Total Carbonate Concentrations (CO ₃)	5-6
6-1	Total Hydrogen Content for Optimized Zircaloy-4, M4, and M5 As a Function of Burnup	6-9

TABLES

Table		Page
2-1	Comparison of Calculated High Burnup Inventory to TPA Code Version 5.0 Inventory (<i>nuclides.dat</i>) for Nuclides Important to Long-Term Performance	2-2
2-2	Comparison of Calculated High Burnup Thermal Load to the U.S. Nuclear Regulatory Commission (NRC) Regulatory Guide 3.54 (1999) and TPA Code Version 5.0 Proposed Average Thermal Load (<i>burnup.dat</i>)	2-6
4-1	Halides and Nitrogen Impurity Levels in Approved Testing Materials	4-3
4-2	Instant Release Fraction Distributions	4-7
4-3	Recommended Instant Release Fraction Values for Triangular Distributions	4-11
5-1	Composition of the Simulated Bicarbonate Groundwater	5-4
5-2	Normalized Dissolution Rate for Swedish Spent Nuclear Fuels	5-4
5-3	Normalized Dissolution Rate for Canadian CANDU Spent Nuclear Fuel	5-5
6-1	Chemical Composition of Zircaloy-2, Zircaloy-4, and Recent Zirconium Alloys in Weight Percent	6-2
6-2	Design Characteristics of Base Case Fuel Assembly	6-3
6-3	Comparison of Predictions from Models of Different Investigators for the General Corrosion of Zircaloy after 10,000 years at 180 °C [356 °F]	6-13

ACKNOWLEDGMENTS

This report was prepared to document work performed by the Center for Nuclear Waste Regulatory Analyses (CNWRA) for the U.S. Nuclear Regulatory Commission (NRC) under Contract No. NRC-02-02-012. The activities reported here were performed on behalf of the NRC Office of Nuclear Material Safety and Safeguards, Division of High-Level Waste Repository Safety. This report is an independent product of the CNWRA and does not necessarily reflect the view or regulatory position of the NRC.

The work on this report was initiated during staff exchange at the NRC. V. Jain gratefully acknowledges discussions with T. Ahn of the Division of High-Level Waste Repository Safety, C. Brown of Spent Fuel Project Office, and H. Scott of the Office of Nuclear Regulatory Research at the NRC that helped initiate the work on this report. The comments from the NRC staff also helped in improving the report.

The authors gratefully acknowledge L. Yang and K. Chiang for technical reviews, the programmatic review of B. Sagar, and the editorial reviews of C. Cudd, J. Pryor, and A. Woods. Appreciation is due J. Gonzalez for assistance in preparing this report.

QUALITY OF DATA: Sources of data are referenced in each chapter. CNWRA-generated data contained in this report meet quality assurance requirements described in the CNWRA Quality Assurance Manual. Data from other sources, however, are freely used. The respective sources of non-CNWRA data should be consulted for determining levels of quality assurance.

ANALYSES AND CODES: ORIGEN-ARP 2.00 (Bowman and Leal, 2002) was used for the radionuclide and decay heat calculations. This code is controlled according to requirements of CNWRA Technical Operating Procedure (TOP-18). Detailed calculations can be found in scientific notebook number 650.

REFERENCES:

Bowman and Leal. "Isotope Generation and Depletion Code System—Matrix Exponential Method with GUI and Graphics Capability." Oak Ridge, Tennessee: Oak Ridge National Laboratory. 2002.

EXECUTIVE SUMMARY

One of the major goals of this study is to evaluate existing literature on the behavior of the high burnup spent nuclear fuel under disposal conditions after failure of confinement barriers such as breach of a waste package, that allows interactions between the spent nuclear fuel and groundwater. Spent nuclear fuel exceeding 45 GWd/MTU is classified as high burnup and below 45 GWd/MTU as moderate (or medium) burnup. Based on 1998 projections, high burnup fuel will constitute more than 70 percent of the total inventory of the spent nuclear fuel generated between 1998 and 2015. Assuming 63,000 MTU capacity for commercial spent nuclear fuel of a total capacity of 70,000 MTU at the potential Yucca Mountain repository, 30 percent of the 63,000 MTU of the commercial spent nuclear fuel could be classified as high burnup fuel. It should be noted, however, spent nuclear fuel inventory is expected to exceed 63,000 MTU planned for potential Yucca Mountain repository. A significant quantity of the future spent nuclear fuel will be classified as high burnup. In this review, no attempt is made to examine fuels beyond the current capacity of the potential Yucca Mountain repository. Currently, the operating U.S. nuclear reactors average burnup is limited to 62 GWd/MTU for the fuel rod with the maximum or peak burnup (Meyer, 2000). However, nuclear industry seeks to increase peak rod burnup from 62 to 75 GWd/MTU. An increase in burnup could impact pellet morphology, fission gas distribution, and cladding performance.

During irradiation, UO_2 fuel undergoes significant changes in chemical composition, which includes generation and decay of fission products, and changes in microstructure, which includes formation of rim structure. Steep radial thermal gradient during irradiation results in pellet cracking that allows fission gases and volatile fission products to migrate to gap regions in the fuel rod. These changes become more prominent as the burnup increases. In light water reactor fuels with burnups below 50 GWd/MTU, only a small fraction of radionuclides are present at the gap and grain boundaries. These radionuclides are bounded by the fraction of fission gas release, mainly xenon. The literature review indicates a high burnup structure begins forming between 60 and 75 GWd/MTU and reaches completion around 100 GWd/MTU average burnup. The burnup around the rim region is approximately 1.3 times the average burnup attributed to epithermal fissions. High burnup or rim structure is characterized by a formation of a porous structure {1 to 2 μm [3.9×10^{-2} to 7.9×10^{-2} mils] diameter pores} and loss of optically definable grain structure {0.2 to 0.3 μm [7.87×10^{-3} to 11.8×10^{-3} mils] grain diameter} in the rim region. Furthermore, formation of rim structure impacts the temperature distribution in the pellet.

The changes in the radionuclide inventories for a high burnup fuel were calculated using ORIGEN-ARP 2.00 to evaluate the effects of the increase in radionuclide inventory and assess the impact on the source term for the postclosure period of the potential repository. Comparisons are made for the inventory and decay heat load produced by a 15 \times 15 pressurized water reactor fuel assembly with 5.0 wt% enriched U-235 fuel at 65 GWd/MTU burnup versus 4.0 wt% enriched U-235 fuel at 45 GWd/MTU burnup. Calculations were conducted over the 10,000 year regulatory repository period for the potential repository. Pressurized water reactor fuel was analyzed because it has a higher inventory of most radionuclides and generally has a higher range of burnup than boiling water reactor fuel. Increasing fuel burnup changes the radionuclide inventory in spent nuclear fuels. The activities of short-lived fission products tend to remain constant or decrease slightly, while activities of activation products and actinides tend to increase with increasing burnup, thus also increasing the amount of decay heat the waste will generate at a given point in time.

Fission gas release characteristics are different for the boiling water reactor and pressurized water reactor. Several studies have assessed that a pressurized water reactor has a slightly lower fission gas release as compared to the boiling water reactor. Fission gas release, however, is highly dependent on design and operating conditions. The fission gas release increases sharply at burnups exceeding 55 GWd/MTU. The cesium release from the fuel after a puncture is similar in concentration to the fission gas release. Furthermore, studies conducted about spent nuclear fuel rods exceeding 50-GWd/MTU burnup and stored during dry storage conditions for 15 years indicate the fission gas release could range from 1.4 to 17 percent.

The fraction of radionuclides present at the grain boundaries and in the gap is referred to as an instant release fraction. Instant release fraction refers to a combined inventory of soluble fission products, such as cesium, iodine, chloride, and carbon, located in the gap; and fission products, such as cesium, iodine; and segregated metallic phases, such as technetium, located at the grain boundaries. Studies have shown that in the presence of water, fission products present at the grain boundaries are released at a slower rate as compared to the gap. Because of difficulties in separating gap and grain boundary contributions, however, fractions are combined and are assumed to be released instantly upon contact with water. Despite the lack of experimental data on values exceeding 50-GWd/MTU burnup, an estimate of instant release fraction is determined based on the fission gas release data from the high burnup spent nuclear fuel. As a result of the formation of a high burnup rim structure, significant uncertainties remain however, for the estimate of instant release fraction for important radionuclides for fuels exceeding 60 GWd/MTU. This study estimates the instant release fraction of 34 percent for I-129 at 75-GWd/MTU burnup. I-129 is considered to be the most important contributor to the dose. The instant release fraction for cesium is estimated at one-third of the instant release fraction for I-129 based on available light water reactor data. Uncertainties in Tc-99 are significant because of the limited data and low concentration of Tc-99 present in the grain boundaries that make Tc-99 measurements prone to uncertainties. This study recommends that the upper bound for the instant release fraction for Tc-99 be 0.28 percent, based on the maximum observed concentration of 0.13 percent of Tc-99 in analyzed samples. Because of the lack of data, similarly significant uncertainties exist for the instant release fraction for C-14 and Cl-36, which are results of impurities in the unirradiated fuel and cladding. Because Cl-36 volatility is comparable to I-129, this study recommends the I-129 release fraction for Cl-36. A constant instant release fraction of 10 percent is recommended for C-14 based on this study. Because most of the data were obtained for fuel grains or fragments, the instant release fraction obtained from these samples represent a conservative estimate. The estimate does not take credit for limited access of water to grain boundaries. This study proposes a triangular probability distribution for iodine, cesium, chloride, and technetium. Because high burnup spent nuclear fuel exceeding 65 GWd/MTU could be a very small quantity compared to high burnup fuel between 45 and 65 GWd/MTU, the influence of rim effects on spent nuclear fuel dissolution can be neglected based on the quantity of spent nuclear fuel that will be emplaced at the repository.

Following a rapid release of instant release fraction, spent nuclear fuel dissolves at rates determined by the aqueous chemical environment. Studies have shown that the burnup has no significant effect on the spent nuclear fuel dissolution rate at 25 °C [77 °F]. At 75 °C [167 °F], however, based on the U.S. Department of Energy data, the spent nuclear fuel dissolution rate decreases with an increase in burnup. Furthermore, estimation of surface area is complicated by the pellet fragmentation caused by the radial thermal gradient and microstructural changes in the rim structure. Various authors have assumed different surface area roughness (or

correction) factors to account for such changes. Surface area estimation continues to contribute significant uncertainty in the analysis. Effect of the high burnup spent nuclear fuel dissolution rate can be adequately sampled in the existing U.S. Nuclear Regulatory Commission and the Center for Nuclear Waste Regulatory Analyses performance assessment abstraction model.

Zircaloy cladding exhibits extremely low uniform corrosion rates in aqueous environments and could delay substantially the release of radionuclides from commercial spent nuclear fuel if the cladding remains intact under disposal conditions. Performance assessments show a high correlation between dose and fraction of failed cladding. Cladding is thin, however, and not physically strong. Cladding failure can occur as a result of localized corrosion, stress corrosion cracking, and hydride reorientation and embrittlement, under a combination of adverse environmental and stress conditions. Cladding may also fail as a result of creep caused by hoop stresses due to internal pressure, or mechanically, when subjected to loads associated with seismic events and rockfall.

The most important effect of high burnup on Zircaloy cladding is the increase in the thickness of the ZrO_2 layer as a result of extended exposure to the reactor environment and the concurrent increase of the hydrogen content. Other effects include increased internal fuel rod pressure, fuel pellet swelling, irradiation growth of fuel rods, and, eventually, crud buildup. Under disposal conditions, because of the higher hydrogen content at high burnups, it appears that hydride reorientation and embrittlement upon cooling could have a more adverse effect on the integrity of cladding than that expected for medium burnup fuel. After irradiation in a nuclear reactor, Zircaloy cladding contains hydrides oriented circumferentially that cause little effect on ductility or fracture toughness. If the temperature increases above the solvus temperature following waste emplacement, hydrides can dissolve and reprecipitate in the radial orientation during slow cooling in the presence of hoop stresses of sufficient magnitude. Limited information exists for high burnup fuel cladding after extended dry storage to evaluate the possibility of hydride reorientation and embrittlement. The possibility does exist that cladding may fail by hydride embrittlement under disposal conditions, in particular for high burnup fuel. The introduction of cladding materials with better corrosion resistance than Zircaloy and, as a result, with lower hydrogen content, however, decreases the likelihood of hydride embrittlement.

Creep is considered the dominant process for cladding deformation under normal conditions of dry storage and later during the postclosure period, preceding any breaching of the waste packages. The relatively high temperatures, the outward pressure differential across the cladding wall, and the corresponding hoop stress will, in time, result in permanent deformation of the cladding. Creep analysis needs to be updated based on recent information obtained from dry storage studies although limited information exists for dry storage of high burnup fuel. Because cladding ductility decreases with increasing burnup, it is expected that some of the information available from dry storage studies for burnups lower than 45 GWd/MTU could be applied to higher burnup cladding. Creep models and estimations for medium burnup were reviewed. In general, it can be concluded that (i) deformation caused by creep will proceed slowly through time and will decrease the fuel rod pressure and (ii) the decreasing cladding temperature will also decrease the rod pressure and, therefore, the hoop stress, slowing down the creep rate. In summary, it appears that creep failure is less likely for high burnup fuel than for medium burnup fuel but further evaluation is necessary. More experimental information is needed to reach a definitive conclusion applicable to disposal conditions.

As in the case of medium burnup fuel, localized corrosion and stress corrosion cracking may also be a cause of cladding failure in the in-package aqueous environment. The available information for Zircaloy cladding was reviewed. Localized corrosion of Zircaloy-2 or Zircaloy-4 fuel cladding in the form of pitting may occur in an oxidizing environment (presumably present inside the waste packages), depending on Cl^- concentration and temperature, if the corrosion potential (E_{corr}) is higher than the repassivation potential (E_{rp}). The values of E_{rp} seem to be practically independent of pH and temperature, whereas E_{corr} depends on the presence of oxidizing species (i.e., H_2O_2), temperature, pH, and, to a lesser extent, Cl^- concentration. It can be expected that soluble corrosion products of iron, arising from the dissolution of steel baskets holding the fuel assemblies inside the waste packages, may affect the E_{corr} of Zircaloy. An important limitation to consider for localized corrosion to occur is related to the electronic conductivity of the ZrO_2 layer. Because of the poor electronic conductivity of the oxide, it is possible that, under naturally corroding conditions, and regardless of the nature of the oxidizing species, the cathodic reaction on the oxide-covered surface, needed to sustain the anodic dissolution inside the pit, is severely limited and, therefore, localized corrosion is inhibited.

Stress corrosion cracking of Zircaloy cladding may occur in the presence of hoop stresses of sufficient magnitude under the same environmental and electrochemical conditions that promote pitting corrosion by chloride. These arguments developed for Zircaloy cladding can be extended in general to the behavior of the cladding for high burnup fuel. It was concluded that, if the electrochemical and environmental conditions in terms of potential and Cl^- concentration are appropriate to initiate pitting of Zircaloy fuel cladding, the initiation of cracks could occur even at very low macroscopic stress levels. In the case of high burnup fuel, it is apparent that sufficiently high hoop stresses can be reached. The main limitation for the occurrence of external stress corrosion cracking caused by the in-package environment is related to the environmental and electrochemical conditions, in particular the protection offered by the low electronic conductivity of the oxide, as in the case of localized corrosion.

The likelihood of fuel rod degradation caused by fuel and cladding oxidation under expected repository conditions depends critically on the fuel temperature when the disposal container fails. The fuel temperature, in turn, depends on the mass loading in the waste packages and the stability of the emplacement drifts. Based on temperature estimations, fuel matrix oxidation could be dismissed as precursor of cladding degradation mechanisms as long as the disposal containers are not breached in thousand of years and the temperature is lower than $250\text{ }^\circ\text{C}$ [$482\text{ }^\circ\text{F}$]. It is not anticipated that significant differences would exist with high burnup fuel. However, the effect of possible drift degradation on these oxidation processes needs further evaluation.

Another well-known process of cladding failure is fuel side stress corrosion cracking induced by iodine. Several studies conducted to determine the possibility of these failure processes of Zircaloy cladding under dry storage conditions were briefly reviewed. Because both the critical stress and the stress intensity levels required for iodine stress corrosion cracking, as well as the limiting temperatures of $280\text{--}290\text{ }^\circ\text{C}$ [$536\text{--}554\text{ }^\circ\text{F}$], are not reached, this failure process is not expected to be a major cladding degradation process in the repository for medium burnup fuel. For high burnup fuel, even though the concentration of iodine in the pellet/cladding gap will be higher than that for medium burnup, iodine concentration is not a factor to consider because the threshold concentration is already reached in medium burnup fuel. The important factors are the hoop stress and, in particular, the stress intensity threshold that can be reached in the presence of cracks in the cladding. Additional information is needed to attain a final evaluation.

The negative consequences of corrosion and hydrogen pickup on fuel cladding performance are being attenuated by the use of newly developed zirconium alloys, which are more corrosion resistant, exhibiting significantly lower corrosion rates. Unfortunately, sufficient data are not currently available to evaluate in detail the likelihood of localized corrosion and the stress corrosion cracking resistance of the newly developed cladding alloys under disposal conditions, although some correlations could be established using pitting or repassivation potentials. Specific information, however, will be needed to evaluate the localized corrosion of newly developed zirconium-based cladding alloys, and further evaluation of the initial condition of cladding for high burnup fuel prior to disposal is needed.

Reference

Meyer, R.O. "NRC Activities Related to High Burnup, New Cladding Types, and Mixed-Oxide Fuel." Proceedings of the 2000 International Topical Meeting on Light Water Reactor Fuel Performance, Park City, Utah, April 10–13, 2000. La Grange Park, Illinois: American Nuclear Society. 2000.

1 INTRODUCTION

One of the major goals of this report is to evaluate existing literature to assess the behavior of the high burnup spent nuclear fuel under disposal conditions after failure of confinement barriers, such as breach of a waste package, that allows interactions between the fuel and groundwater. Spent nuclear fuel exceeding 45 GWd/MTU is classified as high burnup spent nuclear fuel. Based on 1998 projections, high burnup will constitute more than 70 percent of the total inventory of the spent nuclear fuel generated between 1998 and 2015. Assuming 63,000-MTU capacity for commercial spent nuclear fuel of a total capacity of 70,000 MTU at the potential Yucca Mountain repository, 30 percent of the spent nuclear fuel could be classified as high burnup fuel. It should be noted, however, spent nuclear fuel inventory is expected to exceed 63,000 MTU planned for potential Yucca Mountain repository. A significant quantity of the future spent nuclear fuel will be classified as high burnup. In this review, no attempt is made to examine fuels beyond the current capacity of the potential Yucca Mountain repository. Currently the commercial spent nuclear fuel average burnup for the operating nuclear reactors in the United States is limited to 62-GWd/MTU for the fuel rod with the maximum or peak burnup (Meyer, 2000). However, nuclear industry seeks to increase peak rod burnup from 62 to 75 GWd/MTU. An increase in burnup could impact pellet morphology, fission gas distribution, and cladding performance.

Several studies discuss the sensitivity of dose to the dissolution rate of the spent nuclear fuel source material and cladding. The spent nuclear fuel degradation models in TPA Version code 4.1 indicate there is a clear correlation between release rate and dose (Mohanty, et al., 2004). Dissolution rate is a relatively important determinant of repository performance, but the ultimate peak dose is less than directly proportional to it because other mechanisms, such as diffusion, advection, and solubility, may limit the ultimate release rates from the engineered barrier. In addition, the introduction of cladding protection (allows radionuclide release from only one percent of the spent fuel) decreases the dose at 10,000 years with respect to basecase from 2×10^{-4} to 3×10^{-6} mSv/yr [2×10^{-2} to 3×10^{-4} mrem/yr]. Release rates of highly soluble and mobile radionuclides such as Tc-99 and I-129, account for most of the 10,000-year calculated dose and are approximately proportional to the amount of spent fuel exposed. Other hazardous but less mobile radioelements such as plutonium and americium, may not be as affected by the amount of spent fuel exposed because their release is likely to be controlled by solubility limits. Based on the available risk insights, the U.S. Nuclear Regulatory Commission ranking of dissolution of spent nuclear fuel and degradation of cladding are considered as having medium significance to waste isolation (NRC, 2004).

It should be noted that current performance analyses do not include the effect of possible drift degradation during the initial few thousand years after repository closure. If drift degradation occurs, the associated increase in waste package temperature could affect: (i) cladding behavior in relation to creep and hydride reorientation; (ii) dry air oxidation of the spent fuel matrix; and (iii) diffusion of dose contributing radionuclides to the grain boundaries of the irradiated UO_2 pellets.

1.1 Organization of the Report

High burnup spent nuclear fuel undergoes significant microstructural changes at the rim such as decrease in the fuel grain size or loss of defined grain structure, high density of small pores, and loss of fission gas xenon from the fuel matrix. Fission gas release characteristics are different

for the boiling water reactors and pressurized water reactors and are highly dependent on design and operating conditions. The fission gas release increases sharply at burnups exceeding 55 GWd/MTU. The characteristics of the high burnup fuel including fission gas release are examined in Chapter 2.

Chapter 3 examines the changes in the radionuclide inventories for high burnup fuel using ORIGEN-ARP 2.00 code to calculate the radionuclide inventories and decay heat loads. Comparisons are made for the inventory and decay heat load produced from a 15 × 15 pressurized water reactor fuel assembly with 5.0-wt% enriched U-235 fuel at 65-GWd/MTU burnup versus 4.0-wt% enriched U-235 fuel at 45-GWd/MTU burnup. Calculations were conducted for the 10,000-year regulatory repository timeframe. Pressurized water reactor fuel was analyzed because it has a higher inventory of most radionuclides and generally has a higher range of burnup than boiling water reactor fuel. The radionuclide inventories were calculated based on three typical depletion (irradiation) case histories in the reactor and 10,000 years of decay.

Radionuclide release from a breached spent nuclear fuel in contact with groundwater occurs via a rapid release of fission products present in the gap, followed by a slow release of fission products from grain boundaries and dissolution of fuel matrix. Combined release of fission products from the gap and grain boundary is termed as instant release fraction. Instant release fraction has a major contribution to the initial dose from the breached waste packages. A review of existing data about instant release fraction and estimation of instant release fraction as a function of burnup is provided in Chapter 4. Following the release of instant release fraction, spent nuclear fuel dissolves at a rate depending on the aqueous chemical environment. An assessment based on the review of the literature data about spent nuclear fuel is provided in Chapter 5.

Most of the cladding of the spent nuclear fuel for power generating reactors is made of two zirconium alloys, Zircaloy-2 and Zircaloy-4, used in boiling water reactors and pressurized water reactors. In addition to the low neutron cross section, zirconium alloys are used as cladding material because they have adequate mechanical properties up to 400 °C [752 °F] and very good corrosion resistance in high-temperature, high-pressure water under operating reactor conditions. In recent years, refinements in the Zircaloy composition (lowering of the tin content) and improved fabrication and control processes have been introduced to attain better corrosion resistance. In addition, other zirconium alloys such as ZIRLO and M5, were developed and introduced as fuel cladding materials to improve the in-reactor fuel performance. The burnup strongly affects the thickness and characteristics of the ZrO₂ layer, the amount of absorbed hydrogen, the fission gas production and, as a result, the internal fuel rod pressure, the fuel pellet swelling, irradiation growth of fuel rods, and, eventually, crud buildup.

As the burnup increases, the performance of the cladding degrades because of the increased thickness of the oxide layer and the associated increase in the hydrogen absorption. Chapter 6 provides a review of the available information and discussion of the possible effects of high burnup on the integrity of spent nuclear fuel cladding under repository conditions.

2 HIGH BURNUP INVENTORY SOURCE TERM

Commercial nuclear power plants use a variety of fuels and fuel configurations in the reactor core to generate power. Each fuel assembly, depending on the reactor configuration, initial fuel enrichment, burnup, and age of the waste, will have a unique isotopic composition. As discussed previously in this report, approximately 97 percent of the 1998 commercial spent nuclear fuel inventory in the United States is classified as medium burnup (less than 45-GWd/MTU). High burnup spent nuclear fuel, which has been used for fuel at greater than 45 GWd/MTU burnup, is expected to substantially increase in the coming years and could account for as much as 30 percent of the total projected inventory to be placed at the potential high-level waste repository at Yucca Mountain.

Radionuclide inventories for high burnup fuels were calculated using ORIGEN-ARP 2.00 code (Bowman and Leal, 2000). ORIGEN-ARP 2.00 code performs burnup calculations using libraries (files of radionuclide characteristics such as decay parameters and neutron cross sections) defined for different types of assemblies and uranium enrichments. The library for the 15 × 15 pressurized water reactor assembly was used because the relative increase in radionuclide inventory with burnup does not change significantly with fuel design. Because the principal purposes of this study were to evaluate the effects of the increase in radionuclide inventory and assess the impact on the source term for postclosure, the 15 × 15 pressurized water reactor library was used for a 5.0-wt% enriched U-235 fuel at 65 GWd/MTU burnup. The results were compared to a 15 × 15 pressurized water reactor with a 4.0-wt% enriched U-235 fuel at 45 GWd/MTU burnup and to literature values and TPA Version 5.0 code¹ inventory values. Cross sections used in the calculations were obtained by interpolation between the cross sections in the libraries for various fuel exposures.

Pressurized water reactor fuel was analyzed because it has a higher inventory of most radionuclides and generally has a higher range of burnup than boiling water reactor fuel. The radionuclide inventories were calculated based on a typical three depletion case (irradiation) in the reactor with a 10,000-year decay case in which the cooling time is assumed to be 10 years prior to emplacement in the potential repository. This calculation provides radionuclide inventories for direct comparison to the inventory used in the TPA Version 5.0 code in curies/metric ton of uranium at 10 years from the reactor and important radionuclide concentrations as the waste decays during the 10,000-year regulatory period for the potential repository.

2.1 Assessment of the Source Term

The calculated source term was compared to a number of source term analyses in the literature to ensure a realistic calculation was made. These calculations include those used in this report such as Ramsdell, et al. (2001) and Sanders and Gauld (2003). Significant work was also accomplished in bench marking and validation of the ORIGEN code calculations against isotopic analyses of high burnup fuels, such as Sanders and Gauld (2003), and a number of references included in Bowman and Leal (2000). Although most of the radionuclide

¹The TPA Version 5.0 code is currently under review and revision, including update and verification of parameter values. Therefore, the analysis accomplished for this report using the code is for comparison purposes only since the parameter values may be updated in the revised TPA Version 5.0 code.

Nuclide	65 GWd/MTU Inventory at 10 Years Decay (Ci/MTU)	TPA Version 5.0 Code Initial (at 10 Years) Inventory (Ci/MTU)	Difference to TPA Version 5.0 Code Inventory (%)	45 GWd/MTU Inventory at 10 Years Decay (Ci/MTU)	Difference to TPA Version 5.0 Code Inventory (%)
Am-241	2.88×10^3	2.08×10^3	40	2.35×10^3	14
Pu-240	7.32×10^2	5.44×10^2	35	6.11×10^2	12
Pu-239	3.84×10^2	3.69×10^2	4	3.57×10^2	-3
Tc-99	2.42×10^1	1.45×10^1	67	1.78×10^1	23
Np-237	7.28×10^1	4.34×10^1	68	4.69×10^1	8
Cs-135	1.10	5.36×10^1	105	6.91×10^1	29
I-129	6.13×10^2	3.57×10^2	72	4.30×10^2	20
Total: 43 Nuclide TPA Version 5.0 Code Inventory	4.23×10^5	2.57×10^5	65		

concentrations important to risk over the potential repository lifetime increase with increasing burnup, as shown in Table 2-1 and by comparing Figure 2-1 for the 45-GWd/MTU case and Figure 2-2 for the 65-GWd/MTU case, the increase in the source term is not large in magnitude. In terms of the source term, the bounding performance assessment inventory would be entirely made up of high burnup spent nuclear fuel. As previously discussed, the potential repository inventory could be as much as 30-percent high burnup spent nuclear fuel.

Table 2-1 provides a comparison between important long-lived radionuclides in the source term calculated for the 65-GWd/MTU high burnup fuel, the 45-GWd/MTU burnup fuel, and the representative repository inventory used in the current TPA Version 5.0 code. The TPA code uses the INVENT utility module to centralize the computation and storage of radionuclide-specific information and inventory, accounting for the chain decay and ingrowth of daughters (Mohanty, et al., 2000). The data file *nuclides.dat* provides the inventory in Curies/MTU of 43 radionuclides at 10 years out-of-reactor decay age. To provide risk insight into the source term effects of a high burnup fuel, the inventory of the *nuclides.dat* file was changed to the calculated high burnup 65-GWd/MTU fuel inventory for the 43 radionuclides tracked by the TPA Version 5.0 code. This change provides a conservative calculation of the source term effects on the dose calculation of the TPA Version 5.0 code because this file would provide a risk calculation assuming 100 percent of the inventory of the potential repository commercial spent nuclear fuel was high burnup fuel. Using mean value for single realization TPA Version 5.0 code runs to highlight the change in dose risk caused by the source term change, the peak dose at 10,000 years increases from the nominal basecase of 0.162 to 0.297 mrem/yr [1.62 to 2.97 μ SV/yr], an increase of 1.8 times but still within the same order of magnitude for the risk calculation.

Nuclides - 45 GWd/MTU Case

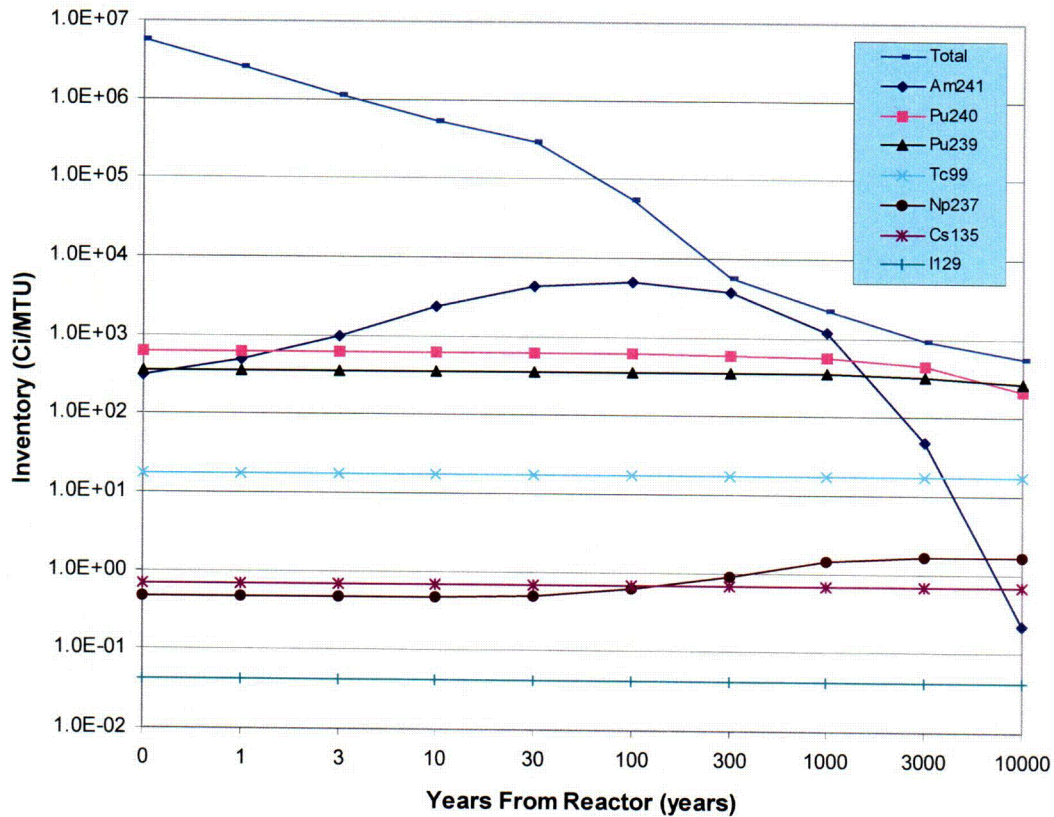


Figure 2-1. Radionuclide Inventory and Decay—45 GWd/MTU Fuel

The U.S. Department of Energy (DOE) source term calculations can be reviewed in two primary references, the Preclosure Safety Analysis Guide (DOE, 2002) for the preclosure source term and the Inventory Abstraction Analysis Model Report (DOE, 2001a) for the postclosure source term. Both references calculate the source term using a weighted average method in which the pressurized water reactor and boiling water reactor commercial spent nuclear fuel waste forms are determined using weighted averages of the reported enrichments, burnup, and ages from the reactor. The weighting terms are provided based on the number of fuel assemblies with a given value of each characteristic in the waste stream. Characteristics of the bounding pressurized water reactor and boiling water reactor waste forms are the maximum reported burnup, maximum reported enrichment, and the minimum reported age in the waste stream for each fuel type (DOE, 2001a). DOE presents the radionuclide source terms in curie (and gram) per fuel assembly basis compared to curie per metric ton of uranium presented in this report and used in the TPA Version 5.0 code inventory abstraction.

2.2 Assessment of the Thermal Load

The decay heat load in Watts/MTU for the two spent nuclear fuel burnup cases discussed above was calculated to analyze the impact of higher burnup fuel. The 45 GWd/MTU and 65 GWd/MTU cases are compared to literature values from Ramsdell, et al. (2001). The

Nuclides - 65 GWd/MTU Case

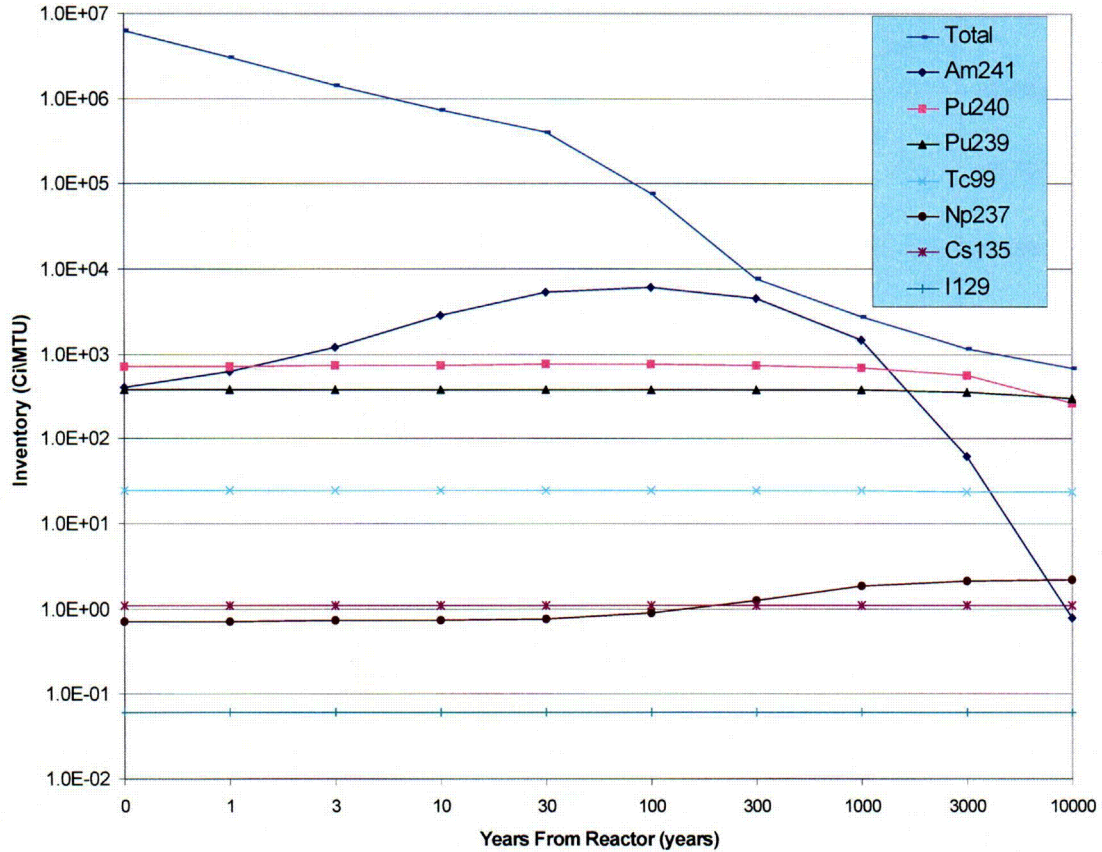


Figure 2-2. Radionuclide Inventory and Decay—65 GWd/MTU Fuel

literature values for comparison encompass 1 to 30 years decay. The recommended TPA Version 5.0 code pressurized water reactor decay heat profile (*burnup.dat* file) for pressurized water reactor spent nuclear fuel is also presented in Figure 2-3 for comparison.

The range of thermal output from the various burnup levels presented here is relatively small and shows good agreement with the calculated profiles for this report. Because most (approximately 70 percent) of the potential repository spent nuclear fuel will have been irradiated at burnups of less than 45 GWd/MTU and, thus, have lower magnitude decay heat profiles than those presented in Figure 2-3, the repository decay heat load as a whole is bounded well by the recommended profile from the TPA Version 5.0 code used to assess performance of the potential repository.

Table 2-2 provides a comparison between the calculated high burnup fuel and average pressurized water reactor spent nuclear fuel thermal outputs used in performance assessment in the TPA Version 5.0 code (*burnup.dat* file). The thermal output used for performance assessment is a weighted average of the pressurized water reactor and boiling water reactor waste packages and weighted average fuel enrichment and burnup values taken from the

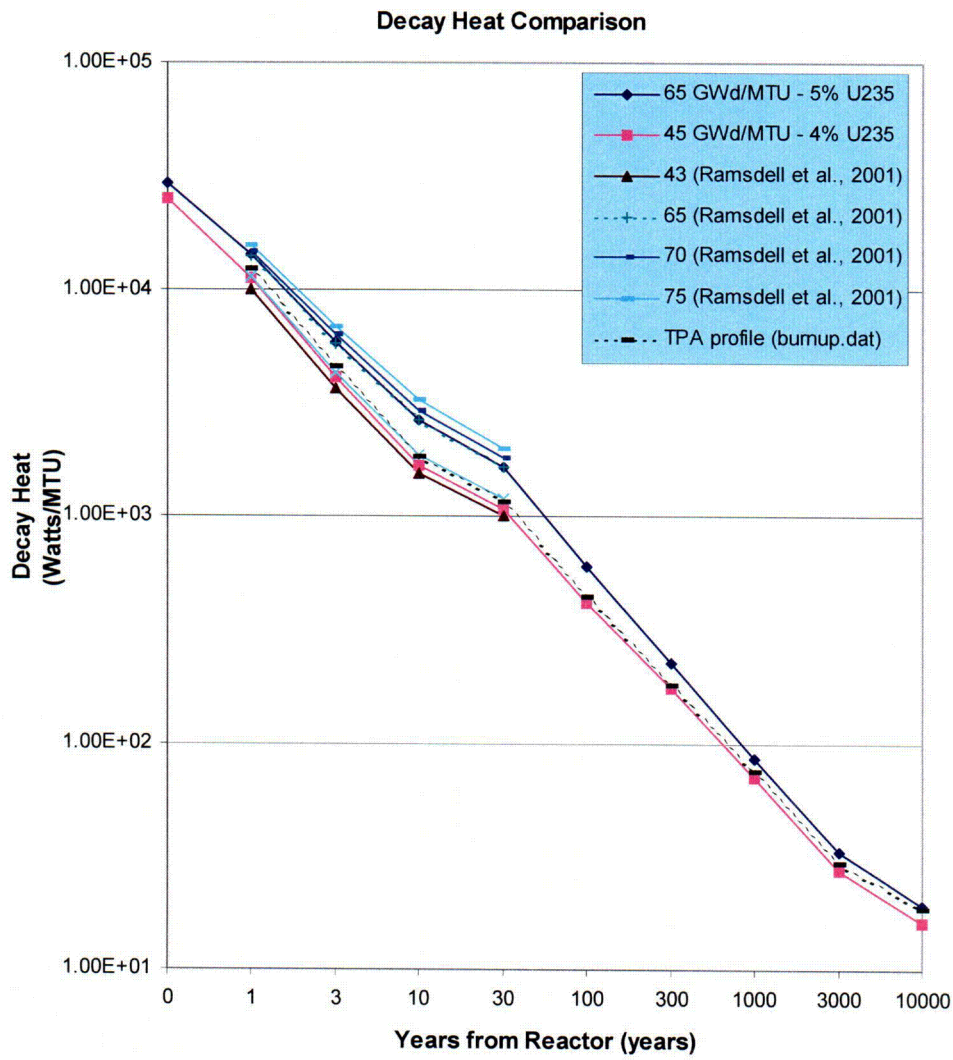


Figure 2-3. High Burnup Fuel Decay Heat Comparison

Table 2-2. Comparison of Calculated High Burnup Thermal Load to the U.S. Nuclear Regulatory Commission (NRC) Regulatory Guide 3.54* and TPA Version 5.0 Code Proposed Average Thermal Load (<i>burnup.dat</i>)			
Decay Time (Time from Reactor)	Calculated (ORIGEN-ARP 2.00) High Burnup Fuel Decay Heat: 5% Enrichment, 65 GWd/MTU (watts/MTU)	NRC Regulatory Guide 3.54–4.2 Percent Enrichment, 50 GWd/MTU (watts/MTU)	Values for TPA Version 5.0 Code Average Pressurized Water Reactor Fuel from the Recommended <i>burnup.dat</i> File (watts/MTU)
1 year	14,100	13,466	12,140
3 years	5,860	5,267 (2.8 years)	4,610
10 years	2,650	1,936	1,853

*NRC. "Spent Fuel Heat Generation in an Independent Spent Fuel Storage Installation." Regulatory Guide 3.54. Washington, DC: NRC. 1999.

literature. The typical age of waste at the time of emplacement is assumed to be 26 years. As can be seen from this example, the percentage of waste packages in the potential repository at higher burnup would increase the thermal output assuming the same decay time. The potential repository however, will have significant numbers of waste packages at lower thermal outputs than those shown here because of lower enrichments and burnup and longer decay times from the reactor prior to emplacement in the potential repository.

2.3 Summary

Literature review and analysis indicate increasing fuel burnup changes the radionuclide inventory in spent nuclear fuels. The activities of short-lived fission products tend to remain constant or decrease slightly, while activities of activation products and actinides tend to increase with increasing burnup, thus also increasing the amount of decay heat the waste will generate at a given point in time from the reactor. For use in performance assessment calculations, the source term and thermal load values are weighted averages that are used to model the potential repository inventory as a whole. An analysis using a calculated source term as a nonweighted, 100-percent high burnup fuel inventory does not demonstrate high risk significance in the performance assessment calculation, nor does the variation in decay heat load caused by a relatively small range of decay heat with varying burnup and the representative profile used in performance assessment calculations.

3 HIGH BURNUP SPENT NUCLEAR FUEL STRUCTURE AND FISSION GAS RELEASE

During irradiation, UO_2 fuel undergoes significant changes in chemical composition which includes generation and decay of fission products and changes in microstructure, which includes formation of rim structure. Steep radial thermal gradient during irradiation results in pellet cracking that allows fission gases and volatile fission products to migrate to gap regions in the fuel rod. These changes become more prominent as the burnup increases. Another change that occurs is the formation of a pellet-cladding bonding layer. When the burnup increases, the pellet swells causing the pellet-cladding gap to close; this contact eventually develops into a bond. In addition to transmitting stresses to cladding, pellet-cladding interactions could prevent axial movement of fission gases.

In light water reactor fuels with burnups below 50 GWd/MTU, only a small fraction of radionuclides are present at the gap and grain boundaries. These radionuclides are bounded by the fraction of fission gas release, mainly xenon (Johnson and Tait, 1997). When the burnup exceeds 65 GWd/MTU, significant changes characterized by formation of a porous structure {1 to 2 μm [3.9×10^{-2} to 7.9×10^{-2} mil] diameter pores} and loss of optically definable grain structure {0.2 to 0.3 μm [7.87×10^{-3} to 11.8×10^{-3} mil] grain diameter} in the rim region are observed (Barner, et al., 1993). Lassmann, et al. (1995) demonstrated that high burnup rim structure originates between 60 and 75 GWd/MTU. Furthermore, formation of rim structure impacts the temperature distribution in the pellet. According to Une, et al. (1997), the centerline temperatures of 1,000 °C [1,832 °F] and 1,450 °C [2,642 °F] of the pellet in an 80-GWd/MTU burnup fuel is increased by 50 and 100 °C [122 and 212 °F] at linear power of 150 and 250 W/cm [1,300 and 2,166 Btu/hr-in], respectively.

There have been numerous studies that examined fission gas release from spent nuclear fuel assemblies. Barner, et al. (1993) conducted extensive measurements of fission gas release in 82 different Zircaloy light water reactor spent nuclear fuel rods ranging from average fuel burnup of 22–69 GWd/MTU with a peak pellet burnup of 83 GWd/MTU. The study showed that for both low and high burnup fuels, the fission gas release depends on design and irradiation history. Barner, et al. (1993) further concluded that in fuels with similar design, the fission gas release increases as burnup increases. In addition, fuels with high internal helium fill gas pressure has less fission gas release compared to fuels with low internal helium pressure. Helium gas introduced during manufacturing and fission gases produced during irradiation are the primary sources of internal pressure inside a spent nuclear fuel rod. The internal pressure increases as the amount of fission gas increases. The high burnup spent nuclear fuels have a larger amount of fission gases. Fission gases present inside the fuel pellet do not contribute to the internal pressure. Figure 3-1 shows fission gas release data from boiling water reactor fuels in different pellet-to-cladding gaps (Van Swam, et al., 1997a). In large diametral {0.21–0.23 mm [8.27–9.06 mil]} pellet-to-cladding gaps, fission gas release is 26 percent while in samples with small diametral gaps {0.15–0.17 mm [5.91–6.69 mil]}, fission gas release was less than 1 percent. Measurable fission gas release is observed in samples exceeding 30 GWd/MTU. Data clearly show that fission gas release depends on the design of the assembly and irradiation cycles. Stroes-Gascoyne, et al. (1997a) studied fission gas release from Canada Deuterium Uranium (CANDU) fuels and reported that the differences in the instantaneous release fraction is a result of differences in the microstructure. High burnup fuels showed significant fission gas bubble formation and in some cases grain growth that allowed noble gases and fission products to escape to the fuel-sheath gap.

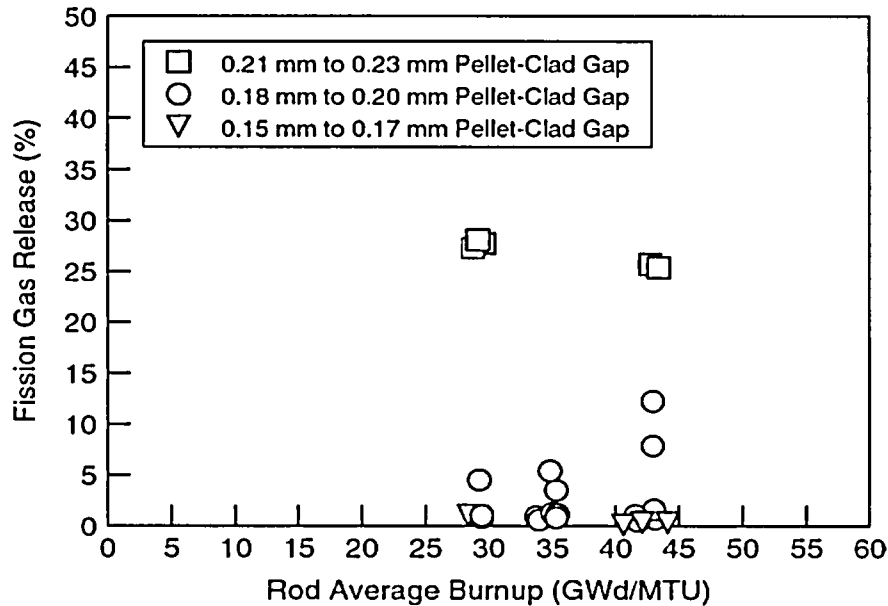


Figure 3-1. Fission Gas Release for Boiling Water Reactor Fuel Rods with Dry Conversion Pellets and Pellet-Cladding Gap Variations (Van Swam, et al., 1997a) (Reproduced with Permission from the American Nuclear Society, Inc.)
 Note: 1 mm = 39.37 mil

Van Swam, et al. (1997a) studied fission gas release from both boiling water and pressurized water reactors. Figure 3-2 shows fission gas release from a 15 × 15 assembly in a pressurized water reactor for burnup ranging as much as 73 GWd/MTU for UO₂ pellets and Gd₂O₃ doped UO₂ pellets. Fission gas release measurements on UO₂ spent nuclear fuel rods after 5 cycles showed a release of 3–7 percent while on Gd₂O₃-doped UO₂ spent nuclear fuel rods after 5 cycles showed a release between 0.5 and 2 percent. The spent nuclear fuel rods were subjected to a different number of time cycles operating at different linear heat generation rates to provide equivalent burnups. The effect of power history on fission gas release is clearly evident from these results. Manzel and Coquerelle (1997) studied irradiation of a 15 × 15 rod array in a pressurized water reactor in 7 cycles with a maximum burnup of 82 GWd/MTU. The fission gas release of 7 and 14 percent as observed at 50 and 80 GWd/MTU burnups from a pressurized water reactor is shown in Figure 3-3. Most of the fission gas release was observed at the center of the pellets. However, on increasing the burnup, low temperature regions were saturated with fission gases and significant amounts of fission gases were confined to the small bubbles in the rim region. Gray (1998) studied spent nuclear fuels ranging from 30 to 50 GWd/MTU and examined fission gas release. Fission gas release ranged from 0.25 to 18 percent.

Figure 3-4 (Lassman, et al., 1995) shows a comparison between predicted and measured local xenon concentrations as a function of local burnup. This data clearly showed the xenon concentration peaks at approximately 1 wt% between 60–75-GWd/MTU burnup, and stabilizes at an equilibrium value of 0.25 wt% beyond 120 GWd/MTU. Furthermore, results indicate fission gases that are continuously released from the grains during fission migrate to the newly

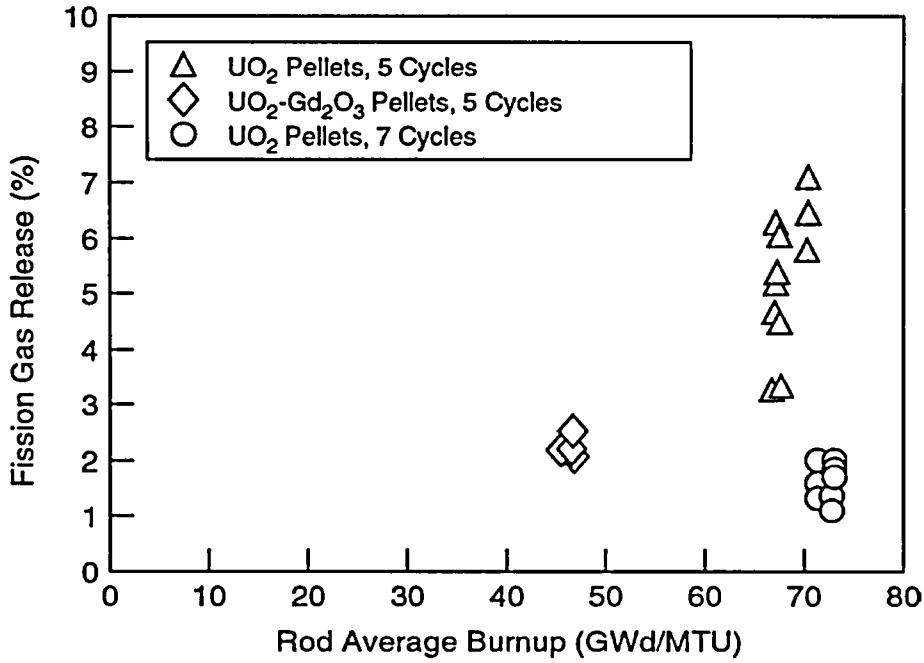


Figure 3-2. Pressurized Water Reactor Fuel Rod Fission Gas Release (Van Swam, et al., 1997a) (Reproduced with Permission from the American Nuclear Society, Inc.)

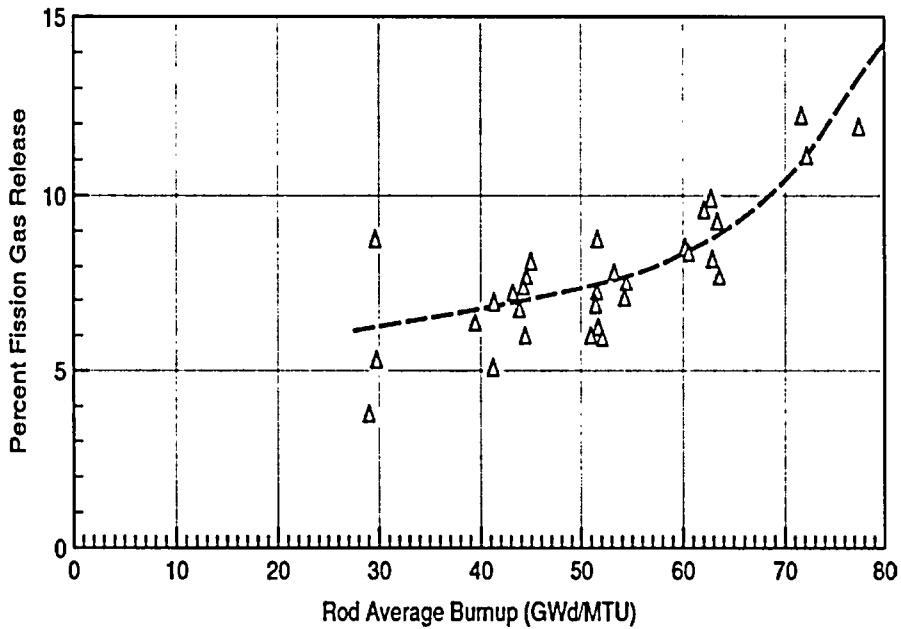


Figure 3-3. Fractional Fission Gas Release of Pressurized Water Reactor Fuel Rods with Enrichments of 3.5 to 4.2 wt% As as a Function of Rod Burnup (Manzel and Coquerelle, 1997) (Reproduced with Permission from the American Nuclear Society, Inc.)

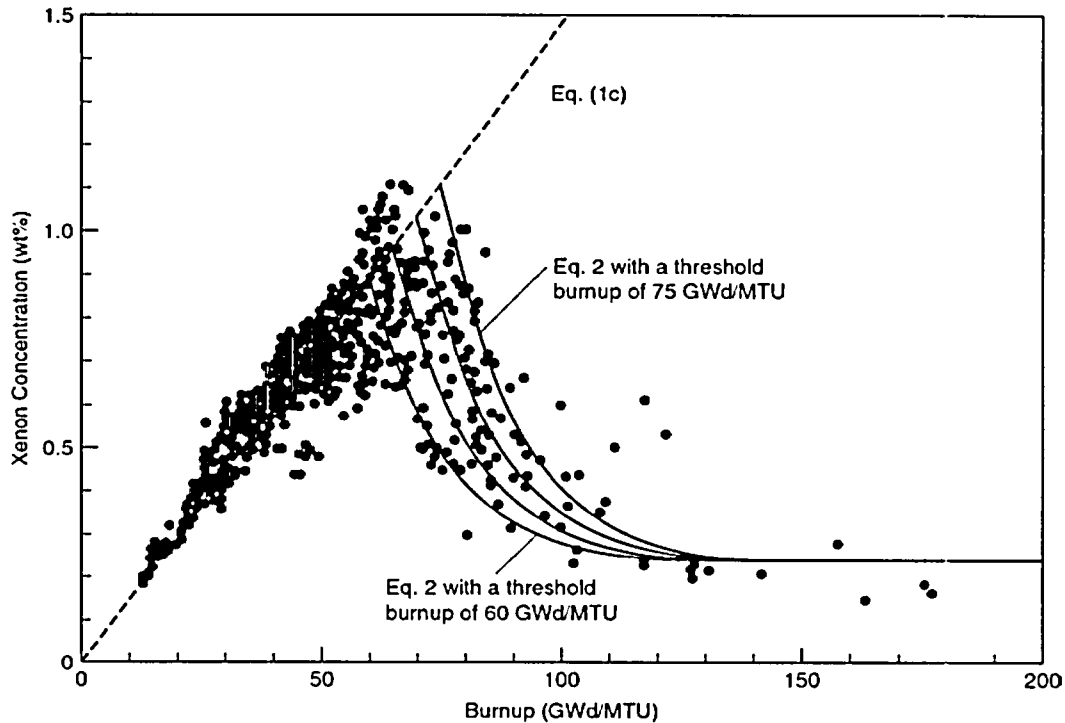


Figure 3-4. Comparison Between Predicted and Measured Local Xenon Concentrations As a Function of the Local Burnup; the Threshold Burnup Was Varied Between 60 and 75 GWd/MTU in Steps of 5 GWd/MTU (Lassmann, et al., 1995). Details for Eqs. (1c) and (2) Are Provided in Lassmann, et al., 1995. (Reproduced with Permission from Copyright Clearance Center)

formed pores in the high burnup structure. Mogensen, et al. (1999), in addition to reaching a similar assessment concluded, based on the rod-puncturing test, that only a small fraction of fission gases are released from the rim structure. Barner, et al. (1993) also demonstrated burnup and temperature dependence of grain boundary bubble precipitation. For fuels greater than 65-GWd/MTU burnup, dependant microstructural changes occurred around the rim of the pellet. The results also showed fission gas migration from the grain boundaries to this porous structure which could enhance fission gas release.

Lassmann, et al. (1995) showed the thickness of this high burnup structure increases with an increase in the burnup as shown in Figure 3-5. These changes are attributed to increased production of Pu-239, which are caused by the capture of epithermal neutrons by U-238, and its subsequent fissioning. This process resulted in a substantial increase in the local burnup around the rim. Walker (1999) characterized high burnup spent nuclear fuel from 60 to 120 GWd/MTU using electron microprobe analysis and showed that the microstructural changes at the rim/edges caused by high burnup, were much deeper than characterized by optical methods. Koo, et al. (2001) showed that local burnup at the rim is approximately 33 percent higher than the average pellet burnup. In an average burnup of 70 to 75 GWd/MTU, the rim burnup exceeds 100 GWd/MTU. While fission gas release is expected to increase with burnup because of an increased number of fissions, the high burnup structure tends to retain fission

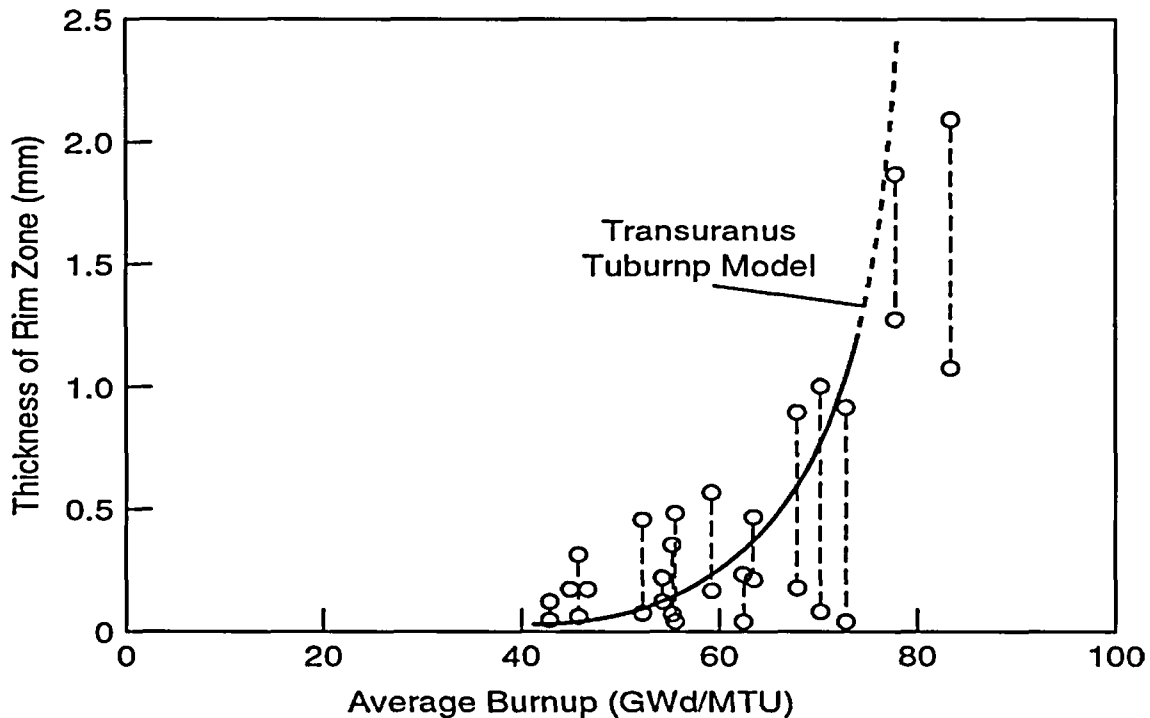


Figure 3-5. The Thickness of the High Burnup Structure (Rim Zone) As a Function of the Cross Section Average Burnup As Revealed by Xenon Measurements. The Prediction of the TRANSSURANUS TUBRNP Model Serves Only to Demonstrate the Theoretical Trend. It Is Not Known Whether the Model Is Valid at Burnups Above 75 GWd/MTU and Hence, the Line of the Model Prediction Is Shown Dashed (Lassmann, et al., 1995). (Reproduced with Permission from Copyright Clearance Center).

gases especially xenon in the pores. Only an additional small fraction of fission gases are released from the structure. At an average burnup of 80 GWd/MTU, assuming no fission gas is released, 10–20 percent of xenon can be accommodated in the pores of the rim region (Koo, et al., 2001). Despite higher fission gas concentrations in the rim region, however, diffusion from the rim structure is significantly lower because of the lower temperature in the rim region compared to the central region of the pellet.

Bremier, et al. (2000) examined fission gas release from the pressurized water reactor spent nuclear fuel rods with average burnups reaching 98 GWd/MTU and showed that the fission gas release increased from 10 percent at 50 GWd/MTU to 25 percent at 98 GWd/MTU burnup, as shown in Figure 3-6, with most of the gas release occurring from the central region of the fuel pellet. Bremier, et al. (2000) also examined the radial distribution of xenon retained in the UO_2 grains using electron microprobe analysis. The xenon profiles at different burnups are shown in Figure 3-7. Formation of a high burnup structure starts at 55 GWd/MTU, with a sharp drop observed in xenon concentration at the surface of the pellet, and continues to grow radially inward with the increase in burnup as shown in the figure. At 102-GWd/MTU burnup, the high burnup structure extended to the entire pellet and xenon concentration in UO_2 grains was uniformly distributed, with slightly lower concentration at the center, between 0.1 and 0.3 wt%.

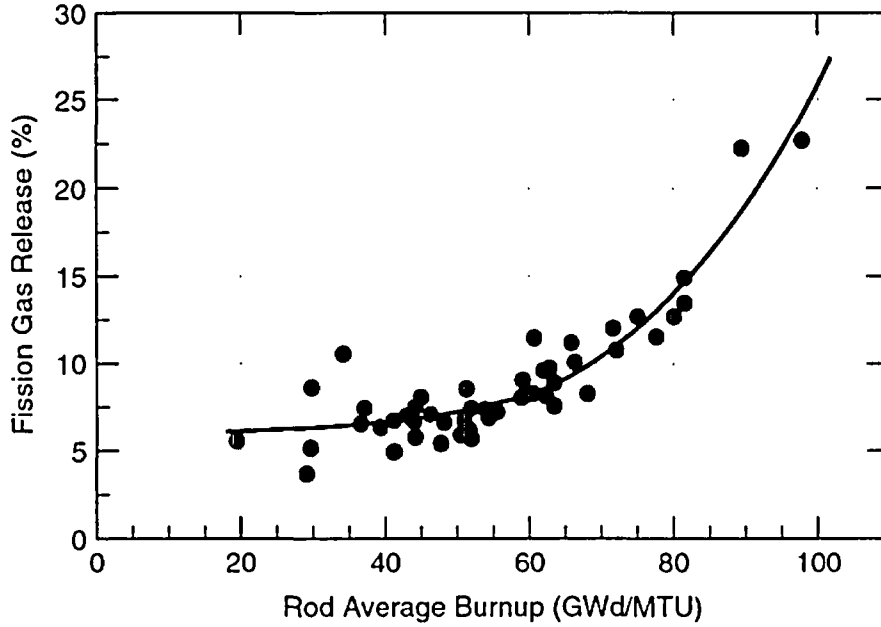


Figure 3-6. Percentage of Fission Gas Released to the Rod-Free Volume (Manzel and Walker, 2000) (Reproduced with Permission from the Nuclear Energy Agency)

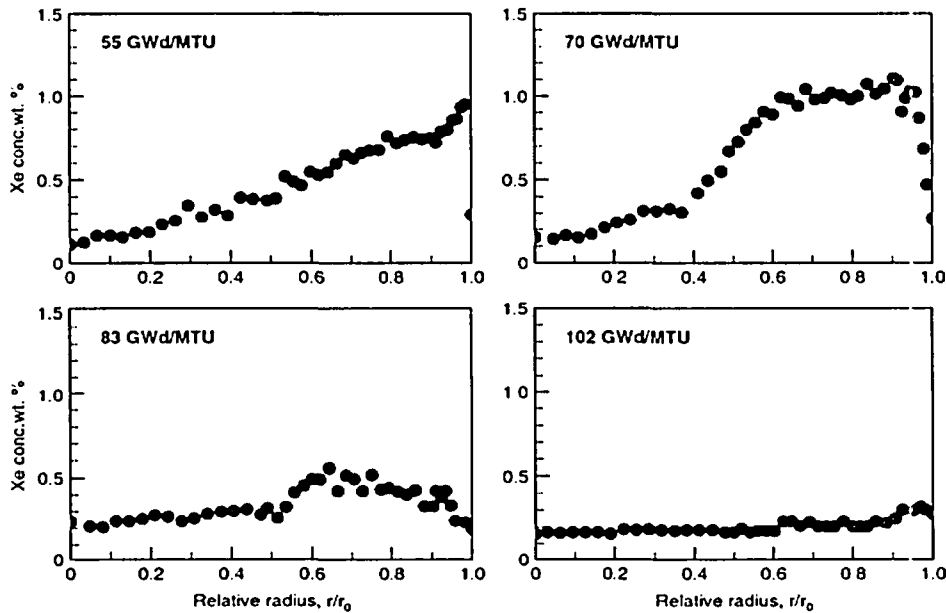


Figure 3-7. Microprobe Analysis Concentration Profiles for the Radial Distribution of Xenon Retained in the UO₂ Grains of Four Pressurized Water Reactor Fuels with Burnups of 55, 70, 83, and 102 GWd/MTU (Manzel and Walker, 2000) (Reproduced with Permission from the Nuclear Energy Agency)

Furthermore, an optical microscopy examination indicated growth in size and number of the gas pores in the high burnup structure. The large increase in the pore size at the pellet rim interface is attributed to the existence of a large reservoir of vacancies where the fission density is two to three times higher than in the body of the fuel. The comparison of fission gas release and percentage of cesium release from the fuel sample using puncture tests showed that cesium release was similar to the fission gas release at all burnups.

Tsai¹ analyzed spent nuclear fuel from Surry reactor (15 × 15 Westinghouse, 3-cycle, 36-GWd/MTU fuel stored in dry cask for 15 years), H.B. Robinson (15 × 15 FRA-ANP, 5–7 cycle, 57 GWd/MTU), and Limerick (9 × 9 GE, 3-cycle, 56 GWd/MTU) for fission gas release. While the Surry reactor spent nuclear fuel sample showed 0.5–1-percent fission gas release and no obvious changes in microstructure, the Limerick spent nuclear fuel sample had 5–17 percent and Robinson spent nuclear fuel had 1.4–2.4 percent fission gas release. The high fission gas release from Limerick spent nuclear fuel was attributed to fuel microcracking.

In this report, a limited discussion on MOX spent nuclear fuel is provided because the disposal plans at the potential Yucca Mountain repository includes less than 1 percent (1,800 MOX assemblies out of 220,000 total assemblies) of MOX spent nuclear fuel (DOE, 2001b). Furthermore, MOX spent nuclear fuel will be limited to only a few commercial reactors and DOE plans to replace each MOX assembly with an energy-equivalent uranium enriched assembly. Currently no MOX spent nuclear fuel is generated in the United States from the weapons-usable plutonium. While the quantity of MOX spent nuclear fuel is small, it should be noted that for the same burnup, MOX spent nuclear fuel shows a larger fission gas release than UO₂ spent nuclear fuel due to reactivity drop in MOX fuel with burnup resulting in a higher linear heating rate during the second cycle (Lippins, et al., 2002). The higher fission gas release lowers the thermal conductivity leading to a higher centerline temperature. Furthermore, helium generation in MOX spent nuclear fuel could be significantly higher compared to UO₂ spent nuclear fuel. In MOX fuel, during irradiation Cm-244 is a principle source of helium and during disposal, Cm-244, Pu-238, and Am-241 dominate helium generation with time. Piron, et al. (2000) compared, using CESER database, UO₂ spent nuclear fuel (47.5 GWd/MTU burnup, 4 percent enrichment) and MOX spent nuclear fuel (47.5 GWd/MTU burnup, 8.277 percent plutonium enrichment) and showed that for alpha activity of MOX spent nuclear fuel is 5 to 8 times higher than UO₂ spent nuclear fuel. At 10,000 year, the volume of helium produced from MOX spent nuclear fuel was 6,700 cm³ [408.9 in³] and from UO₂ spent nuclear fuel was 1,171 cm³ [71.5 in³]. This corresponds to 9.1 MPa [90 atm] over pressure and 66 MPa [9,572 psi] additional hoop stress for UO₂ spent nuclear fuel, and 52.7 MPa [520 atm] over pressure and 380 MPa [5.51 × 10⁴ psi] additional hoop stress for MOX spent nuclear fuel at 10,000 year. Piron, et al. (2000) warrants that the numbers do not take into account solubility of helium in fuel.

¹Tsai, H. "Characterization of High Burnup Fuel and Cladding." *Presented at the Review of ANL LOCA and Dry-Cask Storage Programs, July 16–17, 2003*. Published on CD-ROM. Argonne, Illinois: Argonne National Laboratory. 2003.

3.1 Summary

Fission gas release characteristics are different for the boiling water reactor and pressurized water reactors. Several studies have assessed that the pressurized water reactor has a slightly lower fission gas release compared to boiling water reactor. Fission gas release, however, is highly dependent on design and operating conditions. This literature review indicates a high burnup structure starts forming between 60 and 75 GWd/MTU and reaches completion at approximately 100-GWd/MTU average burnup. The burnup around the rim region is approximately 1.3 times the average burnup attributed to epithermal fissions. The fission gas release increases at higher burnups. A moderate increase in the fission gas release is observed at burnups exceeding 55-GWd/MTU. This is followed by a sharp increase in the fission gas release at burnups exceeding 75-GWd/MTU. The cesium release from the fuel upon puncturing is similar in concentration to the fission gas release. Furthermore, studies conducted on spent nuclear fuel rods exceeding 50-GWd/MTU burnup and stored in a dry storage condition for 15 years indicate the fission gas release could range from 1.4 to 17 percent. While Bremier, et al. (2000) have shown the restructuring of spent nuclear fuel microstructure could initiate at an average burnup of 55 GWd/MTU, most of the literature data indicate that rim effects are significant for burnups exceeding 60–75 GWd/MTU and have a significant impact of the fission gas release.

4 INSTANT RELEASE FRACTION

During irradiation of nuclear fuel, fissions at grain boundaries, diffusion of fission products to the grain boundaries, and a thermal process (enhancement of local burnup caused by plutonium production and fissioning) at the rim are the key contributors to the grain boundary inventory. Cracks in the fuel pellet, caused by the radial thermal gradient, and interconnected open porosity assist in the contributions to the gap inventory. The fraction of radionuclides present at the grain boundaries and in the gap is referred to as the instant release fraction. Instant release fraction refers to a combined inventory of soluble fission products, such as cesium and iodine; activation products, such as chloride and carbon located in the gap; fission products such as cesium and iodine, and segregated metallic phases, such as technetium, located at the grain boundaries (Poinssot, et al., 2001). Studies have shown that in the presence of water, fission products present at the grain boundaries are released at a slower rate compared to the gap. Because of difficulties in separating gap and grain boundary contributions, however, these fractions are combined and are assumed to be released instantly on contact with water in total system performance assessment (Mohanty, et al., 2000). Key long-lived radionuclides important to repository safety are Cs-135, I-129, Cl-36, C-14, and Tc-99.

4.1 Literature Review

Spent nuclear fuel burnup has a significant effect on the instant release fractions. The following sections provide a literature review of instant release fractions for key long-lived radionuclides and their relationship to burnup. In this report, the fraction release of Cs-135 is assumed to be represented by the fractional release from Cs-137 because Cs-137 is typically analyzed in the samples. Cs-137, however, is not considered an important contribution to the dose because the expected life of the waste package far exceeds the half-life of Cs-137. Data from CANDU spent nuclear fuel is widely used in this chapter to support instant release fraction for two reasons. First, CANDU reactors operate at higher temperature and linear power density compared to light water reactors which results in a higher fraction of fission products at grain boundaries due to thermal diffusion. Second, instant release fraction data for radionuclides such as Cl-36 from light water reactor spent nuclear fuel is lacking. Furthermore, instant release fraction data for UO₂ spent nuclear fuel is limited to 50 GWd/MTU and there is no data for MOX spent nuclear fuel.

4.1.1 Instant Release Fraction for I-129 and Cs-135

Gray (1999) analyzed gap and grain boundary concentrations of spent nuclear fuels with burnups ranging from 30 to 50 GWd/MTU and showed that both the instant release fraction for I-129 and Cs-137 and the fission gas release fraction increase with the increase in the burnup. In addition, the instant release fraction for I-129 was equal to the fission gas release fraction while instant release fraction for Cs-137 was approximately one-third of the total fission gas release fraction. Figures 4-1 and 4-2 show instant release data for I-129 and Cs-137 as functions of burnup. The data include results from boiling water reactor and pressurized water reactor spent fuels. An observed variability in the data is attributed to a combination of differences in the design, operating conditions, and radiochemistry measurements. This result is in contrast to the data on CANDU spent nuclear fuels in which the instant release fraction for Cs-137 and the I-129 were similar and mostly located in the gap (Stroes-Gascoyne, 1996). This difference is attributed to a higher operating linear power density and temperature for CANDU

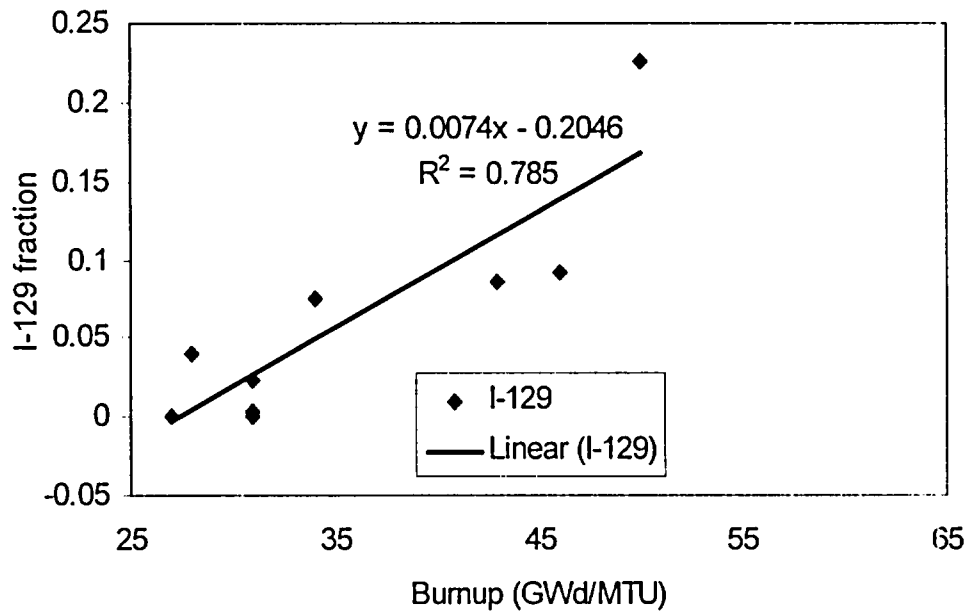


Figure 4-1. Instant Release Fraction for I-129 As a Function of Burnup. Data Are Extracted From Gray (1999) and Johnson and Tait (1997).

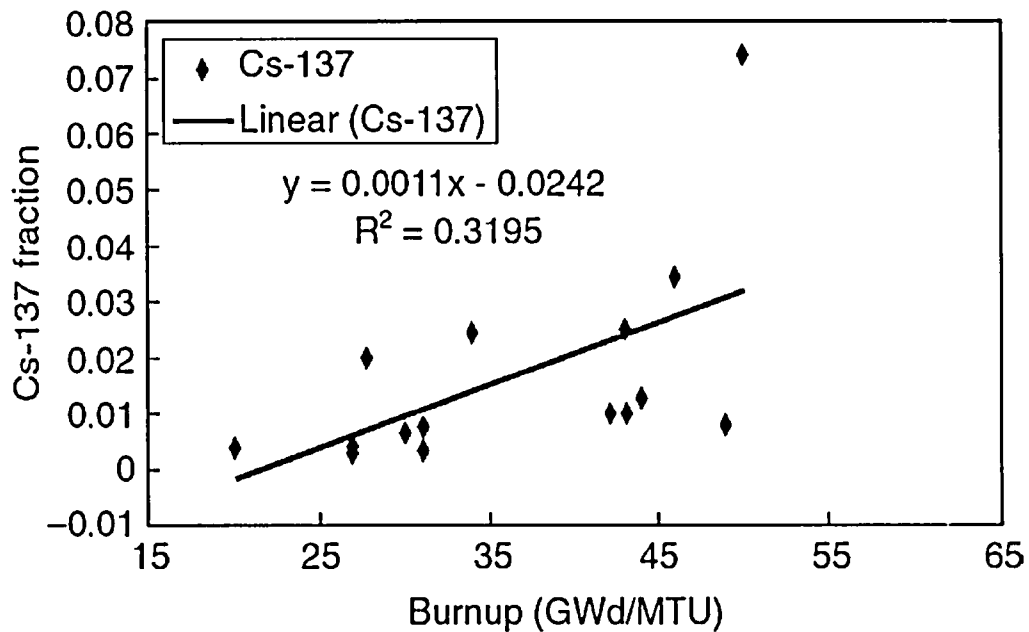


Figure 4-2. Instant Release Fraction for Cs-137 As a Function of Burnup. Data Are Extracted from Gray (1999) and Johnson and Tait (1997).

fuels compared to light water reactors. Furthermore, the data summarized by Johnson and Tait (1997) for Cs-137 and I-129 gap inventory measured by Forsyth and Werme (1992), Forsyth (1997), Wilson (1988), Wilson and Shaw (1987) indicated gap inventory of less than 2 percent for Cs-137 and less than 4 percent for I-129 in spent nuclear fuels with burnups ranging between 20 and 43 GWd/MTU. No estimate was provided, however, for the Cs-137 and I-129 grain boundary inventory. Based on these observations, Johnson and Tait (1997) recommended 3 percent as a best estimate and 6 percent as a bounding estimate for cesium and iodine instant release fractions for the Swedish spent nuclear fuel. This analysis excludes 50-GWd/MTU burnup data for I-129 and Cs-137 by Gray (1999).

The instant release fraction data for Cs-137 and I-129 for spent nuclear fuel are limited to 50-GWd/MTU burnup. Johnson and McGinnes (2002) recommend a log-uniform distribution for both I-129 and Cs-135 with 4 and 25 percent as lower and upper bounds. The data were extrapolated to 75 GWd/MTU to include contributions from the high burnup spent nuclear fuel by combining the instant release fraction analysis by Johnson and Tait (1997) and high burnup fission gas release analysis by Koo, et al. (2001).

4.1.2 Instant Release Fraction for Chloride

In a nuclear reactor Cl-35, which is present as an impurity in the UO₂ fuel pellets, and cladding are activated to Cl-36 by a neutron capture reaction. Based on the analysis of four samples, total chloride impurity in the unirradiated fuel pellets for CANDU fuel was estimated to be 2.3 ± 1 parts per million (ppm) (Tait, et al., 1997). A chemical analysis conducted by Guenther, et al. (1994) on unirradiated UO₂ fuel showed halide impurity below 10 ppm as shown in Table 4-1. Chloride is also present as an impurity in Zircaloy cladding (Tait, et al., 1997). Analyses of Zr/2.5 niobium tubing indicate chloride impurity levels between 1 and 5 ppm.

Tait, et al. (1997) analyzed a Cl-36 instant release fraction from CANDU fuel with burnups ranging between 5.6 and 15.5 GWd/MTU {linear power density between 32 and 50 kW/m

Table 4-1. Halides and Nitrogen Impurity Levels in Approved Testing Materials*		
Sample	Halides (ppm)	Nitrogen (ppm)
ATM-103 UO ₂ pellet	<10	24
ATM-104 UO ₂ pellet	<10	23
ATM-106 UO ₂ pellet	<10	44
ATM-103 cladding	—	42
ATM-104 cladding	—	19
ATM-106 cladding	—	42

*Guenther, R.J., D.E. Blahnik, and N.J. Wildung. "Radiochemical Analyses of Several Spent Fuel Testing Materials." PNL-10113. Richland, Washington: Pacific Northwest National Laboratory. 1994.

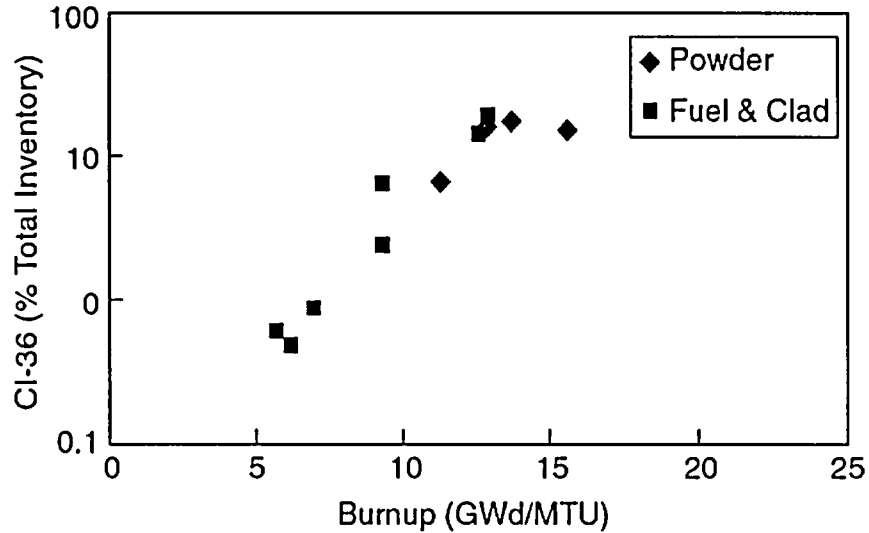


Figure 4-3. Instant Release Fraction for Cl-36 As a Function of Burnup. Data Are Extracted from Tait, et al., (1997).

[3.32×10^4 and 5.20×10^4 Btu/hr-ft]} and showed a strong functional dependence on burnup and linear power density. The instant release fraction measurements for Cl-36 in CANDU fuels ranged from 0.5 at 1.6 GWd/MTU to 20 percent at 12.8 GWd/MTU. Figure 4-3 shows a percentage of Cl-36 released as a function of burnup in a CANDU reactor. It should be noted that this behavior is expected because neutron flux, which is needed for Cl-36 activation, increases with the increase in the burnup. A Cl-36 instant release fraction was measured by the dissolution of powdered spent nuclear fuel samples as well as spent nuclear fuel clad sections. Both forms showed a similar release indicating most of the Cl-36 is released from the gap. It should be noted that the CANDU reactor operates at a much higher temperature and lower burnup compared to light water reactors. Based on the normal operating conditions of CANDU reactors, Tait, et al. (1997) recommended instant release of 5 percent for Cl-36.

There are no data on Cl-36 instant release fraction from spent nuclear fuels in the light water reactors. Johnson and Tait (1997) used Cl-36 data on CANDU fuels and recommended 6 and 12 percent as a best estimate and a pessimistic estimate for the Cl-36 instant release percentage for the Swedish light water reactor spent nuclear fuels. Johnson and McGinnes (2002) recommend a log-uniform distribution for Cl-36, similar to I-129, with 4 and 25 percent as lower and upper bounds. The data were extrapolated to 75 GWd/MTU to include contributions from the high burnup spent nuclear fuel by combining the instant release fraction analysis by Johnson and Tait (1997) and high burnup fission gas release analysis by Koo, et al. (2001).

4.1.3 Instant Release Fraction for C-14

The majority of the C-14 is produced in the light water reactor by neutron capture reactions involving -14 , O-16, and C-12. The dominant reaction is by the activation of -14 which is present as an impurity in the fuel pellet and cladding. The ASTM standard specification C776 limits the nitrogen concentration to 75 ppm in sintered UO_2 pellets. Similarly, ASTM standard specification B353 limits the nitrogen impurity to 80 ppm in Zircaloy cladding. In an analysis conducted by Guenther, et al. (1994) (Table 4-1), nitrogen impurity ranges from 19 to 44 ppm.

According to Van Konynenburg, et al. (1987), nitrogen is present in UO_2 fuel as uranium nitrate and in Zircaloy as a solid solution. Dissolution studies conducted by Wilson and Shaw (1987) and Wilson (1988) on a 31-GWd/MTU burnup spent nuclear fuel showed the C-14 instant release fraction ranged from 0.001 to 0.2 percent at 25 °C [77 °F] and 0.33 percent at 85 °C [185 °F]. The lower value for C-14 percentage at 25 °C [77 °F] was obtained using an unsealed silica crucible that could have allowed C-14 to escape as CO_2 . The higher C-14 numbers were obtained using a sealed Type 304 SS vessel. Wilson (1988) postulated that the higher values for C-14 could originate from the contributions of cladding hulls included in the test. Neal, et al. (1988) studied dissolution of ATM-101 fuel with 28-GWd/MTU burnup. Washed samples were reacted in a simulated Hanford groundwater at 200 °C [392 °F] and 25 MPa [3,626 psi] for a period of 9 months. Fractional release for C-14, Cs-137, and I-129 ranged from 3.2×10^{-4} to 1×10^{-4} /gm [0.143 to 0.45/lb] of solution which converts to 2.4 to 7.3 percent (this could include some matrix contribution). The combination of data by Wilson and Shaw (1987) and Neal, et al. (1988) indicates a strong temperature dependence on instant release fraction for C-14. For light water reactors, the C-14 release fraction at 25 and 85 °C [77 and 185 °F] ranges from 0.2 to 0.33 percent and at 200 °C [392 °F] ranges from 2.4 to 7.3 percent. Data from CANDU fuels, however, indicate that instant release fraction for C-14 has no correlation with burnup or linear power density (Stroes-Gascoyne, et al., 1994). The observed C-14 instant release fraction ranged from 1 to 5 percent. Based on these observations, Johnson and Tait (1997) recommended 5 percent as a best estimate and 10 percent as a bounding estimate for the Swedish spent nuclear fuel. Johnson and McGinnes (2002) also recommend a constant value of 10 percent for the instant release of C-14 for the Swiss spent nuclear fuel after considering the effect of high burnup fuel as much as 75 GWd/MTU.

4.1.4 Instant Release Fraction for Tc-99

Tc-99 is present in spent nuclear fuel as alloy inclusions. Since the diffusion coefficient of technetium in UO_2 is smaller than iodine, cesium, and xenon, only a small fraction is expected to be available as gap and grain boundary inventory (Prussin, et al., 1988). Wilson (1998) and Gray, et al. (1992) summarized Tc-99 instant release fraction measurements. Dissolution studies conducted by Wilson and Shaw (1987) and Wilson (1988) on spent nuclear fuel of 30-GWd/MTU burnup from the Turkey Point 1 and H.B. Robinson pressurized water reactor plants showed that the Tc-99 release was approximately 0.01 percent. Gray, et al. (1992) measured the Tc-99 gap and grain boundary inventory from ATM-103 and ATM-106 fuels with burnups ranging from 30 to 50 GWd/MTU. The measured gap and grain boundary inventory for Tc-99 was less than 0.13 percent. The measured values were near detection limits for the method used for the analysis and were much less than Cs-137 and I-129. Figure 4-4 shows a plot of measured Tc-99 instant release fraction as a function of burnup. Stroes-Gascoyne, et al. (1992) analyzed the Tc-99 instant release fraction from 13 fuel elements originating from 7 CANDU fuel bundles ranging from 5.4 to 15.6 GWd/MTU {linear power density of 29 to 50 kW/m [3.02×10^4 to 5.00×10^4 Btu/hr-ft]}. In CANDU fuels the instant release fraction for Tc-99 varied between 0.001 and 0.23 percent. Based on these observations, Johnson and Tait (1997) recommended 0.2 percent as a best estimate and 1 percent as a bounding estimate for the Swedish light water reactor spent nuclear fuel. Johnson and McGinnes (2002) recommend a log-uniform distribution for Tc-99 with 2 and 17 percent as lower and upper bounds. The data were extrapolated to 75 GWd/MTU to include contributions from the high burnup spent nuclear fuel by combining the instant release fraction analysis by Johnson and Tait (1997) and high burnup fission gas release analysis by Koo, et al. (2001).

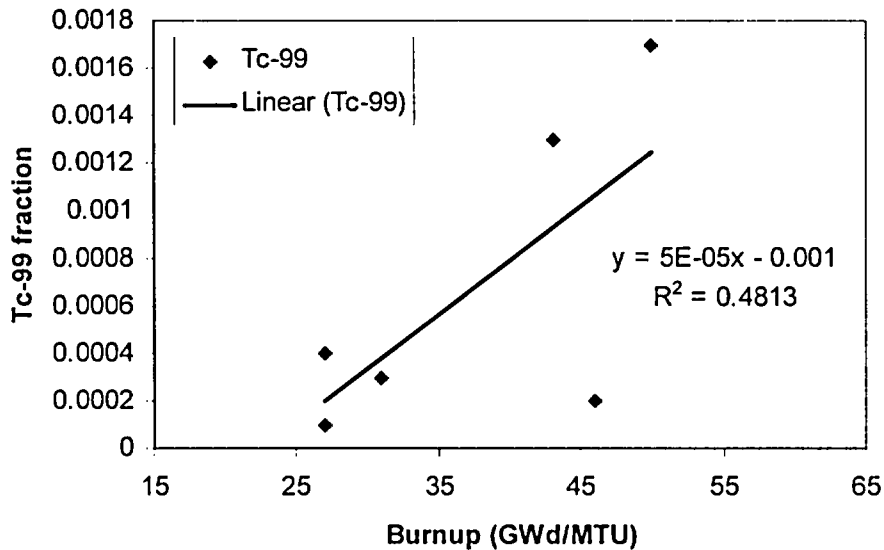


Figure 4-4. Instant Release Fraction for Tc-99 As a Function of Burnup. Data Are Extracted from Johnson and Tait (1997).

4.1.5 Instant Release Fraction for Other Radionuclides

Sr-90 is present as a dissolved species in the spent nuclear fuel (Kleykamp, 1985). A very small fraction, however, could originate at grain boundaries that could contribute to grain boundary instant release fraction. Gray, et al. (1992) measured the Sr-90 gap and grain boundary inventory from ATM-103 and ATM-106 fuels with burnups ranging from 30 to 50 GWd/MTU. The measured gap and grain boundary inventory for Sr-90 was less than 0.13 percent. The measured values were near detection limits for the method used for the analysis and were similar to Tc-99 and much less than Cs-137 and I-129. Stoes-Gascoyne, et al. (1992) analyzed 13 fuel elements from 7 CANDU fuel bundles ranging from 5.4 and 15.6 GWd/MTU {linear power density of 29 to 50 kW/m [3.02×10^4 to 5.00×10^4 Btu/hr-ft]} for Sr-90 instant release fraction. In CANDU fuels the instant release fraction for Sr-90 varied between 0.0005 and 0.04 percent. Based on these observations, Johnson and Tait (1997) recommended 0.25 percent as a best estimate and 1 percent as a bounding estimate for the Swedish light water reactor spent nuclear fuel. Sr-90, however, is not considered an important contributor to the dose because the expected life of the waste package far exceeds its half-life.

There are no instant release fraction data for radionuclides, such as Se-79, Zr-93, Nb-94, Pd-107, Cd-113m, and Sn-126, that could be present in the gap and grain boundary. Johnson and Tait (1997) conservatively paired these radionuclides with either I-129, Cs-135, or Tc-99. To extrapolate instant release fractions for these radionuclides to 75 GWd/MTU, Johnson and McGinnes (2002) adopted a similar approach and recommended a log-uniform distribution based on instant release fractions for existing radionuclides. However, these radionuclides are not considered important to waste isolation at the potential Yucca Mountain repository.

Table 4-2 provides a summary of distributions or ranges proposed for instant release fraction by various high-level waste disposal programs. Stoes-Gascoyne (1996) and Johnson and

Element	Swiss for Sensitivity Analyses*	Canadian†	DOE‡	NRC/CNWRA§	Swedish
Distribution	Log-uniform Lower: best estimate at 48 GWd/MTU Upper: Extrapolated to 75 GWd/MTU	Normal distribution: mean; standard deviation	Triangular distribution: lower, apex, upper	Constant	Not specified: (best estimate, conservative)
I-129	4, 25	3.6, 2.4	2.04, 11.24, 26.75	6	3, 6
Cs-135	4, 25	3.9, 1.9	0.39, 3.63, 11.06	6	3, 6
Tc-99	2, 17	—	0.01, 0.10, 0.26	1	0.2, 1
Se-79	4, 25	—	—	6	3, 6
Cl-36	0, 25	—	—	12	6, 12
C-14	10, 10	2.7, 1.6	—	10	5, 10

*Johnson, L.H. and D.F. McGinnes. "Partitioning of Radionuclides in Swiss Power Reactor Fuels." NAGRA Technical Report 02-07. Wetingen, Switzerland: National Cooperative for Disposal of Radioactive Waste. 2002.
†Stroes-Gascoyne, S. "Measurements of Instant-Release Terms of Cs-137, Sr-90, Tc-99, I-129 and C-14 in Used CANDU Fuels." *Journal of Nuclear Materials*. Vol. 238. pp. 264-277. 1996.
‡Bechtel SAIC Company, LLC. "Technical Basis Document No. 7: In-Package Environment and Waste Form Degradation and Solubility." Rev. 1. Las Vegas, Nevada: Bechtel SAIC Company, LLC. 2004.
§Mohanty, S., T.M. McCartin, and D.W. Esh. "Total System Performance Assessment (TPA) Version 4.0 Code: Module Descriptions and User's Guide." San Antonio, Texas: CNWRA. 2000.
||Johnson, L.H. and J.C. Tait. "Release of Segregated Nuclides From Spent Fuel." SKB Technical Report 97-18. Stockholm, Sweden: Swedish Nuclear Fuel and Waste Management Company. 1997.

McGinnes (2002) proposed normal and log-uniform distributions for the Canadian and Swiss high-level waste disposal program, respectively. The Swiss estimate includes contributions based on fission gas release from high burnup fuels and was used for conducting sensitivity analyses. The Swedish high-level waste program provides upper and lower bounds for instant release fraction while the U.S. Department of Energy (DOE) proposed a triangular distribution. Table 4-2 also provides current U.S. Nuclear Regulatory Commission and Center for Nuclear Waste Regulatory Analyses distributions for instant release fractions (Mohanty, et al., 2000). Even though distributions assumed are different, the same database is used for developing estimates for instant release fractions by various high-level waste producers and regulators.

4.2 Review of DOE Approach

DOE proposed ranges for instant release fraction for cesium and iodine based on Gray (1998) and Tc-99 and Sr-90 based on Gray, et al. (1992) studies as discussed in Section 4.1.

Proposed ranges, however, do not include effects of spent nuclear fuels exceeding 50 GWd/MTU. The instant release fraction distributions proposed by the DOE is shown in Table 4-2. The distribution type and the range selected by the DOE is reasonable.

4.3 Discussion and Assessment of the NRC Approach for Instant Release Fraction

4.3.1 Justification for Extrapolation of Instant Release Fraction Data to High Burnups

The following are key observations from the studies about the instant release fraction for spent nuclear fuels

- The amount of fission products released in the gap and grain boundary increase with burnup. This increase is demonstrated in Figures 4-1 through 4-4.
- The instant release fraction for I-129 is similar to the xenon release rate (Gray, 1999).
- A high burnup structure forms between 60 and 75 GWd/MTU at the outer surface of the pellet and moves inward radially (Bremier, et al., 2000; Lassmann, et al., 1995).
- Beyond 50 GWd/MTU, fission products from the high burnup structure are required to be estimated because there are no experimental data beyond 50 GWd/MTU on the release of fission products.
- Beyond 60 GWd/MTU, localized burnup in the rim region is estimated as 1.33 times average burnup (Koo, et al., 2001).
- Xenon is not completely retained in high burnup rim structure (Mogenson, et al., 1999).
- In the rim region, the grain size decreases as the burnup increases. Decrease in grain size will significantly increase the total surface of the grain boundary (Une, et al., 1997). Gray (1999) includes grain boundary contributions from samples crushed to typical fuel grain size, which provides a conservative estimate for grain boundary release for the rim region.
- Poinssot, et al. (2002) considered the instant release fraction present in the rim section as liable.

Because of the lack of instant release fraction data for fuels higher than 50-GWd/MTU burnup, the instant release fraction data for burnup below 50 GWd/MTU is used to extrapolate instant release fractions in the high burnup regime. Johnson and McGinnes (2002) estimated expected instant release fraction for radionuclides by calculating the fraction of xenon removed from the grains as a function of burnup. Such linear extrapolation was justified by the expected capacity xenon fission gas retained in the pores of the rim of the high burnup fuels. Lassmann, et al. (1995) showed that fission gas, which is continuously released from the grains through fission, migrates to the newly formed fission gas pores and is retained in the high burnup structure. Similarly, Mogensen, et al. (1999) concluded that in some cases, up to 90 percent of

the fission gas released to the gap inventory came from the high burnup structure. Normally maximum fission gas release occurs in the central region because of thermally active diffusion. Because in some cases, xenon release could occur from a high burnup structure, it is prudent to assume the entire fraction of xenon gas present in the pores of the high burnup structure is available for release.

Koo, et al. (2001) developed an empirical linear relationship between the observed high burnup rim thickness as a function of burnup. Rim thickness is a measure of high burnup structure in a pellet. This relationship was based on a large number of studies published in the literature as shown in Figure 4-5. While some studies showed exponential growth of the rim region, others support linear increase of the rim region with increase in burnup. Recent studies indicate that the width of the rim structure increases linearly up to 70 GWd/MTU burnup and is followed by an exponential increase thereafter. Using Koo, et al. (2001) relationship and assuming a limiting average high burnup of 75 GWd/MTU, a rim thickness of 169 and 342 μm [6.65 and 13.46 mil] is estimated as best and conservative estimates. This rim thickness corresponds to 8- and 16-percent volume of the fuel pellet {assuming fuel pellet dimensions of 13.5-mm [0.53-in] thickness and 8.2-mm [0.32-in] diameter}. Furthermore, best and conservative estimates for burnup in the pellet excluding the rim area are approximately 72.8 and 70.3 GWd/MTU, for an average burnup of 75 GWd/MTU and rim burnup of 100 GWd/MTU. From the linear regression equation shown in Figure 4-1, I-129 releases from the fuel pellet, excluding the rim and the high burnup rim

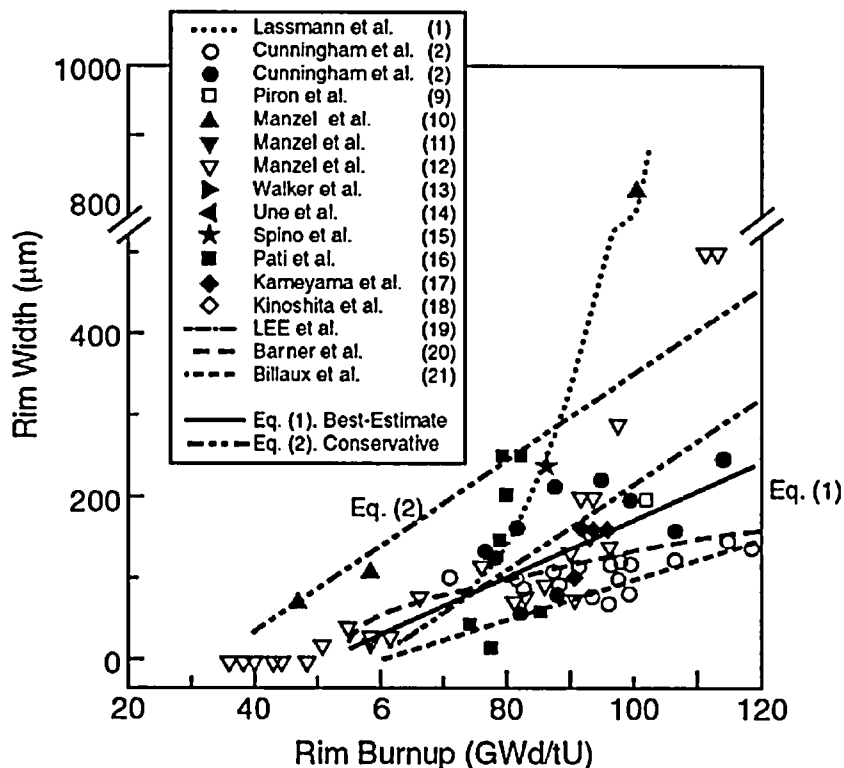


Figure 4-5. Measured Rim Width Both by Electron Microprobe Analyzer and Optical Microscopy (Koo, et al., 2001). (Reproduced with Permission from Copyright Clearance Center). NOTE: Refer to Koo, et al. (2001) for Information on References Cited in the Figure.

region are 28.5 and 49.5 percent. Therefore, the average I-129 instant release at 75 GWd/MTU average burnup, which is a combination of fractional release from the pellet excluding the rim and the high burnup rim region is 30 percent for the best estimate and 32 percent for the conservative estimate. Studies, however, indicate that, for burnups exceeding 60 GWd/MTU, most of the xenon is captured in the pores. Given a similar mobility of I-129 compared to xenon, I-129 is also expected in the rim structure porosity. Studies also have shown that, in infrequent cases, xenon is released to the gap inventory from the rim structure. To ensure fission release from the pellet captures the potential for I-129 release to an instant release fraction, 100 percent of the I-129 present in the high burnup rim region should be assumed as liable (Poinsett, et al., 2002). Conservative and best estimates for I-129 instant release fractions at 75 GWd/MTU, assuming 100 percent of the I-129 present in the rim structure is available for release, are 34 and 40-percent, respectively. It is recommended that an upper limit of 34 percent be used as an estimate for I-129 release at 75 GWd/MTU burnup. The 40 percent release for I-129 represents an extremely conservative position that includes conservative estimates of rim thickness combined with an assumption that 100 percent of I-129 in the high burnup region is present in pores.

Based on the data by Gray (1999), it is recommended to tie the Cs-135 release to one-third of I-129. This is a conservative recommendation based on available data. Lassmann, et al. (1995) showed that cesium is retained within the high burnup rim structure. Combined with expected low temperatures {less than 800 °C [1,472 °F]} around the rim region and its observed retention in the structure, cesium is expected to contribute only from the center of the pellet and follow the relationship shown in Figure 4-2 as a function of burnup. Similarly Tc-99 is expected to follow the relationship shown in Figure 4-4 because of its extremely low mobility.

Cl-36 originates because of neutron capture by Cl-35 impurity in the pellet. Cl-36 concentration increases with the increase in burnup. Cl-36, like xenon and I-129, is volatile and is expected to follow I-129 or xenon release behavior. While there are no data for instant release for Cl-36 in light water reactors, the Cl-36 instant release fraction data obtained from CANDU fuels are considered conservative because CANDU fuels operate at much higher temperatures {1,400 °C [2,552 °F]} compared to light water reactor fuels. The release to the gap and grain boundary is expected to be significantly lower in light water reactor fuels whose operating temperatures are approximately 1,200 °C [2,192 °F]. Because of the high volatility of Cl-36 and lack of data from light water reactors, Cl-36 instant release fraction is assumed to follow I-129 release for high burnup spent nuclear fuels. This assumption includes contribution from cladding.

C-14 originates because of neutron activation of N-14 impurity in the pellet. C-14 instant release fraction studies by Stroes-Gascoyne (1996) on CANDU fuels indicated an average C-14 concentration of 2.7 percent (ranged from 0.06 to 5.4 percent) with no burnup dependence. While 30-GWd/MTU light water reactor fuel release data indicate C-14 concentration below 0.33 percent at 85 °C [185 °F], the C-14 instant release fraction of 10 percent selected by Tait and Johnson (1997) is 30 times higher than the observed concentration of C-14. This C-14 concentration is considered very conservative. Since CANDU data showed no burnup dependence and was obtained at higher operating temperatures {1,400 °C [2,552 °F]} compared to light water reactors {1,200 °C [2,192 °F]}, a constant value 5-percent release for C-14 instant release fraction is appropriate for light water reactor fuels. If a similar contribution from cladding is added, however, 10-percent instant release fraction from spent nuclear fuel and cladding is appropriate.

Table 4-3. Recommended Instant Release Fraction Values for Triangular Distributions			
Instant Release Fraction	Lower (Percent)	Apex (Percent)	Upper (Percent)
I-129 and Cl-36	0.50	11	34
Cs-135	0.16	3.7	11.3
Tc-99	0.05	0.13	0.28
C-14	10	10	10

4.3.2 Proposed Instant Release Fraction Distribution

Figures 4-1 through 4-4 show plots of instant release fraction data for iodine, cesium, chloride and technetium as a function of burnup. Despite a large variance in data for cesium and technetium, the trend shows an increase in the instant release fraction with the increase in the burnup of the spent nuclear fuel. The increase in the gap and grain boundary inventory with the increase in the burnup are attributed to the increased fissions at the grain boundaries coupled with the contributions from the diffusion of fission products to the grain boundary. While temperature does not undergo significant change with burnup, the fission product concentration at grain boundaries tends to increase with time at any given temperature.

Because 97 percent of the present spent nuclear fuel in the United States according to a 1998 inventory, is <45 GWd/MTU burnup and the instant release fraction for important species increases with the increase in burnup, a triangular distribution is recommended with lower and upper bounds represented by 30 and 75 GWd/MTU with an apex at 45 GWd/MTU. Projected data show the high burnup spent nuclear fuel (>45 GWd/MTU) is expected to substantially increase and could account for as much as 30 percent of the total projected inventory to be placed in the potential high-level waste repository at Yucca Mountain. The recommended ranges are shown in Table 4-3. The instant release fraction for I-129 was estimated as 34 percent at 75 GWd/MTU. The recommended instant release fraction for cesium is one-third of the instant release fraction for I-129 based on available light water reactor data. Because of the high volatility of Cl-36 and the lack of Cl-36 data in light water reactors, a release fraction similar to I-129 is recommended. Uncertainties in Tc-99 are significant because of the limited data and low concentration of Tc-99 present in the grain boundaries that makes Tc-99 measurements prone to method uncertainties. The observed concentration of Tc-99 in analyzed samples does not exceed 0.13 percent, which is much lower than the upper bound of 17 percent selected by the Swiss program. Based on the CANDU fuel data that showed no dependence on burnup, the instant release fraction for C-14 was fixed at 10 percent. The instant release fraction for Cl-36 and C-14 includes contributions from both fuel and cladding.

4.4 Summary

Because the high burnup fuel (exceeding 45 GWd/MTU) is expected to be between 30 and 35 percent of the total inventory, the fuel contribution to the source term from the instant release fractions could be significant and should be considered in the assessment. Despite the lack of

experimental data exceeding 50-GWd/MTU burnup, an estimate of instant release fractions is determined based on the fission gas release data from the high burnup spent nuclear fuel. Significant uncertainties remain, however, in the estimate of the instant release fraction for important radionuclides above 60 GWd/MTU because of the formation of the high burnup rim structure. An instant release fraction of 34 percent for I-129, which is considered most important to the dose, is estimated by linear extrapolation of existing data for as much as 50-GWd/MTU burnup, assuming 100 percent of the I-129 present in the rim is available for release and justifying the high burnup rim region based on fission gas release data. The instant release fraction for cesium is similarly justified. The instant release fraction for cesium, however, is one-third of the instant release fraction for I-129 based on available light water reactor data. Uncertainties in Tc-99 are significant because of the limited data and low concentration of Tc-99 present in the grain boundaries that make Tc-99 measurements prone to method uncertainties. The observed concentration of Tc-99 in analyzed samples does not exceed 0.13 percent, which is much lower than the upper bound of 17 percent selected by the Swiss program. It is recommended that the upper bound for the instant release fraction for Tc-99 should be 0.28 percent. Similarly, significant uncertainties exist for the instant release fraction for C-14 and Cl-36, which are a result of impurities in the fuel and cladding caused by the lack of data for light water reactor spent nuclear fuels. Because Cl-36 volatility is comparable to I-129 {boiling point 184 °C [363 °F]} during reactor operations, I-129 release fraction is recommended for Cl-36. A constant instant release fraction of 10 percent is recommended for C-14. Because most of the data were obtained on fuel grains or fragments, the instant release fraction obtained from these samples represents a conservative estimate; the instant release fraction does not take credit for limited access of water to grain boundaries. A triangular probability distribution is proposed for iodine, cesium, chloride, and technetium. Unlike normal distribution, this distribution bounds upper and lower ends while accommodating expected uncertainties.

5 HIGH BURNUP SPENT NUCLEAR FUEL DISSOLUTION RATE

In 1993, the Center for Nuclear Waste Regulatory Analyses (CNWRA) reviewed characteristics of spent nuclear fuel and cladding relevant to high-level waste source terms (Manaktala, 1993). Recent reviews by Oversby (1999) and Poinsett, et al. (2001) provide an overview of the spent nuclear fuel dissolution and long-term behavior of spent nuclear fuel. While these reports provide state-of-the-art reviews of the spent nuclear fuels issue important to disposal, an assessment of burnup on the spent nuclear fuel dissolution rate is not adequately addressed.

As discussed in Chapter 3, as burnup increases, spent nuclear fuel exceeding 60 GWd/MTU undergoes significant microstructural changes at the rim, including a decrease in the fuel grain size, a loss of defined grain structure, a decrease in the high density of small pores, and a loss of the fission gas xenon from the fuel matrix. In addition, grain fusion could occur at burnup exceeding 60 GWd/MTU. These microstructural changes could influence the spent nuclear fuel dissolution rate. In the following sections, an assessment of high burnup spent nuclear fuel dissolution under oxidizing conditions relevant to potential Yucca Mountain high-level repository conditions is provided.

5.1 Literature Review

In the United States, spent nuclear fuel dissolution studies have been conducted under the U.S. Department of Energy (DOE) program for the disposal of the high-level waste at the potential Yucca Mountain repository. These DOE studies are summarized in the Gray and Wilson (1995), Stout and Leider (1998) and Civilian Radioactive Waste Management Systems Management and Operating Contractor (CRWMS M&O) (2000a) reports and are used for the development of a parametric model to describe the spent nuclear fuel dissolution behavior for the TPA Version 5.0 code. Most of the data used for the development of the abstraction model were collected using a single-pass, flow-through test method (Gray and Wilson, 1995). CRWMS M&O (2000a) analyzed spent nuclear fuel dissolution rates on samples ranging from 15 to 70-GWd/MTU burnup, including unirradiated fuel. The dissolution rate of spent nuclear fuel by the single-pass flow-through test method is considered conservative because the dissolution rate data are not influenced by the saturation of uranium in solution. DOE conducted these tests by systematically varying temperature {21 to 75 °C [69.8 to 167 °F]}, pH (8–10), oxygen partial pressure {0.002–0.2 atm [0.0029–2.94 psi]}, and carbonate concentrations (0.0002–0.02 M) to obtain a parametric model as shown by Eqs. (5-1) and (5-2), to describe spent nuclear fuel dissolution behavior in the alkaline and acidic region.

For pH > 7

$$\log DR = 4.69 - 1085 \times IT - 0.12 \times pCO_3 - 0.32 \times pO_2 \quad (5-1)$$

For pH < 7

where

$$\log DR = 7.13 - 1085 \times IT - 0.32 \times pCO_3 - 0.41 \times pO_2 \quad (5-2)$$

DR — dissolution rate (mg/m²-d)
IT — inverse temperature (K)

pCO_3 — $-\log$ (total molar carbonate)
 pO_2 — $-\log$ (pressure O_2)

The parametric model developed by DOE showed the spent nuclear fuel dissolution rate in the alkaline range (pH 8–10) has a strong functional relationship with temperature and total carbonate concentration and a weak functional relationship with pH. DOE, however, did not provide any functional relationship to burnup. Furthermore, DOE excluded 70-GWd/MTU burnup data in their abstraction model. To estimate a spent nuclear fuel dissolution rate in $mg/m^2\text{-d}$, CRWMS M&O (2000a) used the geometrically measured surface area and multiplied by a surface area roughness factor of three. Details are discussed in Section 5.2.

Röllin, et al. (2001) systematically examined the effect of pH on the spent nuclear fuel dissolution rate using a 43-GWd/MTU burnup sample. Spent nuclear fuel dissolution rate were obtained using a crushed sample of $300\text{-cm}^2/g$ [$2.11 \times 10^4\text{-in}^2/lb$] surface area in flow-through tests. The surface area was determined by Brunauer Emmett and Teller method. Tests were conducted in solutions containing 10 mM NaCl and the pH was adjusted by adding sodium bicarbonate or hydrochloric acid. The oxidizing conditions were established by direct contact of test solution to atmospheric conditions and sparged with pressurized air or gas mixture containing 20% $O_2/0.03\%CO_2/80\%Ar$. The reducing conditions were established by bubbling H_2 containing 0.03% CO_2 . The spent nuclear fuel dissolution rate was obtained as a function of pH (3 to 9.3) in both oxidizing and reducing conditions. Figure 5-1 shows the observed spent nuclear fuel dissolution rate as a function of pH. Data indicate the spent nuclear fuel dissolution rate is systematically higher in oxidizing conditions compared to reducing conditions irrespective of the pH, and in solution pH less than 6, spent nuclear fuel dissolution rate increases with the decrease in pH. At pH higher than 6, dissolution rate remained constant at a value of $3\text{ mg}/m^2\text{-d}$ [$6.13 \times 10^5\text{ lb}/ft^2\text{-d}$].

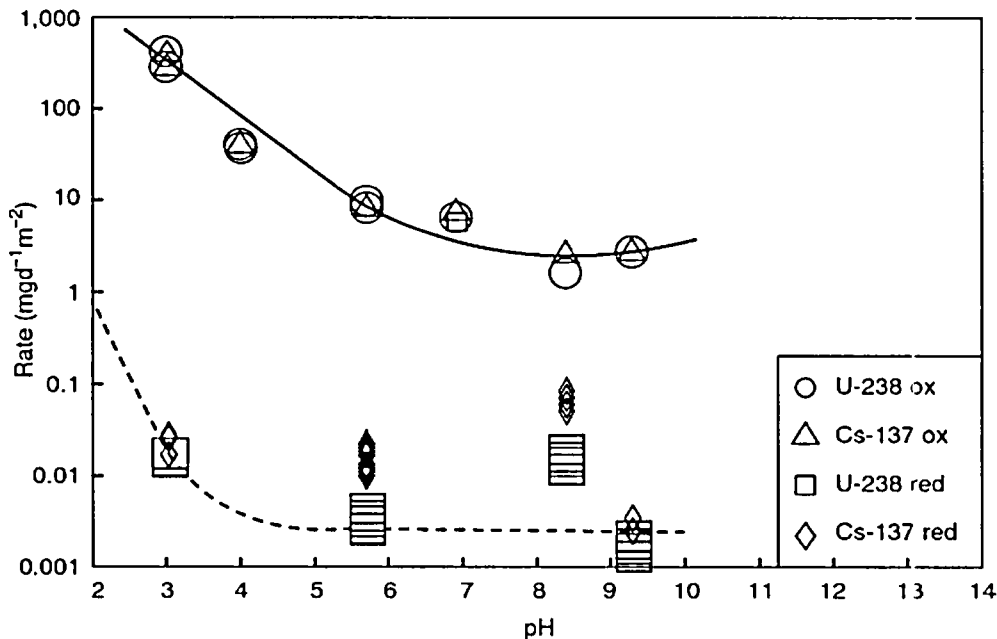


Figure 5-1. Spent Nuclear Fuel Dissolution Rates (R), Based on U-238 and Cs-137 for Different pH Under Oxidizing and Reducing Conditions (Röllin, et al., 2001) (Reproduced with Permission from Copyright Clearance Center)

Jégou, et al. (2001) described ongoing studies about the dissolution behavior of the high burnup spent nuclear fuel from French nuclear power reactors. Jégou, et al. (2001) studied the dissolution behavior of spent nuclear fuel samples with burnups 22, 37, 47, and 60 GWd/MTU in granitic groundwater {composition not provided in Jégou, et al. (2001)} at 25 °C [77 °F] under oxidizing conditions. The clad fuel rod samples, after washing for a period of 3 years to remove gap and grain boundary fractions, were immersed in sealed stainless steel vessels and periodically sampled. The study showed that strontium is a good matrix dissolution rate indicator. The average fractional release rate for the first 8 days in a 1-year-long test ranged from 1 to 4 × 10⁻⁶ per day for all samples irrespective of burnup. The spent nuclear fuel dissolution rate stabilized at 1 × 10⁻⁷ per day for all fuel samples, irrespective of the burnup, between 8 and 126 days as shown in Figure 5-2. Higher initial release rate during first 8 days is attributed to dissolution of a thin uranium (VI) oxide layer formed on the surface during storage. This portion of the spent nuclear fuel dissolution curve is neglected in the calculation for average spent nuclear fuel dissolution rate. Average fractional release rate, were converted to mg/m²-d by multiplying the surface area of open faces with a correction factor of 4.5 to account for surface fragmentation and were estimated as 2 mg/m²-d [4.09 × 10⁻⁷ lb/ft²-d]. The observed dissolution rate behavior at 25 °C [77 °F] is similar to the spent nuclear fuel dissolution rate observed for the DOE samples despite the differences in the test method, surface area correction factor, and sample. Jégou, et al. (2001) used a surface area correction (or roughness) factor of 4.5 for a fuel rod sample in an immersion-type test while CRWMS M&O (2000a) used a correction factor of three for the powder sample in a flow-through test. It is possible that the differences in the spent nuclear fuel dissolution rate are masked by inadequate estimation of surface area in both Jégou, et al. (2001) and CRWMS M&O (2000a) studies.

Forsyth (1997) examined the spent nuclear fuel dissolution from boiling water reactor from the Righhals-1 reactor in Sweden with burnups ranging from 27 to 48.8 GWd/MTU. Tests were conducted using a 20-mm [0.79-in] length of fuel/clad sample under static, oxidizing conditions.

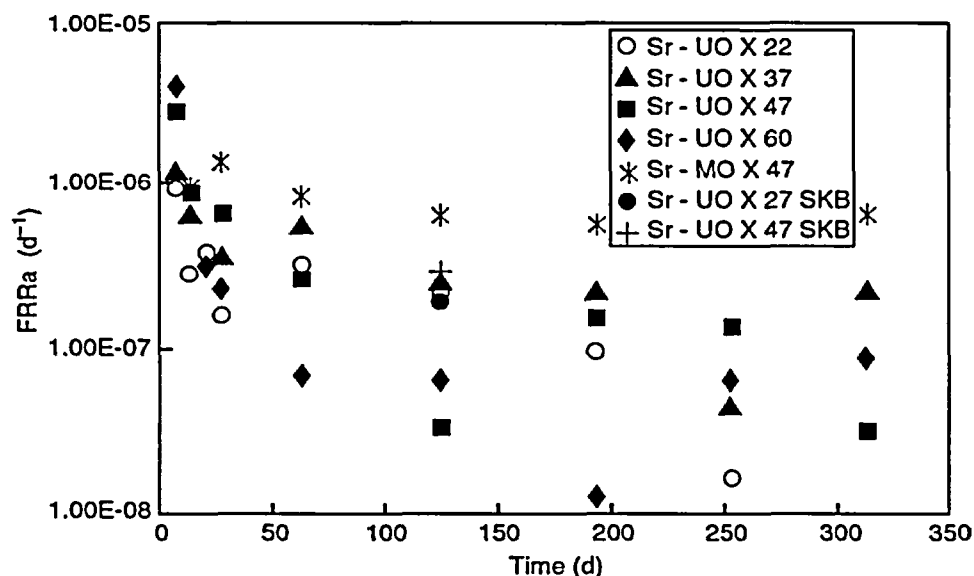


Figure 5-2. Average Fractional Release Rate FRRa (d⁻¹) for Strontium As a Function of Time for Different Burnup Spent Nuclear Fuel Samples (Jégou, et al., 2001)

Tests were either conducted in the deionized water or the Swedish reference simulated bicarbonate groundwater of composition shown in Table 5-1. Free volume between fuel and cladding was estimated as 0.06 and 0.04 cm³ [3.66×10^{-3} and 2.44×10^{-3} in³] for low and high burnup samples, respectively. The release rate for samples with different burnups converge with time. The cumulated cesium during a 5.09-year dissolution period peaked at 45 GWd/MTU. Table 5-2 shows the results of the Forsyth (1997) study. For series three fragment tests, the surface area was calculated using a surface roughness factor of three. For segment tests, majority of the dissolution was assumed to occur at the open ends of the segments, therefore, the calculated surface area was increased by 50 percent and then multiplied by a roughness factor of 3. Depending on the surface area, the spent nuclear fuel dissolution rate could range from 0.7 to 8 mg/m²-d [1.43×10^{-7} to 16.3×10^{-7} lb/ft²-d] in a static immersion type test.

Species	HCO ₃ ⁻	SiO ₂	SO ₄ ²⁻	Cl ⁻	Ca ²⁺	Mg ²⁺	K ⁺	Na ⁺
Molarity	2.01 × 10 ⁻³	2.05 × 10 ⁻⁴	1.0 × 10 ⁻⁴	1.97 × 10 ⁻³	4.47 × 10 ⁻⁴	1.77 × 10 ⁻⁴	1.0 × 10 ⁻⁴	2.83 × 10 ⁻⁴
ppm	123	12	9.6	70	18	4.3	3.9	65

Note: pH: 8.0–8.2; Ionic Strength: 0.0085.
 *Forsyth, R.S. and L.O. Werme. "Spent Fuel Corrosion and Dissolution." *Journal of Nuclear Materials*. Vol. 190. pp. 3–19. 1992.

Loida, et al. (2004, 2003, 2001, 1996) extensively studied the dissolution behavior of the high burnup spent nuclear fuel (50 GWd/MTU, linear power 260 W/m) in environments relevant to a deep geological repository to be located in rock salt formations such as in the salt dome of Gorleben in Germany. Studies showed that, in the reducing condition, the instant release fraction and spent nuclear fuel dissolution rate are not affected by the presence of backfill materials such as magnetite and hydroxylapatite (Loida, et al., 2004). In their study, leachate was entirely replaced with fresh water several times in the first 41 days to remove the easily leachable gap and grain boundary inventory. The spent nuclear fuel dissolution rate was 1×10^{-6} per day based on a fraction of the inventory in aqueous phase [FIAP(Sr)]. FIAP and sorption of radionuclides, such as americium, neptunium, plutonium, uranium, and strontium, however, depended on backfill material. The sorption of radioelements was highest for plutonium, followed by americium, uranium, and technetium, and significantly below strontium. In this study, strontium dissolution was considered an indicator of the matrix dissolution rate because of its low sorption capacity of backfill materials. In samples where a small quantity of air was allowed to contact fuel surface, the spent nuclear fuel dissolution rate was one order of magnitude higher in comparison to nonoxidized fuel (Loida, et al., 2004). The studies were conducted in 5 m sodium chloride and saturated magnesium chloride solutions. After 4.5 years of testing preoxidized samples, however, the dissolution rate based on Sr-90 release was reduced significantly. In an earlier study, Loida, et al. (1996) showed the dissolution rates encountered by powdered samples were lower compared to pallets and fragments and attributed this effect to an enhanced depletion of oxidative reactants (dissolved oxygen, radiolytic products, and radicals) from solution.

Table 5-2. Normalized Dissolution Rate for Swedish Spent Nuclear Fuels*				
Fuel	Series 3 Boiling Water Reactor	Series S Boiling Water Reactor	Series 7 Pressurized Water Reactor	Series 11 Boiling Water Reactor
Type	Fragment	Segment	Segment	Segment
Burnup (GWd/MTU)	42	42	43	34.9–45.8
Fractional release rate (/d)	2.27×10^{-6}	3.58×10^{-7}	3.25×10^{-7}	3.56×10^{-7}
Surface area (fragments) (m ²) [ft ²]	3.74×10^{-4} [4.03×10^{-3}]	8.61×10^{-3} [9.27×10^{-2}]	6.72×10^{-3} [7.23×10^{-2}]	8.61×10^{-3} [9.27×10^{-2}]
Surface area (segment ends) (m ²) [ft ²]	—	7.79×10^{-4} [8.39×10^{-3}]	5.73×10^{-4} [6.17×10^{-3}]	7.79×10^{-4} [8.39×10^{-3}]
Fragments release rate (mg/m ² -d) [lb/ft ² -d]	5.97 [1.22×10^{-6}]	0.72 [1.47×10^{-7}]	0.58 [1.19×10^{-7}]	0.72 [1.47×10^{-7}]
Segment ends release Rate (mg/m ² -d) [lb/ft ² -d]	—	7.97 [1.63×10^{-6}]	6.75 [1.38×10^{-6}]	7.93 [1.62×10^{-6}]
*Forsyth, R.S. "An Evaluation of Results from the Experimental Programme Performed in the Studsvik Hot Cell Laboratory." Technical Report 97-25. Stockholm, Sweden: Swedish Nuclear Fuel and Waste Management Company. 1997.				

Stroes-Gascoyne, et al. (1997b) reviewed the results from an 19-year leach test on a 7.06 GWd/MTU CANDU fuel. These tests were conducted by immersing fuel samples in a polypropylene bottle. After each leaching period, samples were transferred to bottles containing fresh leachate. The studies were conducted in aerated aqueous solutions of distilled water containing 2 mg/L CO₃²⁻ and tap water containing 50 mg/L CO₃²⁻ at 25 °C [77 °F]. Results showed the dissolution becomes congruent with time and only 5- to 7.7-percent cesium leached from the samples. While this study does not support light water reactor spent nuclear fuels operated at low operating temperatures and higher burnups, it shows that in immersion tests the grain boundary releases for cesium could be limited. Tait and Luht (1997) examined spent nuclear fuel dissolution of a 12.8-GWd/MTU {linear power rating of 50 kW/m [5.2×10^4 Btu/hr-ft]} CANDU fuel sample. The crushed samples were tested in deionized water, standard Canadian Shield saline solution (Table 5-3), and a standard carbonate water (0.01 mol/L NaHCO₃ and 0.1 mol/L NaCl) using a flow-through test. A surface area of 267 cm²/gm [1.88×10^4 in²/lb], determined from Brunauer Emmett and Teller method for unirradiated UO₂ samples were used to estimate the release rate in mg/m²-d [lb/ft²-d]. Average dissolution rates are shown in Table 5-4. The spent nuclear fuel dissolution rate in deionized water is a factor of three lower compared to standard carbonate water. The surface area was attributed as the largest uncertainty in determining spent nuclear fuel dissolution rate.

Ion	Concentration (mol·L ⁻¹)	Ion	Concentration (mol·L ⁻¹)
Na ⁺	0.22	HCO ₃ ⁻	0.00016
K ⁺	0.0013	Cl ⁻	0.97
Mg ²⁺	0.0082	SO ₄ ²⁻	0.0082
Ca ²⁺	0.37	NO ₃ ⁻	0.00081
Sr ²⁺	0.00023	—	—
Si	0.00054	—	—
pH	7 ± 0.5	—	—
Ionic Strength	1.37	—	—

*Tait, J.C. and J.L. Luht. "Dissolution Rates of Uranium from Unirradiated UO₂ and Uranium and Radionuclides from Used CANDU Fuel Using the Single-Pass Flow-Through Apparatus." Report No. 06819-REP-01200-0006 R00. Toronto, Canada: Atomic Energy of Canada, Ltd. 1997.

Leachant	Dissolution Rate (mg/m ² -d) [lb/ft ² -d]
Deionized water {25 °C [77 °F]}	3.6 [7.36 × 10 ⁻⁷]
Standard carbonate {25 °C [77 °F]}	10 [2.04 × 10 ⁻⁶]
Standard carbonate {25 °C [77 °F]}	13 [2.66 × 10 ⁻⁶]
Standard carbonate {35 °C [95 °F]}	19.7 [4.03 × 10 ⁻⁶]
Standard carbonate {75 °C [167 °F]}	45 [9.20 × 10 ⁻⁶]

*Tait, J.C. and J.L. Luht. "Dissolution Rates of Uranium from Unirradiated UO₂ and Uranium and Radionuclides from Used CANDU Fuel Using the Single-Pass Flow-Through Apparatus." Report No. 06819-REP-01200-0006 R00. Toronto, Canada: Atomic Energy of Canada, Ltd. 1997.

The studies conducted by CRWMS M&O (2000a), Röllin, et al. (2001), and Jégou, et al. (2001) indicate spent nuclear fuel dissolution rates, within the uncertainty associated with the measurement of the surface area, are similar in near-neutral pHs at 25 °C [77 °F]. Canadian (Stroes-Gascoyne, et al., 1997a) and Swedish (Forsyth, 1997) studies show a wide range of dissolution rates.

5.2 Assessment of DOE Spent Nuclear Fuel Data

The current spent nuclear fuel model proposed by DOE is based on the parametric relationship of single-pass flow-through test that excludes precipitation of uranium in solution and formation of secondary phases. This parametric model was obtained by excluding high burnup spent nuclear fuel samples. Figure 5-3 shows the same DOE spent nuclear fuel dissolution rate data plotted as a function of burnup for four different cases. The figure illustrates the spent nuclear fuel dissolution rate decreases with the increase in burnup at 75°C [167 °F]. Burnup, however, does not show any functional dependence at 25°C [77 °F]. At 70 GWd/MTU burnup, the spent nuclear fuel dissolution rate at 75 °C [167 °F] is similar to the rate at 25 °C [77]. Given the limited information available for the burnup, such changes could be attributed to the changes in the microstructure or the surface area of the fuel pellets that can change the accessibility of water to grain boundaries. Data used by the DOE and presented in Figure 5-3 assume surface area does not change with burnup. This assumption of using same surface area or similar factor to account for fragmentation cannot be adequately justified at 75 °C [167 °F]. Based on the DOE data, the spent nuclear fuel dissolution rate decreases with increases in burnup.

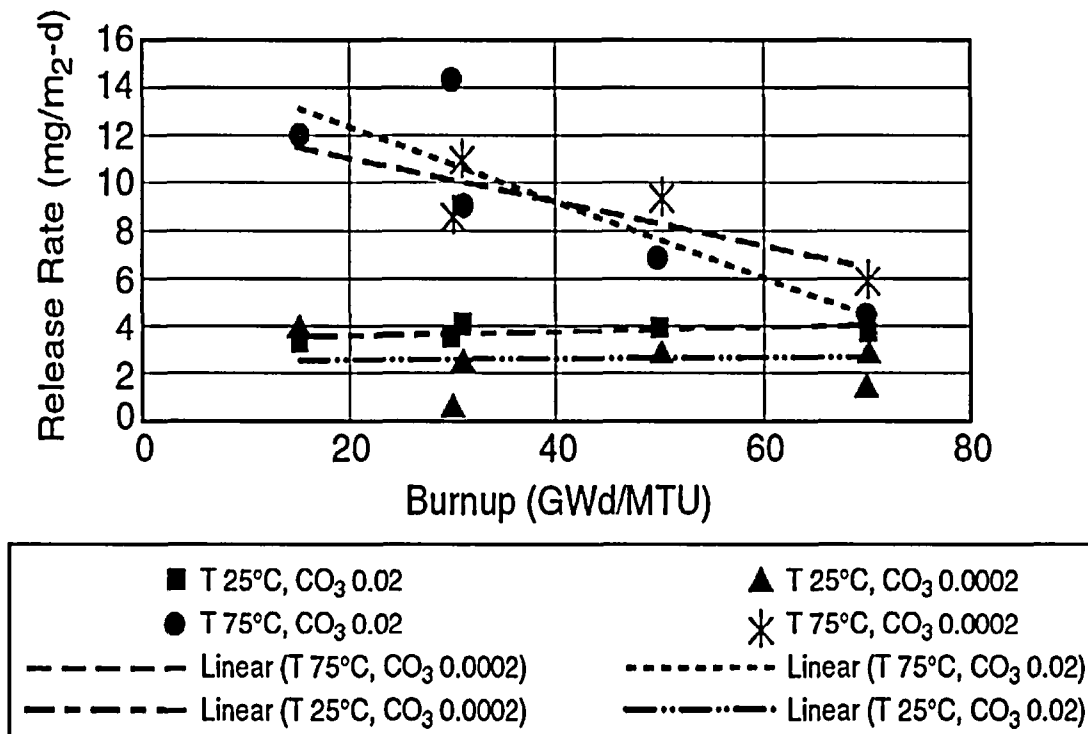


Figure 5-3. Spent Nuclear Fuel Dissolution Rate As a Function of Burnup Under Different Temperatures (T) and Molar Total Carbonate Concentrations (CO₃). Data Extracted from CRWMS M&O (2000a).

Another term in the parametric model that is important in estimating spent nuclear fuel dissolution rate is surface area. The exposed surface area of a fuel pellet after burnup is a complex combination of fragmentation that increases the surface area and fusion of grain that decreases the surface area. If the measured release for the high burnup sample is based on geometric area, the spent nuclear fuel dissolution rate estimated will be much higher as compared using measured surface area. Alternatively, if the measured surface area using the Brunauer Emmett and Teller method is used for estimating surface area, the measured spent nuclear fuel dissolution rate will be nonconservative because the Brunauer Emmett and Teller method tends to include porosity not accessible to water. The surface roughness factor brings the surface area somewhere in between geometric and the Brunauer Emmett and Teller method of surface area measurement. This factor is acceptable provided uncertainty associated with the change in surface area with burnup is adequately addressed. The effect of estimating the surface area is clearly evident from Table 5-2.

5.3 Assessment of NRC and CNWRA Approaches for High Burnup Spent Nuclear Fuel

The abstraction model used in the TPA Version 4.1 code is based on an empirical relationship as shown by Eq. (5-3) (Ahn and Mohanty, 2004).

$$r = r_o \times \exp\left[-\frac{E_a}{RT}\right] \quad (5-3)$$

where

r	—	dissolution rate (mg/m ² -d)
r_o	—	preexponential factor, log-uniform distribution (1.2×10^3 , 1.2×10^6)
E_a	—	activation energy (29 kJ/mol)
R	—	gas constant (kJ/mol-K)
T	—	temperature (K)

This abstraction was developed based on the observed spent nuclear fuel dissolution rates reported in literature and covers a wide range of dissolution rates. Values for the preexponential factors are distributed based on a log-uniform distribution. Because of the log-uniform distribution, preexponential factor values at the lower end are sampled more frequently compared to the values of preexponential factors at the upper end.

The microstructure of the rim of the pellet changes substantially in spent nuclear fuels exceeding 60 GWd/MTU (Barner, et al., 1993). Because high burnup spent nuclear fuel exceeding 60 GWd/MTU will be a very small quantity compared to high burnup fuel between 45 and 65 GWd/MTU, the influence of rim effects on the spent nuclear fuel dissolution can be neglected based on the quantity of the spent nuclear fuel that will be emplaced in the repository. If the quantity of high burnup spent nuclear fuel exceeding 60 GWd/MTU becomes substantial, however, rim effects should be evaluated for the abstraction model. The upper limit of the log-uniform distribution for the preexponential factor used in the performance assessment abstraction model for spent nuclear fuel dissolution is adequate for high burnup spent nuclear fuel.

5.4 Summary

Based on the CRWMS M&O (2000a), Jégou, et al. (2001), and Forsyth (1997), burnup has no significant effect on the spent nuclear fuel dissolution rate at 25 °C [77 °F]. At 75 °C [167 °F], however, based on the DOE data, the spent nuclear fuel dissolution rate decreases with increases in burnup. Furthermore, estimation of surface area is complicated by the pellet fragmentation caused by the radial thermal gradient and microstructural changes in the rim structure. Various authors have assumed different surface area roughness (or correction) factors to account for such changes. Thus, surface area estimation continues to account for significant uncertainty in the analysis.

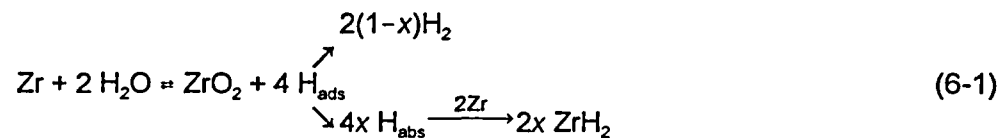
Because high burnup spent nuclear fuel exceeding 65 GWd/MTU could be a very small quantity compared to high burnup fuel between 45 and 65 GWd/MTU, the influence of rim effects on spent nuclear fuel dissolution can be neglected based on the quantity of spent nuclear fuel that will be emplaced at the repository. Furthermore, the effect of high burnup spent nuclear fuel dissolution rate can be adequately sampled in the U.S. Nuclear Regulatory Commission and CNWRA performance assessment abstraction model.

6 HIGH BURNUP SPENT NUCLEAR FUEL CLADDING

Most of the nuclear fuel cladding for power-generating reactors is made of two zirconium alloys, Zircaloy-2 and Zircaloy-4, used in boiling water reactors and pressurized water reactors, respectively. The chemical compositions of these zirconium alloys are given in Table 6-1. In addition to the low neutron cross section, zirconium alloys are used as cladding material because they have adequate mechanical properties up to 400 °C [752 °F] and good corrosion resistance in high-temperature, high-pressure water under operating reactor conditions. In recent years, better corrosion resistance is required to assure fuel reliability in order to improve fuel cycle economy by increasing fuel burnup through longer cycle operation, longer total residence time, and higher heat rating. This need for better corrosion resistance has prompted refinements in Zircaloy-4 composition, especially lower tin content, and an improved cladding fabrication and control process. In addition, other zirconium alloys such as ZIRLO and M5 (Mardon, et al., 2000; Comstock, et al., 1996) have been developed and introduced as fuel-cladding materials to improve the in-reactor fuel performance. The chemical compositions of these alloys are also listed in Table 6-1.

6.1 Cladding Degradation Processes Under Disposal Conditions

The excellent corrosion resistance of zirconium and its alloys in aqueous solutions over a wide range of pH levels and temperatures is due to the formation of an extremely adherent, protective, and thermodynamically stable ZrO₂ film. The main limitation of zirconium alloys, however, is the absorption of hydrogen, a process associated with aqueous corrosion, according to the following overall reaction



which leads to the precipitation of platelets of brittle zirconium hydrides in the zirconium matrix along preferential crystallographic planes in the metal. The fraction of atomic hydrogen absorbed or hydrogen pickup, given by x in Eq. (6-1), depends on the stage in the kinetics of the corrosion reaction in high-temperature, high-pressure aqueous solutions and the hydrogen dissolved in the water or produced by its radiolysis. Under certain conditions of stress, embrittlement of zirconium alloys can be promoted, depending on hydride content, distribution, and orientation (circumferential or radial).

Under disposal conditions, spent nuclear fuel cladding can act as a barrier to the release of radionuclides. Therefore, the U.S. Department of Energy (DOE) has included the consideration of cladding as an additional metallic barrier in the Total System Performance Assessment for the License Application (Bechtel SAIC Company, LLC, 2002a). It is generally recognized, however, that several potential degradation processes of Zircaloy—indistinctive name to be used for Zircaloy-2 and Zircaloy-4—can impair the beneficial action of spent nuclear fuel cladding in controlling radionuclide release in a high-level radioactive waste repository (Cragolino, et al., 1999). These processes include general and localized (pitting and crevice) corrosion, stress corrosion cracking, microbially influenced corrosion, delayed hydride cracking, hydrogen embrittlement, creep, mechanical failure caused by rockfall or seismic events, fuel and cladding

Alloy	Tin	Iron	Chromium	Nickel	Niobium	Oxygen
Zircaloy-2	1.2–1.7	0.07–0.20	0.05–0.15	0.03–0.08	—	0.14 max
Zircaloy-4	1.2–1.7	0.18–0.24	0.07–0.13	0.007 max	—	0.14 max
ZIRLO*	0.9–1.2	0.09–0.12	—	—	0.9–1.3	N/A
M5†	—	0.015–0.06	—	—	0.8–1.2	0.09–0.18

*Cornstock, R.J., G. Shoenberger, and G.P. Sabol. "Influence of Processing Variables and Alloy Chemistry on the Corrosion Behavior of ZIRLO Nuclear Fuel Cladding." Zirconium in the Nuclear Industry: Eleventh International Symposium. E.R. Bradley and G.P. Sabol, eds. ASTM STP 1295. West Conshohocken, Pennsylvania: ASTM International. pp. 710–725. 1996.

†Mardon, J.P., D. Charquet, and J. Senevant. "Influence of Composition and Fabrication Process on Out-of Pile and In-Pile Properties of M5 Alloy." Zirconium in the Nuclear Industry: Twelfth International Symposium. G.P. Sabol and G.T. Moan, eds. ASTM STP 1354. West Conshohocken, Pennsylvania: ASTM International. pp. 505–524. 2000.

oxidation, and pellet/cladding interaction failure. Even though cladding interaction with the internal environment contacting the irradiated UO₂ pellets may occur in several forms (i.e., internal oxidation and pressurization caused by fission gases and helium), only pellet/cladding interaction failure resulting from stress corrosion cracking caused by fission products such as iodine is considered by DOE.

Reviews of most of these potential failure processes have been conducted previously and discussed for the specific case of the potential Yucca Mountain repository in Rothman (1984), Cragolino, et al. (1999), and Ahn, et al. (1999).

As part of the assessment of the cladding failure processes, DOE conducted the screening of features, events, and processes to define those failure processes most likely to occur in the repository for their inclusion of the respective model abstractions in the total system performance assessment. As a result of such analyses (CRWMS M&O, 2000b), the following cladding degradation processes were screened out on the basis of low consequence or low probability (i) general corrosion, (ii) crevice corrosion, (iii) delayed hydrogen cracking, and (iv) hydride embrittlement. Within the scope of (iv), there were several specific processes related to hydride embrittlement that were screen out: (a) reorientation or redistribution (axial migration) of existing hydrides, (b) absorption of hydrogen under disposal conditions such as absorption caused by general and galvanic corrosion of cladding or reaction with irradiated fuel. Specific comments related to the excluded features, events, and processes have been presented by the U.S. Nuclear Regulatory Commission (NRC) (2002).

DOE conducted the features, events, and processes analysis using the Westinghouse 17 by 17 Lopar (W1717WL) fuel assembly as a reference design because it is one of the most commonly used fuel assemblies. Its design characteristics are summarized in Table 6-2. This assembly constitutes 21 percent of the discharged pressurized water reactor fuel assemblies and is the largest fraction of the more general W1717-type design that constitutes 33 percent of the discharged pressurized water reactor fuel. Because the pressurized water reactor fuel operates

**Table 6-2. Design Characteristics of Base Case Fuel Assembly
(Westinghouse W1717WL)***

Characteristic	Numerical Value	Characteristic	Numerical Value
Cladding outer diameter†	0.950 cm [0.37 in]	Irradiation time¶	4.5 years¶
Cladding thickness†	0.05715 cm [0.0025 in]	Reactor coolant pressure§	14–16 MPa [2.0–2.3 ksi]
Cladding inner diameter†	0.836 cm [0.329 in]	Reactor coolant temperature§	300–330 °C [572–626 °F]
Rod length†	385 cm [152 in]	Clad ID temperature§	340–370 °C [664–698 °F]
Active core length†	366 cm [144 in]	Burnup (mean)‡	44 MWd/kgU
Plenum length†	16.00 cm [6.30 in]	Oxide thickness‡	50 µm [1.97 mils]
Plenum volume/rod‡	8.77 cm ³ [0.53 in ³]	Fission gas release‡	2.5 percent
Effective gas volume/rod‡	23.3 cm ³ [1.42 in ³]	Plenum pressure. {27 °C [80 °F]}‡	4.4 MPa [0.64 ksi]
Active fuel volume/rod‡	201 cm ³ [12.3 in ³]	Stress {27 °C [80 °F]}‡	29 MPa [4.21 ksi]
Initial fill pressure†	2.0–3.5 MPa [0.29–0.50 ksi]	Stress {350 °C [662 °F]}‡	59 MPa [8.6 ksi]
Rods/assembly†	264	Fuel volume/waste package‡,	1.112 m ³ [39.29 ft ³]

*CRWMS M&O. "Initial Cladding Condition." ANL-EBS-MD-000048. Rev. 00 ICN 01. Las Vegas, Nevada: CRWMS M&O. 2000.

†DOE. DOE/RW-0184-R1, "Characteristics of Potential Repository Wastes." Vol. 1. Washington, DC: CRWMS M&O. pp. 2A-30. 1992.

‡From this analysis.

§Pescatore, C., M.G. Cowgill, and T.M. Sullivan. "Zircaloy Cladding Performance Under Spent Fuel Disposal Conditions, Progress Report May 1–October 31, 1989." BNL 52235. Upton, New York: Brookhaven National Laboratory. p. 7. 1990.

¶21 pressurized water reactor assemblies per waste package.

||18-month cycle, one-third core per cycle change-out.

under higher pressure than the boiling water reactor fuel, its cladding is thinner {0.57 mm [22.4 mil] wall thickness}, and it is not protected by a fuel channel, DOE considered that the analysis conservatively represents the behavior of all fuel assemblies.

Following such analysis, DOE considered the most likely forms of degradation that may affect the integrity of the commercial spent nuclear fuel cladding during disposal conditions. DOE developed a model to evaluate cladding degradation as part of the waste form degradation model (CRWMS M&O, 2000c) to determine the rate at which the commercial spent nuclear fuel matrix would be exposed to the in-package environment. The degradation of the commercial spent nuclear fuel cladding is assumed to occur in two stages (CRWMS M&O, 2000c,d). The first stage of degradation corresponds to rod failure as a result of cladding perforation. The second stage involves progressive exposure of the spent nuclear fuel matrix as a result of splitting (unzipping) of the cladding through oxidation of the irradiated UO₂ pellets either by moisture or by an aqueous environment.

The model abstraction for clad degradation to be included by DOE in Total System Performance Assessment—License Application (Bechtel SAIC Company, LLC, 2002a), even though some modifications have been introduced, was described in some detail previously (CRWMS M&O, 2000e). The components of the model abstraction corresponding to the cladding perforation as a precursor to wet unzipping include (i) initial condition of the cladding as a result of in-reactor exposure followed by wet and dry storage, (ii) failure by localized corrosion induced by halide anions, (iii) failure by creep or stress corrosion cracking, and (iv) failure by ground motion or acceleration induced by earthquakes.

6.2 Effect of Burnup on Spent Fuel Cladding

The initial condition of the cladding and the percentage of rods perforated at the time of disposal are mainly affected by reactor operation, but than also depend on pool storage, dry storage, and transportation, including fuel handling. Among the most important factors associated with the initial condition of the fuel cladding is the burnup. The burnup strongly affects the thickness and characteristics of the ZrO₂ layer, the amount of absorbed hydrogen, the fission gas production, and, as a result, the internal fuel rod pressure, the fuel pellet swelling, irradiation growth of fuel rods, and, eventually, crud buildup.

The discharge average burnup of pressurized water reactor and boiling water reactor fuels was reaching approximately 44 and 36 GWd/MTU, respectively, in 1999, but a clear trend to higher burnups exist (Yang, et al., 2000). Prompted by the requirements of the utilities, the current regulatory burnup limit for dry storage is 62 GWd/MTU, taking into account that the UO₂ enrichment is limited by fabrication, shipment, and storage to 5 percent. The NRC approved that burnup limit (Brach, 2003). The approval is based on the belief that the embrittlement criteria used for analyzing loss of coolant accident consisting of 17-percent cladding oxidation (the calculated total oxidation of the cladding shall nowhere exceed 0.17 times the total cladding thickness before oxidation) and 1,204 °C [2,200 °F] peak cladding temperature (10 CFR 50.46) will be unaffected by extended burnup operation (Meyer, 2000).

6.3 Characteristics of Spent Fuel Cladding

6.3.1 General Corrosion and Oxide Thickness of Cladding

Zirconium is a hexagonal-close-packed metal at normal temperatures. Although both Zircalloys are single-phase, α - or hexagonal-close-packed zirconium-tin alloys, they contain intermetallic precipitates formed by the minor alloying elements listed in Table 6-1. The composition, size, and distribution of these precipitates inside the equiaxed grains {5–10 μm [0.2–0.4 mil] in diameter} typical of the annealed material are important factors in determining the corrosion and hydrogen pickup rates in high-temperature water (Garzarolli, et al., 1996). The predominant intermetallics in Zircaloy-2 are $\text{Zr}(\text{Fe}_x\text{Cr}_y)_2$ and $\text{Zr}_2\text{Fe}_x\text{Ni}_y$, with $x + y = 1$ (Kai, et al., 1992; Cox, 1976). For Zircaloy-4, the existence of $\text{Zr}_x\text{Fe}_5\text{Cr}_2$ has been reported (Van der Sande and Bement, 1974), although other authors have mentioned $\text{Zr}(\text{Fe}_x\text{Cr}_y)_2$ as the predominant intermetallic (Adamson, et al., 1992). As noted, nickel was eliminated as an alloying element in Zircaloy-4 to reduce the hydrogen pickup in high-temperature water. Indeed, Zircaloy-4 is used in pressurized water reactors as fuel-cladding material instead of Zircaloy-2 because of the more reducing conditions prevailing in the core of this type of light water reactor as a result of hydrogen overpressure. These conditions suppress water radiolysis but tend to promote hydrogen entry. The size and distribution of the intermetallic precipitates are important because they become easy paths for electronic conduction when dispersed and embedded in the insulating, growing oxide film (Garzarolli, et al., 1996; Cox, 1976). Long-term irradiation experiments revealed neutron-induced dissolution of the second-phase particles in the matrix (Garzarolli, et al., 2001). With increasing neutron exposure under pressurized water reactor and boiling water reactor conditions, the precipitates gradually become amorphous and lose most of the iron (Adamson, et al., 1992; Kai, et al., 1992).

Corrosion of zirconium and its alloys, in particular Zircaloy-2 and Zircaloy-4, has been extensively studied in water at temperatures up to 350 °C [662 °F], and a large database exists as a result of the broad experience with light water reactors. The subject has been reviewed by Cox (1988, 1976), Franklin and Lang (1991), and Garzarolli, et al. (1996). The initial review by Cox (1988, 1976) deals with fundamental aspects of the high-temperature aqueous corrosion of zirconium and its alloys. The other reviews, in addition to certain mechanistic aspects, examine the behavior in-reactor of the most widely used alloys.

The growth of the uniform, adherent oxide film according to the reaction described by Eq. (6-1) is followed through the measurement of the weight gain (usually in units of mg/dm^2) or the increase of oxide thickness as a function of time. The oxide thickness is measured directly by in-pool examination of irradiated fuel using an eddy-current distance probe, based on the fact that ZrO_2 has good electrical insulating properties (Knaab and Knetch, 1978), or other specific devices. It should be noted that 15 mg/dm^2 [0.49 oz/ft^2] of weight gain correspond approximately to 1 μm [0.039 mil] of oxide and 0.66 μm [0.026 mil] of metal consumed by the corrosion reaction. The oxide growth takes place following a rate law that initially is close to cubic. After a transitory period of cyclic oxidation comprised of a series of successive, short cubic law curves, a transition to an approximately linear post-transition occurs (Garzarolli, et al. 1996; Hillner, et al., 1994; Cox, 1988).

The growth of the oxide film of Zircaloy-4 in pressurized water reactors for burnups up to 50 GWd/MTU leads to average oxide thicknesses of up to 60 μm [2.36 mil], well in the post-transition region (Adamson, et al., 1992; Cox, 1988) since the transition occurs at

approximately 2–3 μm [0.079–0.118 mil] (Garzarolli, et al., 1996). However, no spalling or other damage of the uniform, thick oxide films has been generally observed in pressurized water reactor fuel cladding. Nevertheless, failures are possible at higher burnups and operating temperatures close to 350 °C [662 °F]. Under such conditions, oxide thicknesses greater than 130 μm [5.12 mil] and hydrogen concentrations of 600 ppm have been measured in some fuel rods (Cox, 1988). This situation may occur when relatively high concentrations of LiOH are attained on the fuel-cladding surface, presumably in the pores of thick oxide films, although other factors have been considered by Cox (1988) to explain the accelerated corrosion rate. LiOH is added in the pressurized water reactor coolant for pH control in conjunction with H_3BO_3 , which is used for reactivity control.

The lithium and boron concentration in pressurized water reactor coolant system has been increasing with increasing fuel cycle length. For a 24-month cycle the startup boron concentration has been increased from the approximately 1,200 ppm used in the 12-month cycle to 1,700 to 2,000 ppm. Lithium was increased from 2.2 to 3.5 ppm to keep a pH of 6.8 at 300 °C [572 °F]. The lithium level could be even higher to attain a pH {300 °C [572 °F]} of 7.4 to minimize plan shutdown radiation dose rate (Cheng, et al., 1997). However, pool examinations of pressurized water reactor fuel operating in the high lithium regime have indicated increases in oxide thickness of no more than 15 percent (Cheng, et al., 1997). Most recent observations indicate that optimized (low tin) Zircaloy-4 fuel cladding in pressurized water reactor cores has been reported to reach its useful limit of 100–120 μm [3.93–4.72 mil] oxide thickness at the high burnup regime of 50–55 GWd/MTU (Cheng, et al., 2000). However, data to confirm the adequacy in the oxide thickness margin for new alloys cladding at the high burnup regime of >60 GWd/MTU are still lacking (Cheng, et al., 2000).

In summary, uniform corrosion rate of Zircaloy-4 cladding is becoming a major concern for high burnup fuel in pressurized water reactors arising from these three correlated factors: (i) oxide thickness exceeding 80–100 μm [3.15–3.94 mil] when cracks or pores may exist in the oxide layer, (ii) significant subcooled boiling, and (iii) crud deposition. Subcooled boiling would cause local deposition of iron and nickel corrosion products on the cladding surface. Even though crud deposition in pressurized water reactors is relatively mild compared to that in boiling water reactor, local crud loading could be as significant (Cheng, et al., 2000). Crud deposition promotes hideout of sodium metaborate or LiOH, leading to a significant enhancement of the uniform corrosion of Zircaloy. As a matter of fact, crud-induced localized corrosion of cladding has been observed in several pressurized water reactor plants. Accurate poolside measurements of oxide thickness under such circumstances seem to be impaired by the presence of crud (Cheng, et al., 2000). Nevertheless, local enhancement of corrosion rates has been confirmed by examination in hot cells as well as the closely related phenomenon of axial offset anomalies promoted by local power suppression in the upper half of the core that promoted a skewed flux distribution at the bottom.

To improve the corrosion resistance of Zircaloy-4 in the pressurized water reactor environment, its chemical composition was modified because it was found that the corrosion rate increased with increasing tin. As a result, low tin-Zircaloy-4 was specified and used in pressurized water reactors since 1988 (Garzarolli, 2001). Further studies revealed that the transition metal alloying and the microstructure also have important effects on corrosion rates. Optimized Zircaloy-4 was developed with iron in the upper range of the ASTM International specification and an optimized microstructure (Garzarolli, 2001). This microstructure, determined by the size and distribution of the precipitates, is the result of the quenching rate from the β -phase and the subsequent

annealing time and temperature in the α -phase during fabrication combined with the effect of wall thickness resulting from tube manufacturing (Garzarolli, et al., 1996). Each of these two development steps led to an increase of approximately 10 GWd/MTU in the peak rod burnup (Garzarolli, 2001).

As noted earlier, these increases of waterside corrosion at high burnup and, as a consequence to oxide thickness close to the accepted limit, led to the development of improved zirconium alloys such as ZIRLO. The performance of ZIRLO was evaluated in a pressurized water reactor demonstration program and in plant operation (Sabol, et al., 1997). ZIRLO fuel rods were compared with rods made of conventional Zircaloy-4 and optimized Zircaloy-4 (low tin and improved thermal treatment). For the rods having an average burnup of 52.5 GWd/MTU, the average peak oxide thickness in Zircaloy-4 was 31 μm [1.22 mil], which was approximately 25 and 30 percent of those of conventional and optimized Zircaloy-4. Poolside measurements in pressurized water reactor plants, despite being affected by crud deposition, indicated thicker oxides in the Zircaloy-4 fuel rods than in the ZIRLO rods.

The uniform black oxide formed in the 288 °C [550 °F] boiling water reactor environment has a very slow growth rate and frequently reaches a thickness of less than 10 μm [0.39 mil] at a burnup of 40 GWd/MTU. However, transition to a white uniform oxide, similar to that in pressurized water reactors, has been found on some fuel rods with a burnup in the range of 22 to 45 GWd/MTU (Cheng, et al., 1997). Cheng, et al. (1997) reported that the only available hot cell data for a white oxide show thickness ranging from 20 to 60 μm [0.79 to 2.36 mil] at a burnup of 45 GWd/MTU. More recent poolside examinations of fuel with a burnup greater than 50 GWd/MTU revealed an uniform oxide film thickness of approximately 30 μm [1.18 mil] (Cheng, et al., 2000).

Nodular corrosion of Zircaloy-2 had been a problem in boiling water reactor operation, but it was eliminated several years ago by using β -quenched cladding (Cox, 1988, Cheng, et al., 1997). Fuel rods affected by nodular corrosion exhibit oxide thickness in the white nodules of approximately 120 μm [4.72 mil].

Many cases of crud-induced localized corrosion have also been observed in boiling water reactors, mainly caused by a lack of control of the water quality. This phenomenon is characterized by locally enhanced corrosion resulting from copper-enriched crud deposition in the presence of copper ions, mainly generated by the corrosion of brass condensers, coupled to subsequent localized overheating as a result of poor heat transfer conditions. After the irradiation cycle in the reactor core, fuel cladding is covered with a relatively adherent crud, formed by deposition of corrosion products transported by the coolant from out-of-core components, that reaches a steady-state thickness. The crud, is either a ferrite $\text{FeMe(II)Fe(III)O}_4$ (spinel structure) in pressurized water reactor fuel or a double layer composed of ferrite overlaid with $\alpha\text{-Fe}_2\text{O}_3$ (corundum structure) in boiling water reactor fuel (Macdonald and Cragolino, 1989; Cohen, 1980). The symbol Me(II) in the ferrite indicates the incorporation to the lattice of bivalent cations (i.e., nickel, cobalt, and copper) generated by the corrosion of circuit materials. The composition of deposited crud depends on circuit materials, coolant chemistry, and water cleanup methods. The amount is generally significantly less in pressurized water reactor than in boiling water reactor because crud deposition is promoted by boiling and steam formation. However, local crud deposits can become sites for concentration and hideout of lithium and boron from the coolant, resulting in precipitation of lithium metaborate, which is believed to be

the main cause of axial offset anomalies. Also crud-induced localized corrosion has been observed in two pressurized water reactors (Cheng, et al., 2000).

A more detailed discussion on the effect of high burnup on cladding corrosion for both boiling and pressurized water reactors has been presented by Garzarolli, et al. (2001). These authors concluded that fuel-cladding materials can be optimized to achieve higher burnups under different reactor operating conditions.

6.3.2 Hydrogen Content and Distribution

As shown by Eq. (6-1), hydrogen absorption as a result of the corrosion reaction occurs in the relatively high reactor. Hydrogen pickup is rather low in the oxidizing boiling water reactor environment but in hydrogenated environments such as in pressurized water reactors. Indeed, Zircaloy-4 was developed to reduce the hydrogen pickup, mainly attributed to the nickel content of Zircaloy-2. Typically, the pickup is approximately 16 to 24 percent for a medium burnup Zircaloy-4 fuel rod in a pressurized water reactor. At the usual levels of burnup (< 50 GWd/MTU), hydrogen is in solid solution at the reactor operating temperatures up to 100 to 150 ppm, corresponding to an oxide layer thickness of 10 to 50 μm [0.39 to 1.96 mil] for the usual cladding wall thickness (Garzarolli, et al., 1996). At higher concentrations, precipitation of hydrogen platelets occurs. Because of the lower solubility of hydrogen in the colder outside region and due to diffusion of atomic hydrogen driven by the temperature and stress gradients, precipitation of hydride occurs mainly in the outer 10 to 40 percent of the cladding wall. As noted by Garzarolli, et al. (1996), a substantial amount of data including fuel rods with peak oxide layer thickness in excess of 100 μm [3.94 mil], and average hydrogen contents above 500 ppm, indicates that generally such hydrogen concentrations do not affect adversely the fuel rod behavior in reactor.

For pressurized water reactor Zircaloy-4 fuel cladding with a burnup of 57 GWd/MTU, hydrogen concentrations ranging from 135 to 290 ppm were measured in five fuel rods in the location of the highest oxide thickness (Van Swam, et al., 1997b). The concentrations included 10–15 ppm hydrogen initially present in the cladding. The hydrogen pickup fraction, calculated using a Pilling-Bedworth ratio¹ of 1.75 and correcting for the initial hydrogen content, ranged from 0.125 to 0.20, although it was higher at the spacer regions where the oxide layer was thinner (Van Swam, et al., 1997b). It should be noted that the theoretical value of the Pilling-Bedworth ratio for ZrO_2 is 1.56. If a density lower than the theoretical is assumed or measured and compositional changes are considered, higher values up to a maximum of approximately 1.75 can be estimated, which lead to higher values of the hydrogen pickup fraction. Metallographic examination of polished and etched specimens revealed the circumferential (and axial) orientation of the hydride platelets that were found distributed predominantly in the vicinity of the outer surface of the cladding (Van Swan, et al., 1997b). This region is cooler as a result of the temperature gradient through the wall thickness. In Zircaloy-4 cladding with an inner zirconium liner, hydride platelets were found concentrated in the liner as a result of the lower solubility of hydrogen in the liner.

Sabol, et al. (1997) compared the hydrogen pickup of ZIRLO fuel rods with that of the optimized Zircaloy-4 and found the theoretical hydrogen pickup of both alloys similar, ranging from 10 to

¹The Pilling-Bedworth ratio is defined as the ratio of the molar volume of the oxide to that of the metal underneath.

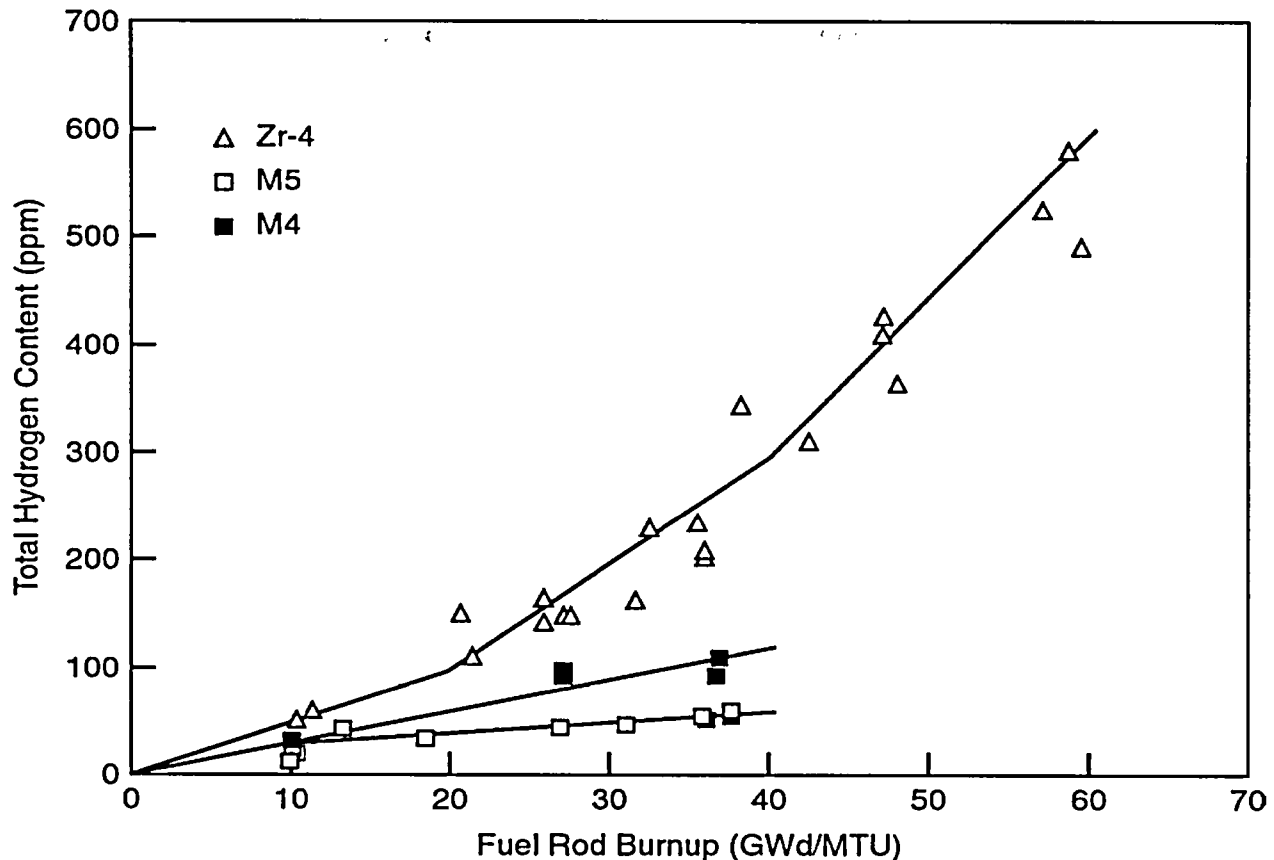


Figure 6-1. Total Hydrogen Content for Optimized Zircaloy-4, M4, and M5 As a Function of Burnup (Mardon, et al., 1997) (Copyright Permission Obtained for Figure Reprint from the American Nuclear Society, Inc.)

20 percent for a burnup of approximately 45 GWd/MTU. However, the maximum hydrogen concentration in ZIRLO was 240 ppm, compared to 620 ppm for the improved Zircaloy-4 as a result of the lower corrosion of the ZIRLO cladding. Mardon, et al. (1997) compared the hydrogen uptake of optimized Zircaloy-4 with that of M4 (a zirconium-tin-iron-vanadium-oxygen alloy containing 0.3-percent tin, 0.6-percent iron, 0.4-percent vanadium, and 0.125-percent oxygen) and M5 as a function of the burnup. Figure 6-1 shows the difference in the hydrogen absorption among these alloys, which is related to the difference in corrosion rates.

An important observation is that in- and out-reactor corrosion of Zircaloy-4 cladding can be accelerated by concentrated hydrides on the outer cladding surface adjacent to the oxide layer (Kim and Kim, 2000; Kim, et al., 1994; Garde, 1991). The hydride concentration in that outer

region seems to be promoted by circumferential tensile stresses caused by fuel swelling in the upper part of the cladding after the pellet/cladding gap is closed. Cheng, et al. (1996) have reported that up to 170-percent increase in oxide thickness has been observed in laboratory tests at 360 °C [680 °F] when specimens of Zircaloy were precharged with 2,200-ppm hydrogen. Blat and Noel (1996) and Blat, et al. (2000) have confirmed these observations, but no clear

explanation has been provided for the cause of the corrosion rate increase with the exception of remarks regarding the presence of fine cracks in the oxide.

6.3.3 Other Factors Affecting Spent Fuel Cladding

6.3.3.1 Internal Fuel Rod Pressure and Hoop Stress

The internal pressure of the fuel rod has a significant influence on rod failure caused by creep, delayed hydride cracking, hydride reorientation and cracking, and stress corrosion cracking. The internal pressure of the fuel rod is the main factor affecting the cladding hoop stress. The internal pressure of the cladding is determined by the initial prepressurization with helium (used to improve heat transfer through the pellet-cladding gap and to avoid cladding collapse from the external coolant pressure in the reactor), the fission gas pressure, and, in the long-term, by the pressure of helium gas formed by the α -decay of actinides.

DOE has conducted a calculation of the fission gas pressure (CRWMS M&O, 2000f). DOE assumed that the fuel gas production is linearly proportional to the fuel burnup and that most of the fission gas produced is not available to pressurize the cladding because it is held in the irradiated fuel pellets. An evaluation of data from different sources, including different manufacturers and burnups, led to the development of a complementary cumulative distribution function for percentage of fission gas release as a function of burnup. The fission gas pressure will tend to decrease slowly with time after a peak. Helium pressure, however, as a result of the generation of helium as α -particle resulting from the decay of the actinides will increase with time. Rothman (1984) has estimated that a helium partial pressure of 4.7 MPa [0.681 ksi] can be attained after 10,000 years using a prototypical pressurized fuel reactor fuel rod with a burnup of 36 GWd/MTU considering a fuel with the same burnup. Johnson and Gilbert (1983), as quoted in Manaktala (1993), estimated a value of approximately 3.6 MPa [0.52 ksi] after 10,000 years.

Summarizing the approach adopted for the cladding evaluation in the potential repository at Yucca Mountain, Siegmann, et al. (2000) estimated an internal pressure of 4.8 MPa [0.70 ksi] as a mean value for a 44.1-GWd/MTU burnup and an upper 5-percent value of 7.3 MPa [1.06 ksi] for a burnup of 63.3 GWd/MTU. These values correspond to hoop stresses at 27 °C [80.6 °F] of 38.4 and 61.8 MPa [5.60 and 8.96 ksi] for the W1717WL fuel rods.

The use of ZrB₂ in the form of a thin layer coating the pellets as an integral fuel burnable absorber (IFBA) in new fuel assembly designs (e.g., Westinghouse 17×17 VANTAGE 5H [IFBA]) is an additional source of helium. Significant amounts of helium can be produced by the reaction of B-10 with thermal neutrons (Lanning and Beyer, 2004).

6.3.3.2 Fuel Pellet Swelling and Irradiation Growth

When power is initially raised in a reactor, the Zircaloy cladding is ductile and the gap between the fuel pellets and the cladding is sufficient to accommodate the larger thermal expansion of the fuel pellets and dimensional increase caused by fission product swelling. The pellets also crack and relocate outward to contribute to gap closure together with creepdown or inward motion of the thin-walled cladding in response to applied coolant pressure. Under such conditions, if the fuel rod power is increased, local power changes may be of sufficient magnitude to cause direct interaction between the irradiated UO₂ pellet and the Zircaloy cladding, resulting in localized deformation of the cladding. Stresses and strain are localized over the axial lines corresponding

to fuel pellet cracks leading to hoop stress concentration factors close to two (Roberts, 1981). High fuel burnups will tend to increase the significance of this process of localized stress buildup on the inner cladding surface.

Another process to consider for high burnup fuel is irradiation growth. Dimensional instability in reactor, at practically zero stress level, is associated with the effect of high energy (>1 MeV) neutron fluence in promoting growth of the hexagonal close-packed crystalline structure of zirconium (Adamson, 2000). Growth is highly texture dependent and affects predominantly structural components in-core but also boiling water reactor fuel channels. Gilbon, et al. (2000) have compared the axial stress-free irradiation growth of both stress-relieved and recrystallized low-tin Zircaloy-4 with that of M4 and M5 at 280 and 350 °C [536 and 662 °F]. Whereas stress-relieved Zircaloy-4 exhibited a quasi-linear behavior with increasing fluence, recrystallized Zircaloy-4, as well as M4 and M5, underwent an early saturation phenomenon. Among these three materials, M5 had the highest irradiation growth resistance.

6.4 Assessment of High Burnup Fuel Cladding Disposal Performance

The following sections are based on a review previously published (Cragolino, et al., 1999). The sections have been updated on the basis of most recent information for high burnup fuel.

6.4.1 General Corrosion

Rothman (1984) conducted a series of calculations to estimate the weight gain and thickness of the oxide film after exposure to water, taking into consideration the evolution of the fuel-cladding temperature with time after emplacement under the conditions expected in the repository. In these calculations, only growth of the oxide film in the post-transition regime, according to a linear law, is considered by extrapolating the data available in the range of 250 to 360 °C [482 to 680 °F] to low temperatures. In addition, it is assumed that the oxidation behavior of both Zircalloys is similar under the environmental conditions considered in the analysis. Assuming that the container is breached in 1,000 years, the time at which the fuel rod temperature is estimated to be 105 °C [221 °F], Rothman (1984) calculated that the depth of Zircaloy oxidized would be only 0.006 µm [2.4×10^{-4} mil]. If the container is breached in 300 years and the temperature is 143 °C [289 °F], the depth would be 0.03 µm [1.2×10^{-3} mil]. Even this value is too low to affect the integrity of the cladding. Adopting the conservative assumption that the temperature remains constant at 180 °C [356 °F] for 10,000 years after breaching of the container in 1,000 years, calculations using equations and parameters proposed by different investigators led to a maximum depth of 53 µm [2.08 mil] for the oxide growth under disposal conditions. The total oxide thickness, including the in-reactor growth, would be approximately 120 µm [4.72 mil], which is less than 20 percent of the original wall thickness.

A more detailed analysis was conducted by Hillner, et al. (1994) using data from long-term autoclave tests. Twenty-two different tests were analyzed in which 46 different heats of Zircaloy-2 and -4 were used. Specimens with different heat treatments and preoxidized surface conditions were included. The maximum exposure time was 10,507 days (approximately 29 years) in a test at 316 °C [600 °F], and the maximum weight gain was 1,665 mg/dm² [0.034 lb/ft²], corresponding to an oxide film thickness of 114.3 µm [4.5 mil] in a 338 °C [640 °F] experiment. The post-transition linear law is described by the following expression

$$\Delta W = Kt + C \quad (6-2)$$

where

ΔW	—	specimen weight gain in mg/dm ²
t	—	time in days
K	—	linear rate constant in mg/m ² /day
C	—	constant in mg/dm ²

The dependence of K with temperature is given by

$$K = B \exp\left[-\frac{Q}{RT}\right] \quad (6-3)$$

where

B	—	pre-exponential constant in mg/dm ² /day
Q	—	activation energy in cal/mol
R	—	gas constant in cal/mol ^o K
T	—	absolute temperature in ^o K

Using values determined by different authors for the various parameters in Eqs. (6-2) and (6-3) and data obtained by Hillner, et al. (1994) in their own tests using two different expressions, the maximum thickness after 10,000 years at 180 °C [356 °F] was estimated to be 89 μm [35 mil], as shown in Table 6-3. However, when the thickness is calculated by taking into consideration the expected decrease in fuel-cladding temperature with time, Hillner, et al. (1994) concluded that the maximum oxide thickness will be approximately 8 μm [0.31 mil] after 1,000,000 years of exposure. As noted previously, these values of oxide thickness, as those listed in Table 6-3, do not include the in-reactor oxide growth. Several arguments were offered by Hillner, et al. (1994) regarding the validity of these extrapolations.

The previous two analyses were used by the DOE (CRWMS M&O, 2000b) to exclude general corrosion from further consideration in the model abstraction for clad degradation. As a further confirmation, it was noted that Bradley, et al. (1981) examined Zircaloy-clad fuel from two bundles of the Shippingport pressurized water reactor Core 1 “blanket” fuel after extended in water pool storage. The oxide layer thickness was reported to be on average 1.8 and 2.4 μm [0.071 and 0.094 mil] for each bundle after reactor operation and 1.7 and 2.3 μm [0.067 and 0.091 mil] after 16 and 21 years of water pool storage. The almost negligible differences were attributed to differences in measurement techniques and experimental errors. It was concluded that no change occurred in the oxide layer thickness in the water exposure for more than 20 years. A similar observation has been reported for a Canadian Deuterium Uranium (CANDU) fuel rod after 27 years, as quoted in an International Atomic Energy Agency report (1998).

At a drilled hole, a small amount of UO₂ exposed to water for 21 years reacted to form a thin {< 1 μm [0.039 mil]} deposit of UO₃0.8H₂O. It is claimed that the absence of any evidence of degradation in the inner or outer cladding surface provides confidence that cladding can be safely stored in water for periods up to 100 years. It has also been reported (International Atomic Energy Agency, 1998) that fuel with a burnup exceeding 50 GWd/MTU has been in wet storage for more than a decade. The fuel exhibited good performance without any known failure.

Table 6-3. Comparison of Predictions from Models of Different Investigators for the General Corrosion of Zircaloy after 10,000 years at 180 °C [356 °F]*

Investigator	B (mg/dm ² /day)	Q/R (°K)	K (mg/dm ² /day)	ΔW (mg/dm ²)	Oxide Thickness (μm)
†Hillner (1977)	1.12 × 10 ⁸	12,529	1.10 × 10 ⁻⁴	402	27.9
‡Van der Linde (1965)	2.30 × 10 ⁹	14,451	3.25 × 10 ⁻⁵	119	7.6
§Dyce (1964)	6.53 × 10 ⁹	15,109	2.16 × 10 ⁻⁵	79	5.0
Daalgard (1976)	1.84 × 10 ⁷	11,222	3.23 × 10 ⁻⁴	1,181	78.7
¶Billot, et al. (1989)	1.13 × 10 ⁸	12,567	4.95 × 10 ⁻⁵	181	12.7
#Garzarolli, et al. (1982)	1.18 × 10 ⁹	13,815	1.02 × 10 ⁻⁴	374	25.4
**Stehle, et al. (1975)	2.21 × 10 ⁹	14,242	6.80 × 10 ⁻⁵	248	17.8
††Peters (1984)	8.12 × 10 ⁸	13,512	9.12 × 10 ⁻⁵	333	22.9
*Hillner, et al. (1994)	2.46 × 10 ⁸	12,877	112e-5	410	27.9
*Hillner, et al. (1994)	3.47 × 10 ⁷	11,452	3.67 × 10 ⁻⁴	1,341	88.9

*Hillner, E., D.G. Franklin, and J.D. Smee. *The Corrosion of Zircaloy-Clad Fuel Assemblies in a Geological Repository Environment*. WAPD-3173. West Mifflin, Pennsylvania: Bettis Atomic Power Laboratory. 1994.

†Hillner, E. "Corrosion of Zirconium-Base Alloys—An Overview." *Zirconium in the Nuclear Industry: Third International Symposium*. A.L. Lowe, Jr. and G.W. Parry, eds. ASTM STP 633. Philadelphia, Pennsylvania: ASTM International. pp. 211–235. 1977.

‡Van der Linde, A. "Calculation of the Safe Life Time Expectancy of Zirconium Alloy Canning in the Fuel Elements of the NERO Reaction." RCN Report 41. Petten, The Netherlands: Reactor Centrum. 1965.

§Dyce, I.H. "Corrosion of Zircaloy Fuel Cladding: The Influence of High Heat Fluxes." *Nuclear Engineering*. Vol. 9, No. 98. pp. 253–255. 1964.

||Daalgard, S.B. "Long-Term Corrosion and Hydriding of Zircaloy-4 Fuel Clad in Commercial Pressurized Water Reactors with Forced Convective Heat Transfer." *Extended Abstracts of the Electrochemical Society*. Vol. 76-1, No. 31. p. 82. 1976.

¶Billot, P., P. Beslu, A. Giodano, and J. Thomazel. "Development of a Mechanistic Model to Assess the External Corrosion of the Zircaloy Claddings in PWRs." *Zirconium in the Nuclear Industry: Eighth International Symposium*. L.F.P. Van Swam and C.M. Eucken, eds. ASTM STP 1023. Philadelphia, Pennsylvania: ASTM International. pp. 165–184. 1989.

#Garzarolli, F.W. Jung, H. Schoenfeld, A.M. Garde, G.W. Parry, and P.G. Smerd. "Waterside Corrosion of Zircaloy Fuel Rods." EPRI NP-2789. Palo Alto, California: Electric Power Research Institute. 1982.

**Stehle, H., W. Kaden, and R. Manzel. "External Corrosion of Cladding in PWRs." *Nuclear Engineering and Design*. Vol. 33. pp. 155–169. 1975.

††Peters, H.R. "Improved Characterization of Aqueous Corrosion Kinetics of Zircaloy-4." *Zirconium in the Nuclear Industry: Sixth International Symposium*. D.G. Franklin and R.B. Adamson, eds. ASTM STP 824. Philadelphia, Pennsylvania: ASTM International. pp. 507–518. 1984.

It is recognized that the combination of high fluence ($>10^{22}$ n/cm²) and elevated hydrogen content (>600 ppm) results in low room temperature ductility. In the same report (International Atomic Energy Agency, 1998), an analysis of the effect of high burnup on cladding behavior during wet storage is made. In general, it is considered that the performance would be satisfactory for prolonged (several decades) of wet storage, and no additional loss of thickness can be anticipated. Even the possibility of thick oxide spallation is considered unlikely. However, because of the low ductility caused by elevated hydrogen uptake (>600 ppm) produced by in-reactor corrosion and the high fluence ($>10^{22}$ n/cm²) in-core, the risk of low-temperature fracture by impact is noted.

Most of the quantitative comparisons and estimations for disposal conditions presented previously are made on the basis of oxide layer thickness from reactor operation, which are significantly thinner than those expected for high burnup fuel. Thicker films contain defects, pores, and cracks that can affect significantly the corrosion behavior in the in-package environment, an environment that can differ significantly from the recirculating, deionized water used in wet fuel storage. Aggressive anionic species can be concentrated, and many other factors could influence the behavior of the oxide-covered Zircaloy cladding. One main limitation in the analyses presented previously is the lack of consideration of changes in the environmental conditions inside the waste packages, away from the postulated chemistry based in the composition of J-13 Well water as the in-flow water. However, more aggressive environmental conditions may lead to oxide film breakdown and the initiation of localized corrosion during long exposures under disposal conditions.

6.4.2 Localized Corrosion

As reported by Yau and Webster (1987), zirconium is very resistant to corrosion in most inorganic and organic acids, alkalis, and saline solutions over wide ranges of concentrations and temperatures. The thickness of the ZrO₂ passive film increases linearly with increasing potentials, reaching values close to 0.5 μm [0.020 mil] in the presence of many anionic species such as SO₄²⁻, NO₃⁻, PO₄³⁻, and CO₃²⁻, among others, even in very acidic conditions (Young, 1961). The thickness increase with applied potential is approximately equal to 2.5 nm/V. A similar behavior is observed in concentrated KOH solutions. No passivity breakdown is observed in these electrolytic solutions, and relatively high overpotentials are required to detect the onset of the oxygen evolution reaction because the oxide is a very poor electronic conductor. The range of passivity in aqueous solutions is also extended to pH values lower and higher than those predicted through the potential-pH diagram on the basis of thermodynamic data for ZrO₂·2H₂O (Pourbaix, 1974), undoubtedly reflecting the significant stability and low solubility of the passive surface film.

Halides are the most detrimental species affecting the stability of the passive film. The oxide film is dissolved in the presence of F⁻ with the formation of ZrF₆²⁻ complexes, particularly in acidic solutions (Meyer, 1964). All other halides promote the localized breakdown of the passive film, leading to pitting corrosion above a critical potential that increases in the sequence Cl⁻ < Br⁻ < I⁻, as discussed in the review by Knittel and Bronson (1984). Even though all these anions may promote pitting corrosion of zirconium alloys, only F⁻ and Cl⁻ are present in the groundwaters at the vicinity of Yucca Mountain.

Rothman (1984) dismissed the possibility of localized corrosion of fuel cladding on the basis of the low Cl⁻ concentration found in groundwaters near the potential repository. His argument is

also based on the results of investigations reporting the lack of localized corrosion in more concentrated halide solutions. Rothman (1984), however, does not consider the possibility of oxidizing conditions inside the waste packages promoted by γ - or α -radiolysis of water or both or the presence of reducible oxyanions or cations formed by corrosion of structural components inside waste packages. Hillner, et al. (1994), instead, considered that Fe^{3+} cations will not be stable to promote pitting in the presence of Cl^- anions. A different approach for the consideration of the deleterious effect of F^- is offered by Rothman (1984). In this case, even arguments similar to those for Cl^- are used in terms of available anionic concentration. Rothman (1984) suggested that additional experimental work is needed to evaluate any possible detrimental effect of F^- anions. On the other hand, Hillner, et al. (1994) considered that at least 100 ppm F^- must be present to impair the excellent corrosion resistance of Zircaloy. On the basis of the concentration reported for J-13 Well water, Hillner, et al. (1994) believe that Zircaloy will not be affected by F^- anions under disposal conditions. The subject was reviewed for the application to the Yucca Mountain conditions (CRWMS M&O, 2000g).

The localized corrosion behavior of Zircaloy-4 was evaluated under a wide range of environmental conditions (Brossia, et al., 2002; Pan, et al., 2001; Cragnolino, et al., 2001; and Greene, et al., 2000). It was found that Zircaloy-4, either mechanically polished or covered with a hydrothermally grown oxide layer, is susceptible to pitting corrosion in chloride-containing solutions at concentrations above 0.001 M and potentials higher than a repassivation potential. The repassivation potential linearly dependent on the logarithm of the Cl^- concentration, independent of temperature from 25 to 95 °C [77 to 203 °F] and slightly dependent on pH within the pH range of 2 to 1. However, no crevice corrosion was observed under the crevice former used in the specimens, suggesting that Zircaloy-4 is more prone to pitting than to crevice corrosion. The presence of hydrothermally grown oxide films {1.7 to 3.4 μm [0.067 to 0.13 mil]} was not observed to influence the repassivation potential but did increase the breakdown potential and the corrosion potential. The initiation time for pitting increased significantly with the thickness of the hydrothermally grown oxide film (Brossia, et al., 2002; Pan, et al., 2001). It was found that the corrosion potential can reach and even exceed the repassivation potential in FeCl_3 -containing solutions. Therefore, pitting corrosion of Zircaloy cladding may occur after a long time interval under natural corroding conditions inside a breached container. Additional work on the kinetics of the cathodic reactions on oxide-covered surfaces is needed to evaluate the long-term performance of cladding as an additional metallic barrier to radionuclide release in the disposal of spent nuclear fuel.

In agreement with the results previously described, Yau and Webster (1987) reported that zirconium is not susceptible to crevice corrosion in Cl^- solutions, even at low pH levels. More detailed information is provided by Yau (1983), showing that both zirconium and Zr-1.5Sn were resistant to crevice corrosion after 14 days of exposure to boiling {107 °C [225 °F]}, saturated NaCl solution with the pH adjusted to 0 by the addition of hydrochloric acid. Unfortunately, E_{corr} was not measured in those tests in which no pitting corrosion was observed.

Zirconium is not susceptible to galvanic corrosion because the protective ZrO_2 passive film leads to corrosion potential (E_{corr}) values in the galvanic series in flowing seawater close to those of noble metals and graphite, but slightly lower than that of silver (Yau and Webster, 1987). However, local corrosion promoted by galvanic coupling to a more noble metal may occur if the film is mechanically disrupted. Nevertheless, the repassivation rate of zirconium and its alloys is sufficiently fast in many aqueous solutions that, unless fretting is continuously occurring, no substantial corrosion can be expected.

In summary, localized corrosion of Zircaloy-2 or Zircaloy-4 fuel cladding in the form of pitting may occur in an oxidizing environment (as that presumably present inside the waste packages), depending on Cl^- concentration and temperature, if E_{corr} is higher than the repassivation potential (E_{rp}). The values of E_{rp} seem to be practically independent of pH and temperature, whereas E_{corr} depends on the presence of oxidizing species (i.e., H_2O_2), temperature, and pH, and, to a lesser extent, on Cl^- concentration. It can be expected that soluble corrosion products of iron, arising from the dissolution of steel baskets holding the fuel assemblies inside the waste packages, may affect the E_{corr} of Zircaloy. Although it has been claimed that Fe^{3+} ions will not be stable in solution at pH levels above 3, the effect of solid corrosion products of iron, such as Fe_3O_4 or $\text{FeO}(\text{OH})$, should be examined, particularly in the case of Fe_3O_4 . This oxide is a good electronic conductor and may increase E_{corr} of Zircaloy.

It seems from results reported in the literature that pits can be rapidly initiated if the electrochemical conditions discussed previously are fulfilled, but there are no data available to evaluate the penetration rate. As demonstrated by Yau and Maguire (1984), zirconium did not experience pitting in Cl^- solutions even in the presence of high concentrations of Fe^{3+} ions when the potential was maintained below E_{rp} . At potentials lower than E_{rp} , the corrosion rate of Zircaloy, as calculated from measured current densities of approximately $1 \times 10^{-8} \text{ A/cm}^2$ [$6.5 \times 10^{-8} \text{ A/in}^2$], is low {less than $0.1 \text{ }\mu\text{m/yr}$ [0.004 mpy] } as a result of the protective characteristics of the ZrO_2 passive film. However, these rates are several orders of magnitude higher than those extrapolated from high-temperature water exposures, as presented in the previous section.

An important limitation to consider for localized corrosion to occur is related to the electronic conductivity of the ZrO_2 layer. Because of the poor electronic conductivity of the oxide, it is highly possible that under naturally corroding conditions and regardless of the nature of the oxidizing species, the cathodic reaction on the oxide-covered surface needed to sustain the anodic dissolution inside the pit is severely limited. Therefore, localized corrosion is inhibited.

These arguments developed for Zircaloy cladding can be extended in general to the behavior of the cladding for high burnup fuel. However, specific information will be needed to evaluate the localized corrosion resistance of newly developed zirconium-based cladding alloys.

6.4.3 Stress Corrosion Cracking

Cox (1975, 1990a), Speidel (1976), and Yau (1992) have reviewed in great detail most of the reported work on the susceptibility of zirconium alloys to stress corrosion cracking in a variety of aqueous environments. Cox (1990a) noted that intergranular corrosion of zirconium in the absence of externally applied stresses was observed in hydrochloric acid solutions at temperatures ranging from 100 to $250 \text{ }^\circ\text{C}$ [212 to $482 \text{ }^\circ\text{F}$] in the early 1960s. Also, at nearly the same time, intergranular stress corrosion cracking of zirconium and Zircaloy-4 in relatively concentrated FeCl_3 aqueous solutions was reported. Since then, as discussed in those reviews, many observations have confirmed the occurrence of stress corrosion cracking in zirconium and its alloys in aqueous halide solutions. The environments of interest for repository conditions are those that contain Cl^- anions.

Several authors have shown that Zircaloy is susceptible to stress corrosion cracking in the presence of tensile stresses lower than the yield strength in Cl^- solutions under the same environmental and electrochemical conditions that promote pitting corrosion (Mankowski, et

al., 1984; Cragolino, 1975; Cox, 1973; Cragolino and Galvele, 1973). Sufficiently high hoop stresses (60–70 percent of the yield strength) may be present in localized regions of the cladding as a result of fuel-pellet expansion during irradiation. Although some contraction is expected upon removal from the reactor, the stresses are sufficient to promote crack initiation if the required environmental and electrochemical conditions are fulfilled. Indeed, Cox (1990a) remarked that no piece of zirconium alloy, even after annealing, will be unstressed because of its anisotropic physical properties. These local stresses may exceed the yield strength (MacEwen, et al., 1983).

Texture plays an important role in the transgranular stress corrosion cracking of zirconium alloys. Because zirconium is a hexagonal-close-packed metal, a single crystal exhibits a strong directional variation of physical and mechanical properties. The preferred orientation of the crystallites, the texture, results from deformation and subsequent heat treatment as a result of the shortage of slip planes and the strict orientation relationship for slip and twinning that is carried from the single crystal to the polycrystalline material. This anisotropy of mechanical properties affects stress corrosion cracking resistance in specific orientations. As noted, cracks tend to propagate on or near the basal plane. As reported by Speidel (1976), a Zircaloy-4 double cantilever beam specimen with the precrack surface oriented perpendicular to the longitudinal (rolling) direction exhibited a crack that propagated at a right angle to the fatigue precrack in a KI solution because it followed the hexagonal basal plane, regardless of the opening mode of the specimen. Neutron irradiation increases the strength of zirconium alloys and decreases the fracture toughness (Speidel, 1976). This irradiation also increases the susceptibility to stress corrosion cracking in I₂ vapor (Cox, 1990b; Cox and Wood, 1974) and presumably has the same effect in aqueous halide-containing environments.

If the electrochemical and environmental conditions in terms of potential and Cl⁻ concentration are appropriate to initiate pitting of Zircaloy fuel cladding, the initiation of cracks could occur even at low macroscopic stress levels. The texture prevailing in fuel rods combined with the effect of irradiation hardening could then facilitate the propagation of cracks leading to failure of the cladding.

Stress corrosion cracking of Zircaloy cladding may occur in the presence of hoop stresses of sufficient magnitude under the same environmental and electrochemical conditions that promote pitting corrosion by chloride. In the case of high burnup fuel, it is apparent that sufficiently high hoop stresses, approximately 150 MPa [21.8 ksi] can be reached at about 400 °C [752 °F] as a result of increasing pressure caused by fission gases and helium. The main limitation for the occurrence of external stress corrosion cracking caused by the in-package environment is related to the environmental and electrochemical conditions, as in the case of localized corrosion (Pan, et al., 2001; Cragolino, et al., 1999). No sufficient data are currently available to evaluate the stress corrosion susceptibility of the newly developed cladding alloys, although some correlations could be established using pitting or repassivation potentials.

6.4.4 Creep Failure

Creep is considered the dominant process for cladding deformation under normal conditions of dry storage and during the postclosure period preceding any breaching of the waste packages. The relatively high temperatures, the outward pressure differential across the cladding wall, and the corresponding hoop stress will result in permanent deformation of the cladding with time.

The resistance of Zircaloy cladding against creep failure under anticipated repository conditions has been evaluated using phenomenological and mechanistic creep models¹ (Thurber and Marschke, 1998; Siegmann, 1997b). Phenomenological creep models that have been evaluated included those of Peehs, et al. (1985), Matsuo (1987), and Mayazumi and Onchi (1990), while mechanistic creep models included those of Chin, et al. (1986); Chin and Gilbert, (1989), Schwartz and Witte (1987), and Thomas (1999).

A critical creep strain has been used as the failure criterion for assessing cladding integrity. Calculations based on Peehs' model (Peehs, et al., 1985) and the application of a 1-percent creep strain criterion indicate that cladding failure by creep should not be expected for the stress {<100 MPa [<14.5 ksi]} and temperature {< 330 °C [626 °F]} conditions anticipated in the repository.² The evaluation by Siegmann (1997b) is based on the Matsuo (1987) model using a failure criterion of 4-percent creep strain. A direct comparison (Thurber and Marschke, 1998) of the Peehs, Matsuo, and Mayazumi models shows substantial differences in the calculated creep strain. All three models, however, predict that the total creep strain in the cladding would be less than 1 percent after 10,000 years at temperatures on or below 230 °C [446 °F]. At 550 °C [1,022 °F], strain ranges from 0.01 percent for the Matsuo model to as high as 10 percent for the Mayazumi model. The predicted failure response is, therefore, sensitive to the choice of the creep model and the critical creep strain. A limitation in the phenomenological creep models arises from the fact that the operative deformation mechanisms involved in the experimental data used to fit the models are different from those expected under repository conditions. The need to consider the operative deformation mechanism under such conditions led to the use of mechanistic creep models for assessing cladding resistance against creep failure.

Both Pacific Northwest National Laboratory (Levy, et al., 1987) and Lawrence Livermore National Laboratory (Thomas, 1999; Schwartz and Witte, 1987) developed mechanistic-based creep models for predicting creep rupture life of cladding under repository conditions. The Pacific Northwest National Laboratory model is based on the deformation and fracture mechanism maps and treats several creep deformation and failure modes (Chin, et al., 1986). For the low stress and low temperature anticipated in the high-level waste repository, the potential dominant creep failure mechanism was considered to be diffusion-controlled cavity growth. The Lawrence Livermore National Laboratory model, based on diffusion-controlled cavity growth, has been upgraded recently (Thomas, 1999). McCoy and Doering (1994) reviewed these previous models and proposed several refinements. Both models have the same basic form traceable to the original model of Raj and Ashby (1975) and should predict similar results, providing similar values are used for the model parameters. A recent calculation by Thurber and Marschke (1998) indicates that Chin's model predicted 1-percent creep strain after 10,000 years at 237 °C [458 °F]. According to this model, therefore, failure would occur only at temperatures above 237 °C [458 °F] if the criterion adopted for creep failure is 1-percent strain.

As reviewed by Ahn³ and Ahn, et al. (1999), there is a general consensus that cladding failure by creep rupture is unlikely under repository conditions for spent nuclear fuel with burnups lower

¹Ahn, T.M. "Cladding Credit." *Presentation at the DOE/NRC Performance Assessment Technical Exchange Workshop, March 17-19, 1998. San Antonio, Texas. 1998.*

²Ibid.

³Ibid.

than 45 GWd/MTU. Creep rupture data from Peehs and Fleisch (1986) are consistent with this assessment. There is, however, a lack of direct comparison of diffusion-controlled cavity growth model prediction against experimental data, and a lack of experimental evidence for diffusion-controlled cavity growth in Zircaloy cladding materials (Pescatore, et al., 1989). Disagreement exists on the pertinent values of some model constants in the diffusion-controlled cavity growth models and on the validity of extrapolating the results of calculations performed using these models to lower stresses and temperatures. It should be noted that the Spent Fuel Project Office of NRC does not endorse these models to calculate the maximum temperature limit for dry storage.

Siegmann and Macheret (2002) conducted an evaluation of six creep models against five sets of experimental data for which the mean burnup was calculated to be 44.1 GWd/MTU. They selected the Murty creep model rather than one of other five models, including the one by Matsuo for estimating the creep behavior under repository conditions. They claimed that Murty creep equations are accurate at low stresses and low temperatures because the equations incorporate Coble creep, which is dominant at low stresses and low temperatures. In addition to Coble creep, Murty creep equations include primary and steady-state creep by dislocation glide—the same creep mechanisms treated in the Matsuo model. A critical strain criterion was used for creep failure. Upper and lower limits of rod failure by creep were computed based on creep failure strain limits of 0.4 and 11.7 percent. These creep failure strains were supported by experimental data of unirradiated Zircaloy. They corresponded to an average creep failure strain of 3.3 percent used in an earlier analysis concerning cladding failure by creep during dry storage and transportation (Siegmann, et al., 2000). The Murty model and the creep strain criteria seem to be acceptable because they both lead to conservative failure estimates. The Murty creep model has also been adopted for evaluating creep of spent fuel under dry storage conditions (Hayes, et al., 2001).

Besides the choice of a creep model and material constants, failure prediction is sensitive to the effect of temperature. As a result, the maximum cladding temperature in the repository must be predicted with a high level of accuracy, and its possible variation with location of the waste packages in the emplacement drifts and in the repository must be established with reasonable precision. In addition, if the cladding is heated to a sufficiently high temperature (a situation that may occur during vacuum drying, dry storage, or in the initial phase after repository closure), hardening resulting from irradiation could be annealed-out and higher creep rates would be subsequently expected. Results obtained by Tsai (2003) using a fuel rod with high burnup (67 GWd/MTU) showed that a substantial fraction of irradiation hardening can be annealed out at temperatures above 420 °C [788 °F] in a matter of hours to days. Tsai and Billone⁴ reported that fuel rods with a burnup of 36 GWd/MTU from the Surry nuclear power reactor that were stored in a dry cask for 15 years exhibited no discernible changes in their physical conditions. Thermal creep tests confirmed that the cladding has a residual creep ductility > 1 percent at 380 °C [716 °F] and > 8.5 percent at 400 °C [752 °F] even after a pretreatment at 415 °C [779 °F]. The creep ductility of the Surry cladding was greater than that of high burnup cladding, 67 GWd/MTU, from the Robinson reactor, under hoop stresses of 190 and 220 MPa [27.6 and 31.9 ksi] at 380 °C [716 °F]. However, at 400 °C [752 °F] the high burnup cladding exhibited a greater creep rate at hoop strains above 0.5 percent.

⁴Tsai, H. and M.C. Billone. "Thermal Creep of Irradiated Zircaloy Cladding." *Presentation at the 14th International Symposium on Zirconium in the Nuclear Industry, June 13–17, 2004*. Stockholm, Sweden. 2004. Submitted for publication. 2004.

Creep analysis needs to be updated based on recent information obtained from dry storage studies, although limited information exists for dry storage of high burnup fuel. A French program (Bredel, et al., 2000; Limon, et al., 2000) has been initiated to evaluate experimentally, and by modeling for storage and disposal estimations, the creep behavior of Zircaloy-4 cladding using fuel rods with a burnup of 47.2 GWd/MTU though tests lasting from few days at high stresses to several years at low stress levels. At stress values of 150 and 250 MPa [21.8 to 36.3 ksi] and temperatures ranging from 380 to 420 °C [716 to 788 °F], circumferential strains from 0.001 to 0.009 were attained after 23 to 57 days without rupture with the exception of one sample.

Goll, et al. (2001) conducted creep tests using two Zircaloy-4 rods with burnups of 54 and 64 GWd/MTU and stress ranging from 400 to 430 MPa [58 to 62.4 ksi] at 370 °C [698 °F] and 600 MPa [87 ksi] at 300 °C [572 °F]. No cladding failure occurred below 2-percent uniform plastic strain. Above 2-percent elongation, rupture was observed in only 6 out of 15 samples. These results clearly demonstrated that a uniform plastic strain limit of at least 1 percent is safe. In addition, the stresses used by Goll, et al. (2001) were above 400 MPa [58 ksi], which is substantially higher than the stresses expected for high burnup fuel under repository conditions.

Because cladding ductility decreased with increasing burnup as a result of irradiation hardening, it is expected that the information on creep available from dry storage studies for burnups lower than 45 GWd/MTU could be conservatively applied to higher burnup cladding. However, additional evaluation is necessary taking into consideration the results reported by Tsai and Billone.⁵ In general, it can be concluded that (i) deformation caused by creep will proceed slowly over time and will decrease the fuel rod pressure and (ii) the decreasing cladding temperature will also decrease the rod pressure and therefore, the hoop stress, slowing down the creep rate (Gruss, et al., 2003). However, more experimental information is needed to reach a definitive conclusion applicable to disposal conditions taking into account that the creep of high burnup fuel can be affected by the presence of a thicker oxide and a significantly larger hydrogen content.

6.4.5 Hydride Embrittlement and Delayed Hydride Cracking

Zircaloy cladding is susceptible to hydride embrittlement and delayed hydride cracking. Hydride embrittlement is a result of the presence of hydride platelets aligned in the radial direction, which can cause a significant reduction in the tensile ductility of cladding (Marshall and Louthan, 1963). One particular form of hydride embrittlement is called delayed hydride cracking because it is a time-dependent crack propagation process under sustained-load conditions that result from diffusion of hydrogen to the crack tip, followed by the formation and fracture of hydrides in the near-tip region (Cox 1990a; Dutton, et al., 1977). It should be noted that hydrogen entry occurs during reactor operation as a result of high-temperature aqueous corrosion, according to Eq. (6-1), followed by hydride precipitation upon cooling. However, hydrogen entry is not expected under the oxidizing conditions prevailing in the in-package environment after disposal.

Most of the relevant experimental data on delayed hydride cracking in the literature are for Zr-2.5 wt% Nb (Sawatzky and Ellis, 2000; Cox, 1990a; Northwood and Kosasih, 1983). This alloy is used as pressure tube material in CANDU nuclear power reactors, in which this type of

⁵ibid.

failure has occurred. Zirconium, Zircaloy-2, and Zircaloy-4 appear to be less susceptible or even unsusceptible to delayed hydride cracking. Several analytical models of delayed hydride cracking are available in the literature (Eadie and Smith, 1988; Cunningham, et al., 1987; Dutton, et al., 1977). Both Cunningham, et al. (1987) and Ahn⁶ reviewed the Canadian data and evaluated the pertinent modeling in terms of its application to repository conditions. Both assessments concluded that delayed hydride cracking would not be important in the repository because the operating stress intensity, which is approximately $0.5\text{--}2 \text{ MPa}\cdot\text{m}^{1/2}$ [$0.46\text{--}1.82 \text{ ksi}\cdot\text{in}^{1/2}$] (Siegmann, 1997a), is less than the crack-growth threshold, K_{IH} , for delayed hydride cracking.

The value of K_{IH} decreases with hydrogen concentration in solid solution (Shi and Puls, 1994), and values ranging from $5 \text{ MPa}\cdot\text{m}^{1/2}$ [$4.6 \text{ ksi}\cdot\text{in}^{1/2}$] (Shi and Puls, 1994) to $12 \text{ MPa}\cdot\text{m}^{1/2}$ [$10.9 \text{ ksi}\cdot\text{in}^{1/2}$] (Cunningham, et al., 1987) have been reported. Based on the available evidence, it seems that delayed hydride cracking is not important under repository conditions. A similar conclusion was reached by Chung (2000), who was analyzing the possibility that hydrogen blisters can be formed at the outer cladding surface in locations that are colder and higher in stress. These locations are near pellet/pellet boundaries, beneath a spacer grid or beneath a spalled or radially cracked oxide layer. Although such a process was considered unlikely, Chung (2000) stated that high burnup cladding made of standard Zircaloy-4 would be more prone to delayed hydride cracking.

In the absence of cracks and a significant source of atomic hydrogen, the integrity of cladding is determined by the quantity and distribution of radial hydrides existing in the microstructure. Zircaloy cladding generally contains some circumferential hydrides that cause little or no effect on ductility or fracture toughness (Northwood and Kosasih, 1983) and the amount of hydrogen pickup in the repository is expected to be small. As a result, possible hydride embrittlement under repository conditions has not been examined closely. The occurrence of hydride embrittlement depends on the presence or absence of hydride reorientation from the circumferential planes to the radial planes. For hydride reorientation to occur, the existing circumferential hydrides in the microstructure must first dissolve and then reprecipitate radially in the presence of an adequate hoop stress.

An important factor for hydride reorientation is temperature because temperatures as high as $300 \text{ }^\circ\text{C}$ [$572 \text{ }^\circ\text{F}$] are, in general, above the solvus temperature of the hydride. As a function of the hydrogen content, the solvus temperature is $260 \text{ }^\circ\text{C}$ [$500 \text{ }^\circ\text{F}$] at 40 ppm hydrogen by weight, but increases to $400 \text{ }^\circ\text{C}$ [$752 \text{ }^\circ\text{F}$] at 200 ppm hydrogen. At a hydrogen content of 50–70 ppm, a range within which hydride embrittlement is known to occur (Marshall and Louthan, 1963), the solvus temperature is approximately $290\text{--}300 \text{ }^\circ\text{C}$ [$554\text{--}572 \text{ }^\circ\text{F}$] (Northwood and Kosasih, 1983; Kearns, 1967). On the other hand, average temperature of the cladding based on thermal calculations is expected to be less than $237 \text{ }^\circ\text{C}$ [$458 \text{ }^\circ\text{F}$] (Siegmann and Macheret, 2002), but the maximum allowable temperature is $330 \text{ }^\circ\text{C}$ [$626 \text{ }^\circ\text{F}$]. If the temperature of the cladding reaches more than $300 \text{ }^\circ\text{C}$ [$572 \text{ }^\circ\text{F}$], the circumferential hydrides are expected to redissolve, at least partially, into solid solution in the zirconium matrix. It should be noted that the terminal solid solubility for precipitation during cooling is found at significantly lower temperatures than the line representing the logarithm of the hydrogen concentration as a function of the reciprocal of the

⁶Ahn, T.M. "Cladding Credit." *Presentation at the DOE/NRC Performance Assessment Technical Exchange Workshop, March 17–19, 1998. San Antonio, Texas. 1998.*

absolute temperature for dissolution during heating (Sawatzky and Ellis, 2000). As the temperature drops below the solvus temperature, radial hydrides can reprecipitate at slow cooling rates if the cladding hoop stress, which is tensile, exceeds a critical value. Both the average cladding temperature and the maximum allowable temperature could increase significantly if drift degradation occurred, followed by the subsequent accumulation of rubble on top of the drip shield and waste package.

The value of the critical or threshold hoop stress required for hydride reorientation is not well defined. Values ranging from 35 to 138 MPa [5.1 to 20.0 ksi] have been quoted by Einziger and Kohli (1983) and from 35 to 200 MPa [5.1 to 29.0 ksi] by Pescatore, et al. (1989). The critical stress value depends on temperature, alloy composition, fabrication method, texture, microstructure, yield strength, and residual stress (Bai, et al., 1994; Hardie and Shanahan, 1975; Marshall, 1967a; Louthan and Marshall, 1963). The low critical stress value of 35 MPa [5.1 ksi] is for a cold-drawn extruded Zr-2.5Nb (Hardie and Shanahan, 1975) and a Zircaloy-2 tubing of unspecified processing condition (Louthan and Marshall, 1963). For cold-worked Zircaloy-2 and Zircaloy-4, the critical stress value is approximately 84 to 95 MPa [12.2 to 13.8 ksi] (Bai, et al., 1994; Chan, 1996; Marshall, 1967a,b), but higher values in the range of 165 to 220 MPa [23.9 to 31.9 ksi] have also been reported (Pescatore, et al., 1989; Marshall, 1967a,b). Recent results indicate that, for Zircaloy-4, the critical stress values are 95, 187, and 200 MPa [13.8, 27.1, and 29.0 ksi] for recrystallized, beta-treated, and stress-relieved microstructures (Bai, et al., 1994). The first reported case of stress reorientation in actual fuel cladding occurred with a stress of 145 MPa [21.0 ksi] (Einziger and Kohli, 1983). In this particular case, the temperature was 323 °C [613 °F] and the hydrogen content was 90 ppm for fuel rods with a burnup of 31 GWd/MTU (Einziger and Kohli, 1983). In addition to microstructure, texture, and processing conditions, recent work suggests that the large variation in the threshold stress can be explained on the basis of the residual stresses that arise because of the misfit strains of the hydride (Bai, et al., 1994). Plastic relaxation of these residual stresses can potentially decrease the threshold stress for hydride reorientation in the repository.

The cladding stress in the repository is anticipated to be 60 to 100 MPa [8.7 to 14.5 ksi] (Siegmann, 1997b).⁷ With these stress levels, reorientation of hydrides may be feasible at the slow cooling rates anticipated in the repository if the repository temperature ever exceeds the hydrogen solvus temperature {290–300 °C [554–572 °F]} and the threshold stress for reorientation is less than 100 MPa [14.5 ksi]. Radial hydrides formed by slow cooling are thick, long plate-like precipitates, whose morphology is conducive to embrittlement and can lead to decreases in ductility and fracture toughness (Chan, 1996). When the hydrides are long and widely spaced, only small amounts of radial hydrides are required to cause a reduction in tensile ductility. As a result, hydride embrittlement can occur without or with only small amounts of hydride reorientation (Chan, 1996). Recent work indicated that while the fracture strength is insensitive to radial hydrides, the tensile ductility is severely reduced by radial hydrides that exceed 50 to 100 μm [1.96 to 3.94 mil] in length (Puls, 1988). Experimental data (Kreyns, et al., 1996; Simpson and Cann, 1979) indicate that the fracture toughness of Zircaloy cladding is reduced from approximately 44 MPa·m^{1/2} [40 ksi·in^{1/2}] without hydrogen to 7.5 MPa·m^{1/2} [6.83 ksi·in^{1/2}] at 4,000 wt ppm hydrogen (Kreyns, et al., 1996) and to 1 MPa·m^{1/2} [0.9 ksi·in^{1/2}] at higher hydrogen contents (Simpson and Cann, 1979).

⁷Ibid.

On the other hand, redissolution of hydrides and hydride reorientation do not occur if the cladding temperature is lower than 230 °C [446 °F], which is below the solvus temperature, because hydrides should be dissolved to be reoriented (Hardie and Shanahan, 1975). Hydride reorientation also requires cladding hoop stresses higher than a threshold stress. Thus, hydride embrittlement may or may not be an important failure mechanism for fuel cladding in the repository environment, depending on the waste package temperature and the threshold stress for hydride reorientation.

Limited information exists for high burnup fuel cladding after extended dry storage to evaluate the possibility of hydride reorientation and embrittlement. Results from a study (Eizinger, et al., 2003) conducted after a 15-year period of dry storage using fuel rods with a medium burnup of 36 GWd/MTU, in which the oxide thickness was 24 to 40 µm [0.94–1.57 mil] and the hydrogen ranges from 250 to 300 ppm, indicate the absence of significant hydride reorientation. However, more information is needed to reach a definitive conclusion taking into account possible effects of axial migration of hydrogen or cool-down under higher levels of stress. Goll, et al. (2001) conducted a ductility test using two fuel rods irradiated to 54 and 64 GWd/MTU, which had measured peak oxide thicknesses of 50 and 90 µm [1.97–3.54 mil], respectively. A stress of 100 MPa [14.5 ksi] was applied at 150 °C [302 °F] after a creep test at 300 °C [572 °F]. Even though a substantial amount of radially precipitated hydrides were detected metallographically, no cladding failure was observed. The hydrogen content was not reported.

It was reported⁸ that in a creep test at 400 °C [752 °F] using a high burnup (67 GWd/MTU) fuel rod in which the hoop stress was 190 MPa [27.6 ksi], the furnace was shut down. After cooling, the test sample ruptured at 205 °C [401 °F]. The hydrogen content of the test sample was approximately 600 ppm, and the hydrides were circumferentially distributed over an outer rim in the proximity of the metal/oxide interface. Although it was some concern initially regarding the possibility of hydride reorientation and embrittlement, the failure in the test was caused by a fracture in the weld of the cladding sample to the bottom end-cap used in the test. It is important to note that the sample survived a probable impact loading after cooling from 400 to 205 °C [752 to 401 °F] at a high pressure even in the presence of radial hydrides.⁹

It should be emphasized that for hydride reorientation, the relevant stress to consider is the cladding hoop stress at temperatures just below the solvus temperature, which is in the range of 260–300 °C [500–572 °F], depending on the hydrogen content (Northwood and Kosasih, 1983). The hydrogen solubility of Zircaloy-4 at 325 °C [617 °F] is approximately 90 to 100 ppm (Kearns, 1967) and appears to be approximately the same for zirconium, Zircaloy-2, and Zr-2.5Nb (Sawatzky and Ellis, 2000). Consequently, some of the circumferential hydrides in Zircaloy cladding would dissolve into the matrix and subsequently reorient and reprecipitate as radial hydrides for a tensile (hoop) stress when the cladding cools slowly in repository conditions below the solvus temperature. Obviously, the amount of hydrogen available for precipitation will be significantly higher in a high burnup fuel. Thus, it is important to consider the distribution of cladding stresses and temperatures and their evolution following waste package emplacement in

⁸Tsai, H. and M.C. Billone. "Thermal Creep of Irradiated Zircaloy Cladding." *Presentation at the 14th International Symposium on Zirconium in the Nuclear Industry, June 13–17, 2004*. Stockholm, Sweden. 2004. Submitted for publication. 2004.

⁹Ibid.

the repository. Uncertainties exist in both the cladding temperature and the critical threshold stress value that preclude a precise determination of the probability of hydride embrittlement of cladding in the repository.

The possibility does exist that cladding may fail by hydride embrittlement under disposal conditions, in particular for high burnup fuel. As recognized in a DOE analysis of hydride-related degradation of cladding (CRWMS M&O, 2000h). It is argued, however, that it will be confined to a small fraction of fuel-cladding fabricated from standard Zircaloy-4 and operated to burnups higher than 55 GWd/MTU. To evaluate more precisely the possibility of fuel-cladding embrittlement, it is necessary to know with sufficient accuracy (i) the average temperature of the fuel cladding and the range of variation for the conditions expected in the repository, (ii) the average value of hoop stress and its expected range of variation, and (iii) a good estimation of the threshold stress for hydride reorientation. Uncertainties regarding the calculated values of cladding temperatures and stresses, including uncertainties related to the temporal and spatial variations expected for thousands of waste packages, must be taken into account when considering hydride reorientation and hydride-induced failure. Because of the higher hydrogen content of high burnup fuel, the probability of occurrence of hydride reorientation and subsequent cladding failure is higher than for medium burnup fuel. However, the introduction of cladding materials with better corrosion resistance than Zircaloy, and as a result, with lower hydrogen content, could decrease the likelihood of hydride embrittlement. Evaluation of the propensity to hydride reorientation and embrittlement for these new cladding materials is needed.

6.4.6 Fuel and Cladding Oxidation

Fuel and cladding oxidation are potential failure processes if the disposal container fails when temperatures of the fuel assemblies are relatively high. Cladding oxidation would be the predominant failure mechanism if the fuel rods remain intact when the container fails. Fuel oxidation would be the dominant failure mode for perforated or failed fuel rods. The possible failure of fuel rods by cladding and fuel oxidation was examined by Einziger (1994), McCoy (1996), Ahn (1996), Ahn, et al. (1999) and Cragolino, et al. (1999). Einziger (1994) has presented models for computing the times to failure for cladding oxidation and for fuel oxidation. The cladding oxidation model has been developed based on oxidation kinetics data reported by Boase and Vandergraaf (1977) and by Suzuki and Kawasaki (1986). Failure of fuel rods by fuel oxidation is more complex and involves two failure steps including: (i) fuel oxidation near a perforation in the fuel rod and the formation of a split (an axial crack) in the cladding and (ii) continued fuel oxidation near the end of the split, causing the split to propagate axially. For perforated fuel rods, fuel oxidation is not expected to be a problem if the fuel temperature is lower than 250 °C [482 °F] because the fuel oxidation kinetics would be too sluggish. Above 250 °C [482 °F], dry oxidation of irradiated UO₂ to U₃O₈ is possible and will be accompanied by a substantial volume increase. This volume increase provides the driving force for the initiation and propagation of the split in the cladding.

Fuel rod degradation caused by fuel and cladding oxidation under expected repository conditions depends on the fuel temperature when the disposal container fails. The fuel temperature, in turn, depends on the mass loading and the stability of the emplacement drifts. Cladding oxidation can be dismissed as a failure mechanism at temperatures lower than 350 °C [662 °F]. For perforated fuel rods, fuel oxidation would not be a problem if the disposal container does not fail before 35 years after emplacement for a mass loading of 5.93 kg U/m² [0.38 lb U/ft²] and no backfill, or before 500 years for 20.5 kg U/m² [1.32 lb U/ft²] with backfill (McCoy, 1996). In both cases, the

fuel temperature would be sufficiently low that the fuel and cladding oxidation kinetics would be too sluggish to cause cladding failure. Based on these estimates, fuel and cladding oxidation could be dismissed as cladding degradation mechanisms as long as the disposal containers are not breached in thousands of years and the fuel temperature is lower than 250 °C [482 °F]. It is not anticipated that significant differences would exist with high burnup fuel.

6.4.7 Fuel Side Stress Corrosion Cracking

As reviewed by Cragnolino, et al. (1999), a well known process of cladding failure, named pellet/cladding interaction failure, is fuel side stress corrosion cracking induced by iodine (Cox, 1990b). Several studies have been conducted to determine the possibility of iodine-induced stress corrosion cracking of Zircaloy cladding under dry storage conditions (Miller, et al., 1989; Pescatore, et al., 1989; Cunningham, et al., 1987; Tasooji, et al., 1984). Tasooji, et al. (1984) developed a phenomenological model for treating stress corrosion cracking and applied this model to predict iodine-induced stress corrosion cracking in Zircaloy cladding under dry storage conditions. Their calculations indicated that the iodine-induced stress corrosion cracking limiting temperature is 280 °C [536 °F] for the case of 20-percent fission gas release at the maximum internal gas pressure expected in dry storage. For 1-percent fission gas release, the iodine-induced stress corrosion cracking limiting temperature was found to be greater than 450 °C [842 °F]. Based on the iodine-induced stress corrosion cracking crack growth model developed by Kreyns, et al. (1976), Cunningham, et al. (1987) determined that 290 °C [554 °F] is the maximum allowable temperature for crack propagation arrest caused by decreasing temperature. Pescatore, et al. (1989) conducted an extensive review and evaluated the pertinent data on iodine-induced stress corrosion cracking. Their compilation of experimental data in the literature indicated that a threshold of iodine concentration exists below which stress corrosion cracking of Zircaloy cladding does not occur. The minimum iodine concentration required to cause stress corrosion cracking, however, is not a constant but decreases with increasing time. In most instances, the critical iodine concentration can be attained or exceeded during isolation in dry storage.

For uncracked cladding, there exists a threshold stress below which iodine-induced stress corrosion cracking would not occur. That critical stress value was determined to be approximately 200–250 MPa [29.0–36.3 ksi] based on available experimental data. For cracked cladding, crack growth by iodine-induced stress corrosion cracking does not occur at stress intensity levels below a threshold value, which was determined to be approximately 3 MPa·m^{1/2} [2.7 ksi·in^{1/2}]. For dry storage, the worst case maximum stress was 131 MPa [19.0 ksi], which was below the critical stress for iodine-induced stress corrosion cracking for smooth, uncracked materials. At a stress of 131 MPa [19.0 ksi] and a growth threshold of 3 MPa·m^{1/2} [2.7 ksi·in^{1/2}], the critical crack length for the onset of iodine-induced stress corrosion cracking is 0.27 mm [11 mil]. Tasooji, et al. (1984) estimated that, in the worst-case condition, 1 percent of spent nuclear fuel rods would have a defect greater than 0.13 mm [5 mil] deep, which is about 20 percent of the wall thickness. The 1-percent estimate was considered too high by Pescatore, et al. (1989), who concluded that there is a low probability of finding a rod with both a crack of the requisite size and a hoop stress of sufficient magnitude to cause the critical stress intensity for iodine-induced stress corrosion cracking to be exceeded. Because of this, Pescatore, et al. (1989) concluded that iodine-induced stress corrosion cracking would not be a major degradation mechanism of cladding and would affect, at the most, only a very small fraction of the total number of fuel rods in dry storage.

Siegmann reviewed pertinent iodine-induced stress corrosion cracking studies for dry storage and concluded iodine-induced stress corrosion cracking would not play a role in cladding degradation in the repository (Siegmann, 1997a). He indicated that, on discharge, irradiated fuel pellets contract away from the cladding and remove the localized stress that is needed for stress corrosion cracking. Cladding creep in the repository can also cause the cladding to move further away from the pellets, leading to additional reduction in pellet ridging and stress. He also cited several studies that indicated that iodine-induced stress corrosion cracking would not be an important cladding degradation mechanism in dry storage (Pescatore, et al., 1989; Cunningham, et al., 1987; Rothman, 1984; Tasooji, et al., 1984). The assessment is probably also applicable to the repository. As indicated in the sections on delayed hydride cracking and hydrogen embrittlement, the operating stress intensity for the cladding in the repository is approximately $0.5\text{--}2\text{ MPa}\cdot\text{m}^{1/2}$ [$0.46\text{--}1.82\text{ ksi}\cdot\text{in}^{1/2}$], which is slightly below the K_{ISCC} value of $3\text{ MPa}\cdot\text{m}^{1/2}$ [$2.7\text{ ksi}\cdot\text{in}^{1/2}$] for crack growth by iodine-induced stress corrosion cracking. The cladding stress is approximately $60\text{--}100\text{ MPa}$ [$8.7\text{--}14.5\text{ ksi}$], which is well below the critical stress of $200\text{--}250\text{ MPa}$ [$29.0\text{--}36.3\text{ ksi}$] for iodine-induced stress corrosion cracking. Because both the critical stress and the stress intensity levels for iodine-induced stress corrosion cracking are not met, crack initiation and growth by iodine-induced stress corrosion cracking is unlikely in the cladding under disposal conditions. In addition, the expected temperature of the cladding is below $250\text{ }^{\circ}\text{C}$ [$482\text{ }^{\circ}\text{F}$], which is below the calculated iodine-induced stress corrosion cracking limiting temperatures of $280\text{--}290\text{ }^{\circ}\text{C}$ [$536\text{--}554\text{ }^{\circ}\text{F}$] (Cunningham, et al., 1987; Tasooji, et al., 1984). Based on these considerations, iodine-induced stress corrosion cracking is not expected to be a major cladding degradation mechanism in the repository.

For high burnup fuel, even though the concentration of iodine in the pellet/cladding gap will be higher than that for medium burnup, this concentration is not a factor to consider because the threshold concentration is already reached in medium burnup fuel. The important factor is the hoop stress and, in particular, the stress intensity threshold that can be reached in the presence of cracks in the cladding. Additional information seems to be necessary to attain a final evaluation.

6.5 Assessment of the Effect of High Burnup on Spent Fuel Cladding Performance

Zircaloy cladding exhibits extremely low uniform corrosion rates in aqueous environments and could delay substantially the release of radionuclides from commercial spent fuel if it remains intact. Performance assessments show a high correlation between dose and fraction of failed cladding. Cladding failure can occur as a result of localized corrosion, stress corrosion cracking, and hydride reorientation and subsequent embrittlement, under a combination of adverse environmental and stress conditions. Cladding may also fail as a result of creep caused by hoop stresses resulting from internal pressure. Both creep and hydride reorientation are processes affected by temperature, whereas localized corrosion and stress corrosion cracking in the chloride-containing in-package aqueous environment are not influenced by temperature. The most important effect of high burnup on the cladding behavior appears to be related to hydride reorientation and embrittlement and, secondly, to the influence of the hydride content and distribution on the creep behavior.

DOE has considered that cladding can be an effective metallic barrier against the release of radionuclides from commercial spent nuclear fuel. However, little experimental evidence has been provided to support such assessment nor have adequate technical bases for all the

assumptions included in the model abstraction been developed. This is the case for the modeling of localized corrosion and stress corrosion cracking, as well as for the lack of consideration of hydride reorientation and embrittlement as a potential failure process that may be faster and, hence, more detrimental than unzipping alone. Recent performance assessment calculations showed that 95th percentile cladding degradation increased the mean annual dose only slightly over the basecase (Bechtel SAIC Company, LLC, 2002b). Even complete cladding neutralization, only increases the mean dose by only one order of magnitude, and the dose, approximately 5×10^{-5} mSv/yr [5×10^{-3} mrem/yr] is more than four orders of magnitude lower than that specified in the regulations for the reasonably maximum exposed individual. In the nominal case, however, it is assumed that the fraction of failed cladding perforated before unzipping remains constant at 0.08 up to approximately 50,000 years and reaches 0.2 only after 100,000 years (CRWMS M&O, 2000b). Note, however, that these estimates of cladding protection do not consider the full range of possible failure mechanisms nor their probabilities, and therefore may overestimate the effectiveness of cladding as a barrier. In other international programs (e.g., France, Canada, Sweden, Finland), no credit is given to the cladding as a metallic barrier as a result of the uncertainties related to its integrity under repository conditions.

It is apparent in the TPA Version 4.1 code Sensitivity Report (Mohanty, et al., 2004) that the introduction of cladding protection decreases the dose at 10,000 years with respect to that for the basecase from 2×10^{-4} to 3×10^{-6} mSv/yr [2×10^{-2} to 3×10^{-4} mrem/yr]. Release rates of highly soluble and mobile radionuclides like Tc-99 and I-129 account for most of the 10,000-year predicted dose, and are approximately proportional to the amount of spent nuclear fuel exposed.

The specific effect of high burnup fuel in performance assessment calculations has not been evaluated in the total-system performance assessment because a specific model should be introduced to account for the potential detrimental effect on the dose of the various failure processes discussed in this section.

7 CONCLUSIONS

This report has evaluated the existing literature to examine the behavior of the high burnup spent nuclear fuel under disposal conditions after failure of the confinement barriers such as waste package that allows interaction between fuel and groundwater. Based on 1998 projections, high burnup will constitute more than 70 percent of the total inventory of the spent nuclear fuel generated between 1998 and 2015. Assuming 63,000-MTU capacity for commercial spent nuclear fuel of a total capacity of 70,000 MTU at the potential Yucca Mountain repository, 30 percent of the 63,000 MTU commercial spent nuclear fuel could be classified as high burnup fuel. It should be noted, however, for the operating U.S. nuclear reactors the upper limit of the spent nuclear fuel average burnup is 62-GWd/MTU for the fuel rod with the maximum or peak burnup.

The changes in the radionuclide inventories for a high burnup fuel were calculated using the ORIGEN-ARP 2.00 code to evaluate the effects of the increase in radionuclide inventory and assess the impact on the source term for the postclosure period of the potential repository. Comparisons are made for the inventory and decay heat load produced by a 15 × 15 pressurized water reactor fuel assembly with 5.0 wt% enriched U-235 fuel at 65-GWd/MTU burnup versus 4.0 wt% enriched U-235 fuel at 45-GWd/MTU burnup. Calculations were conducted over the 10,000-year regulatory repository timeframe. Pressurized water reactor fuel was analyzed because it has a higher inventory of most radionuclides and generally has a higher range of burnup than boiling water reactor fuel. Increasing fuel burnup changes the radionuclide inventory in spent nuclear fuels. The activities of short-lived fission products tend to remain constant or decrease slightly, while activities of activation products and actinides tend to increase with increasing burnup, thus also increasing the amount of decay heat the waste will generate at a given point in time.

For use in performance assessment calculations, the source term and thermal load values are used to model the proposed repository inventory and thermal loading as representative of the entire repository loading. An analysis using a 65 GWd/MTU high burnup source term as 100 percent of the proposed repository radionuclide inventory in the TPA code version 5.0 does not demonstrate any additional risk significance in the performance assessment calculation. The variation of decay heat load occurs over a relatively small range and is also of low risk significance as long as the thermal load range used in performance assessment calculations takes into account the average thermal loading of the proposed repository as a whole unit.

In light water reactor fuels with burnups below 50 GWd/MTU, only a small fraction of radionuclides is present at the gap and grain boundaries. These radionuclides are bounded by the fraction of fission gas release, mainly xenon. Literature review indicates that high burnup structure starts forming between 60 and 75 GWd/MTU and reaches completion near 100-GWd/MTU average burnup. The burnup around the rim region is approximately 1.3 times the average burnup attributed to epithermal fissions. High burnup structure is characterized by a formation of a porous structure {1 to 2 μm [3.9×10^{-2} to 7.9×10^{-2} mil] diameter pores} and loss of optically definable grain structure {0.2 to 0.3 μm [7.87×10^{-3} to 11.8×10^{-3} mil] grain diameter} in the rim region. Furthermore, formation of rim structure impacts the temperature distribution in the pellet.

Fission gas release characteristics are different for the boiling water and the pressurized water reactors. Several studies have assessed that the pressurized water reactor has a slightly lower

fission gas release compared to the boiling water reactor. Fission gas release, however, is highly dependent on design and operating conditions. Fission gas release increases at higher burnups. The cesium release from the fuel on puncturing is similar in concentration to the fission gas release. Furthermore, studies conducted on spent nuclear fuel rods, exceeding 50 GWd/MTU burnup, stored under dry storage conditions for 15 years indicate that the fission gas release could range from 1.4 to 17 percent.

Increasing fuel burnup changes the radionuclide inventory in spent nuclear fuels. The activities of short-lived fission products tend to remain constant or decrease slightly, while activities of activation products and actinides tend to increase with increasing burnup, thus increasing the amount of decay heat the waste will generate at a given point in time. For use in performance assessment calculations, the source term and thermal load values are used to model the potential repository inventory and thermal loading as a whole. An analysis using a 65-GWd/MTU high burnup source term as 100 percent of the potential repository radionuclide inventory in the TPA Version 5.0 code does not demonstrate high risk significance in the performance assessment calculation. The variation of decay heat load occurs over a relatively small range and is also of low risk significance as long as the thermal loading range used in performance assessment calculations bounds the average thermal loading of the potential repository as a whole.

Instant release fraction refers to a combined inventory of soluble fission products such as cesium, iodine, chloride, and carbon located in the gap, and fission products such as cesium, iodine, and segregated metallic phases such as technetium located at the grain boundaries. Studies have shown that in the presence of water, fission products present at the grain boundaries are released at a slower rate compared to the gap. Because of difficulties in separating gap and grain boundary contributions, however, these fractions are combined and are assumed to be released instantly on contact with water. Despite the lack of experimental data exceeding 50-GWd/MTU burnup, an estimate of instant release fraction is determined based on the fission gas release data from the high burnup spent nuclear fuel. Significant uncertainties remain, however, in the estimate of instant release fraction for important radionuclides for spent nuclear fuels above 60 GWd/MTU as a result of the formation of high burnup rim structure. This study estimates instant release fraction of 34 percent for I-129 at 75-GWd/MTU burnup. I-129 is considered to be the most important contributor to the dose. The instant release fraction for cesium is estimated at one-third of the instant release fraction for I-129 based on available light water reactor data in this study. Uncertainties in Tc-99 are significant because of the limited data, and low concentration of Tc-99 present in the grain boundaries that makes Tc-99 measurements prone to uncertainties. This study recommends that the upper bound for the instant release fraction for Tc-99 should be 0.28 percent based on the maximum observed concentration of 0.13 percent of Tc-99 in analyzed samples. Similarly significant uncertainties exist for the instant release fraction for C-14 and Cl-36, due to the lack of data for light water reactor spent nuclear fuels. Because Cl-36 volatility is comparable to I-129, the I-129 release fraction is recommended for Cl-36 in this study. A constant instant release fraction of 10 percent is recommended in this study for C-14. Because most of the data were obtained from fuel grains or fragments, the instant release fraction obtained from these samples represent a conservative estimate. The estimate does not include limited access of water to grain boundaries. A triangular probability distribution is proposed for iodine, cesium, chloride, and technetium. Because high burnup spent nuclear fuel exceeding 65 GWd/MTU could be a very small quantity compared to high burnup fuel between 45 and 65 GWd/MTU, the influence of rim effects on

spent nuclear fuel dissolution can be neglected, based on the quantity of spent nuclear fuel that will be emplaced at the repository.

Following a rapid release of instant release fraction, spent nuclear fuel dissolves at a rate depending on the aqueous chemical environment. The review of literature data indicates that the burnup has no significant effect on the spent nuclear fuel dissolution rate at 25 °C [77 °F]. At 75 °C [167 °F], however, based on the U.S. Department of Energy data, the spent nuclear fuel dissolution rate decreases with an increase in burnup. The effect of high burnup spent nuclear fuel dissolution rate can be adequately sampled in the U.S. Nuclear Regulatory Commission and the Center for Nuclear Waste Regulatory Analyses performance assessment abstraction model. Estimation of surface area, however, is complicated by the pellet fragmentation caused by the radial thermal gradient and microstructural changes in the rim structure. Various authors have assumed different surface area roughness (or correction) factors to account for such changes. Surface area estimation continues to account for significant uncertainty in the analysis.

Zircaloy cladding exhibits extremely low uniform corrosion rates in aqueous environments and could delay substantially the release of radionuclides from commercial spent nuclear fuel if it remains intact. Performance assessments show a high correlation between dose and fraction of failed cladding. Cladding is thin, however, and not physically strong. Cladding failure can occur as a result of localized corrosion, stress corrosion cracking, and hydride reorientation, under a combination of adverse environmental and stress conditions. Cladding may also fail as a result of creep caused by hoop stresses resulting from internal pressure, or mechanically, when subjected to loads associated with seismic events and rockfall.

The most important effect of high burnup on Zircaloy cladding is the increase in the thickness of the oxide layer as a result of the extended exposure to the reactor environment and the concurrent increase of the hydrogen content. Under disposal conditions, due to the higher hydrogen content at high burnups, it appears that hydride reorientation and embrittlement during cooling could have more adverse effects on the integrity of cladding than that expected for medium burnup fuel. Creep failure requires additional examination for high burnup fuel. The concurrent effect of the higher hydrogen content also needs further evaluation. As in the case of medium burnup fuel, localized corrosion and stress corrosion cracking may also cause cladding failure in the in-package aqueous environment. Quantitative analysis of these failure processes may be needed to assess the risk significance of each of these processes under disposal conditions. Performance confirmation activities aimed to verify the expected behavior of spent fuel cladding under disposal conditions are important to evaluate the relative significance of the various cladding failure processes reviewed in this report.

The negative consequences of corrosion and hydrogen pickup on fuel cladding performance are being attenuated, at least partially, by the use of newly developed zirconium alloys that are more corrosion resistant, exhibiting significantly lower corrosion rates. Nevertheless, further evaluation of the initial condition of high burnup fuel cladding prior to disposal is needed. The experience acquired in the evaluation currently being conducted for dry storage will be valuable in establishing the likelihood of creep failure and hydride reorientation and embrittlement under repository conditions.

8 REFERENCES

- Adamson, R.B. "Effects of Neutron Irradiation on Microstructure and Properties of Zircaloy." Zirconium in the Nuclear Industry: Twelfth International Symposium. G.P. Sabol and G.D. Moan, eds. ASTM STP 1354. West Conshohocken, Pennsylvania: ASTM International. pp. 15–31. 2000.
- Adamson, R.B., B.C. Cheng, and R.M. Kruger. "Zircaloy Performance in Light Power Reactors." Fifth International Symposium on Environmental Degradation of Materials in Nuclear Power Systems—Water Reactors. La Grange Park, Illinois: American Nuclear Society. pp. 59–71. 1992.
- Ahn, T.M. NUREG–1565, "Dry Oxidation and Fracture of LWR Spent Fuels." Washington, DC: NRC. 1996.
- Ahn, T. and S. Mohanty. "Dissolution Kinetics of Spent Nuclear Fuels (SNF) in the Proposed Yucca Mountain Repository Environment." *Presentation at the MRS Symposium CC: Scientific Basis for Nuclear Waste Management XXVIII, April 12–16, 2004*. San Francisco, California. ML041000524. 2004. <www.nrc.gov/reading-rm/adams.html>
- Ahn, T.M., G.A. Cragolino, K.S. Chan, and N. Sridhar. "Scientific Bases for Cladding Credit as a Barrier to Radionuclide Release at the Proposed Yucca Mountain Repository." Scientific Basis for Nuclear Waste Management XXII. Symposium Proceedings 556. D.J. Wronkiewicz and J.H. Lee, eds. Warrendale, Pennsylvania: Materials Research Society. pp. 525–533. 1999.
- Bai, J.B., C. Prioul, and D. Francois. "Hydride Embrittlement in Zircaloy-4 Plate: Part II, Interaction Between the Tensile Stress and the Hydride Morphology." *Metallurgical and Materials Transactions*. Vol. 25A. pp. 1,199–1,208. 1994.
- Barner, J.O., M.E. Cunningham, M.D. Freshley, and D.D. Lanning. "Evaluation of Fission Gas Release in High Burnup Light Water Reactor Fuel Rods." *Nuclear Technology*. Vol. 102. pp. 210–231. 1993.
- Bechtel SAIC Company, LLC. "Total System Performance Assessment—License Application Methods and Approach." TDR–WIS–PA–000006. Rev. 00. Las Vegas, Nevada: Bechtel SAIC Company, LLC. 2002a.
- . "Risk Information to Support Prioritization of Performance Assessment Models." TDR–WIS–PA–000009. Rev. 01 ICN 0. Las Vegas, Nevada: Bechtel SAIC Company, LLC. 2002b.
- Blat, M. and D. Noel. "Detrimental Role of Hydrogen on the Corrosion Rate of Zirconium Alloys." Zirconium in the Nuclear Industry: Eleventh International Symposium. E. Ross Bradley and G.P. Sabol, eds. ASTM STP 1295. West Conshohocken, Pennsylvania: ASTM International. pp. 319–337. 1996.

Blat, M., L. Legras, D. Noel, and H. Amanrich. "Contribution to a Better Understanding of the Detrimental Role of Hydrogen on the Corrosion Rate of Zircaloy-4 Cladding Materials." *Zirconium in the Nuclear Industry: Twelfth International Symposium*. G.P. Sabol and G.D. Moan, eds. ASTM STP 1354. West Conshohocken, Pennsylvania: ASTM International. pp. 563–591. 2000.

Boase, D.G. and T.T. Vandergraaf. "The Canadian Spent Fuel Storage Canister: Some Material Aspects." *Nuclear Technology*. Vol. 32. pp. 60–71. 1977.

Bowman, S.M. and L.C. Leal. NUREG/CR-0200, ORNL/NUREG/CSD-2/V1/R6, "ORIGEN-ARP: Automatic Rapid Process for Spent Fuel Depletion, Decay, and Source Term Analysis." Oak Ridge, Tennessee: Oak Ridge National Laboratory. March 2000.

Brach, E.W. "Approval of Interim Staff Guidance Memorandum No. 11, Cladding Considerations for the Transportation and Storage of Spent Fuel, Revision 3." Memorandum (November 17) to Spent Fuel Project Office Staff members, NRC. ML0330230281. Washington, DC: NRC. 2003. <www.nrc.gov/reading-rm/adams.html>

Bradley, E.R., W.J. Bailey, A.B. Johnson, Jr., and L.M. Lowry. "Examination of Zircaloy-Clad Spent Fuel After Extended Pool Storage." PNL-3291. Richland, Washington: Pacific Northwest Laboratory. 1981.

Bredel, T., C. Cappelaere, R. Limon, G. Pinte, and P. Bouffieux. "Long Term Creep Behavior of Spent Fuel Cladding for Storage and Disposal." *Scientific Basis for Nuclear Waste Management XXIII. Symposium Proceedings 608*. R.W. Smith and D.W. Shoemith, eds. Warrendale, Pennsylvania: Materials Research Society. pp. 11–16. 2000.

Bremier, S., C.T. Walker, and R. Menzel. "Fission Gas Release and Fuel Swelling at Burn-Ups Higher than 50 Mwd/kgU." *Proceedings of the Fission Gas Behavior in Water Reactor Fuels*. Agency, Cadarache, France, September 26–29, 2000. Paris, France: Nuclear Energy Institute. pp. 93–106. 2000.

Brossia, C.S., G.A. Cragnolino, and D.S. Dunn. "Effect of Oxide Thickness on the Localized Corrosion of Zircaloy." *Proceedings of the CORROSION 2002 Conference*. Paper No. 02549. Houston, Texas: NACE International. 2002.

Chan, K.S. "A Micromechanical Model for Predicting Hydride Embrittlement in Nuclear Fuel Cladding Material." *Journal of Nuclear Materials*. Vol. 227. pp. 220–236. 1996.

Cheng, B.C., D. Smith, E. Armstrong, K. Tunage, and G. Bond. "Water Chemistry and Fuel Performance in LWRs." *Proceedings of the 2000 International Topical Meeting on Light Water Reactor Fuel Performance*, Park City, Utah, April 10–13, 2000. Published on CD-ROM. La Grange Park, Illinois: American Nuclear Society. 2000.

Cheng, B.C., J.M. Brown, K.G. Tunage, E.A. Armstrong, and M. Hudson. "Fuel Performance and Water Chemistry Variables in LWRs." *Proceedings of the 1997 International Topical Meeting on LWR Fuel Performance*, Portland, Oregon, March 2–6, 1997. La Grange Park, Illinois: American Nuclear Society. pp. 379–388. 1997.

Cheng, B., P.M. Gilmore, and H.H. Klepfer. "PWR Zircaloy Fuel Cladding Corrosion Performance, Mechanisms, and Modeling." *Zirconium in the Nuclear Industry: Eleventh International Symposium*. E. Ross Bradley and G.P. Sabol, eds. ASTM STP 1295. West Conshohocken, Pennsylvania: ASTM International. pp. 137–158. 1996.

Chin, B.A. and E.R. Gilbert. "Prediction of Maximum Allowable Temperature for Dry Storage of Zircaloy-Clad Spent Fuel in Inert Atmosphere." *Nuclear Technology*. Vol. 85. pp. 57–65. 1989.

Chin, B.A., M.A. Khan, J.C.L. Tarn, and E.R. Gilbert. "Deformation and Fracture Map Methodology for Predicting Cladding Behavior During Dry Storage." PNL-5998. Richland, Washington: Pacific Northwest Laboratory. 1986.

Chung, H.M. "Fundamental Metallurgical Aspects of Axial Splitting in Zircaloy Cladding." *Proceedings of the 2000 International Topical Meeting on Light Water Reactor Fuel Performance*, Park City, Utah, April 10–13, 2000. Published on CD-ROM. La Grange Park, Illinois: American Nuclear Society. 2000.

Cohen, P. *Water Coolant Technology of Power Reactors*. La Grange Park, Illinois: American Nuclear Society. 1980.

Comstock, R.J., G. Shoenberger, and G.P. Sabol. "Influence of Processing Variables and Alloy Chemistry on the Corrosion Behavior of ZIRLO Nuclear Fuel Cladding." *Zirconium in the Nuclear Industry: Eleventh International Symposium*. E.R. Bradley and G.P. Sabol, eds. ASTM STP 1295. West Conshohocken, Pennsylvania: ASTM International. pp. 710–725. 1996.

Cox, B. "Environmentally-Induced Cracking of Zirconium Alloys—A Review." *Journal of Nuclear Materials*. Vol. 170. pp. 1–23. 1990a.

———. "Pellet-Clad Interaction (PCI) Failures of Zirconium Alloys Fuel Cladding—A Review." *Journal of Nuclear Materials*. Vol. 172. pp. 249–292. 1990b.

———. "Degradation of Zirconium Alloys in Water Cooled Reactors." *Third International Symposium on Environmental Degradation of Materials in Nuclear Power Systems—Water Reactors*. Warrendale, Pennsylvania: The Metallurgical Society. pp. 65–76. 1988.

———. "Oxidation of Zirconium and its Alloys." *Advances in Corrosion Science and Technology*. M. Fontana and R.W. Staehle, eds. New York: Plenum Press 5. pp. 173–391. 1976.

———. "Environmentally-Induced Cracking of Zirconium Alloys." *Reviews on Coatings and Corrosion*. J. Yahalom, ed. Vol. 1, No. 4. pp. 367–422. 1975.

———. "Stress Corrosion Cracking of Zircaloy-2 in Neutral Aqueous Chloride Solutions at 25 °C." *Corrosion*. Vol. 29. pp. 157–166. 1973.

Cox, B. and J.C. Wood. "Iodine Induced Cracking of Zircaloy Fuel Cladding—A Review." *Corrosion Problems in Energy Conversion and Generation*. C.S. Tedmon, ed. Princeton, New Jersey: The Electrochemical Society. p. 275. 1974.

Cragolino, G.A. "Stress corrosion cracking of zirconium and its alloys in the presence of chlorides (in Spanish)." Doctoral thesis. University of Buenos Aires (Argentina). Buenos Aires, Argentina. 1975.

Cragolino, G.A., C.S. Brossia, D.S. Dunn, and C.A. Greene. "General and Localized Corrosion of Zircaloy Under High-Level Radioactive Waste Disposal Conditions." Tenth International Symposium on Environmental Degradation of Materials in Nuclear Power Systems—Water Reactors. Houston, Texas: NACE International. 2001.

Cragolino, G.A., D.S. Dunn, C.S. Brossia, V. Jain, and K.S. Chan. "Assessment of Performance Issues Related to Alternate Engineered Barrier System Materials and Design Options." CNWRA 99-003. San Antonio, Texas: CNWRA. 1999.

Cragolino, G.A. and J.R. Galvele. "Stress Corrosion Cracking of Zircaloy-4 in the Presence of Chlorides." Proceedings of the 1st Latin American Conference on Electrochemistry. CNEA Report PMM/I-121. Buenos Aires, Argentina: Comision Nacional de Energia Atomica. 1973.

CRWMS M&O. "CSNF Waste Form Degradation: Summary Abstraction." ANL-EBS-MD-000015. Rev 00. Las Vegas, Nevada: CRWMS M&O. 2000a.

———. "Clad Degradation—FEPs Screening Arguments." ANL-WIS-MD-000008. Rev. 00 ICN 01. Las Vegas, Nevada: CRWMS M&O. 2000b.

———. "Waste Form Degradation Process Model Report." TDR-WIS-MD-000001. Rev. 00 ICN 01. Las Vegas, Nevada: CRWMS M&O. 2000c.

———. "Total System Performance Assessment for the Site Recommendation." TDR-WIS-PA-000001. Rev. 00 ICN 01. Las Vegas, Nevada: CRWMS M&O. 2000d.

———. "Clad Degradation—Summary and Abstraction." ANL-WIS-MD-000007. Rev. 00 ICN 01. Las Vegas, Nevada: CRWMS M&O. 2000e.

———. "Initial Cladding Condition." ANL-EBS-MD-000048. Rev. 00 ICN 01. Las Vegas, Nevada: CRWMS M&O. 2000f.

———. "Clad Degradation—Local Corrosion of Zirconium and Its Alloys Under Repository Conditions." ANL-EBS-MD-000012. Rev. 00. Las Vegas, Nevada: CRWMS M&O. 2000g.

———. "Hydride Related Degradation of SNF Cladding Under Repository Conditions." ANL-EBS-MD-000011. Rev 00. Las Vegas, Nevada: CRWMS M&O. 2000h.

Cunningham, M.E., E.P. Simonen, R.T. Allemann, I.S. Levy, R.F. Hazelton, and E.R. Gilbert. "Control of Degradation of Spent LWR Fuel During Dry Storage in an Inert Atmosphere." PNL-6364. Richland, Washington: Pacific Northwest Laboratory. 1987.

DOE. "Preclosure Safety Analysis Guide." TDR-MGR-RL-000002. Rev. 00. Las Vegas, Nevada: Yucca Mountain Site Characterization Office. 2002.

———. "Inventory Abstraction." ANL-WIS-MD-000006. Rev. 00 ICN 02. Washington, DC: DOE, Office of Civilian Radioactive Waste Management. 2001a.

———. DOE/RW-0539, "Yucca Mountain Science and Engineering Report: Technical Information Supporting Site Recommendation Consideration." Las Vegas, Nevada: DOE, Office of Civilian Radioactive Waste Management. 2001b.

Dutton, R., K. Nuttall, M.P. Puls, and L.A. Simpson. "Mechanisms of Hydrogen Induced Delayed Cracking in Hydride Forming Materials." *Metallurgical Transactions*. Vol. 8A. pp. 1,553–1,562. 1977.

Eadie, R.L. and R.R. Smith. "Modeling Delayed Hydride Cracking in Zirconium Alloys." *Canadian Metallurgical Quarterly*. Vol. 27. pp. 213–223. 1988.

Einziger, R.E. "Preliminary Spent LWR Fuel Oxidation Source Term Model." Proceedings of the Fifth Annual International Conference on High-Level Radioactive Waste Management. La Grange Park, Illinois: American Nuclear Society. Vol. 2. pp. 554–559. 1994.

Einziger, R.E. and R. Kohli. "Low-Temperature Rupture of Zircaloy-Clad Pressurized Water Reactor Spent Fuel Rods Under Dry Storage Conditions." *Nuclear Technology*. Vol. 67. pp. 107–123. 1983.

Einziger, R.E., H. Tsai, M.C. Billone, and B.A. Hilton. NUREG/CR-6831, "Examination of Spent PWR Fuel Rods after 15 Years in Dry Storage." Washington, DC: NRC. 2003.

Franklin, D.G. and P.M. Lang. "Zirconium-Alloy Corrosion: A Review Based on an International Atomic Energy Agency (IAEA) Meeting." *Zirconium in the Nuclear Industry: Ninth International Symposium*. C.M. Eucken and A.M. Garde, eds. ASTM STP 1132. West Conshohocken, Pennsylvania: ASTM International. pp. 3–32. 1991.

Forsyth, R.S. "An Evaluation of Results from the Experimental Programme Performed in the Studsvik Hot Cell Laboratory." Technical Report 97-25. Stockholm, Sweden: Swedish Nuclear Fuel and Waste Management Company. 1997.

Forsyth, R.S. and L.O. Werme. "Spent Fuel Corrosion and Dissolution." *Journal of Nuclear Materials*. Vol. 190. pp. 3–19. 1992.

Garde, A.M. "Enhancement of Aqueous Corrosion of Zircaloy-4 Due to Hydride Precipitation at the Metal-Oxide Interface." *Zirconium in the Nuclear Industry: Ninth International Symposium*. C.M. Eucken and A.M. Garde, eds. ASTM STP 1132. West Conshohocken, Pennsylvania: ASTM International. pp. 566–594. 1991.

Garzarolli, F. "Development of Cladding Materials for BWR and PWR Fuel." Tenth International Symposium on Environmental Degradation of Materials in Nuclear Power Systems—Water Reactors. Houston, Texas: NACE International. Published on CD-ROM. 2001.

Garzarolli, F., R. Manzel, and A. Seibold. "Corrosion Phenomena in Zr Alloy Fuel Claddings at High Burnups." Tenth International Symposium on Environmental Degradation of Materials in Nuclear Power Systems—Water Reactors. Houston, Texas: NACE International. Published on CD-ROM. 2001.

Garzarolli, F., H. Stehle, and E. Steinberg. "Behavior and Properties of Zircalloys in Power Reactors: A Short Review of Pertinent Aspects in LWR Fuel." Zirconium in the Nuclear Industry: Eleventh International Symposium. E. Ross Bradley and G.P. Sabol, eds. ASTM STP 1295. West Conshohocken, Pennsylvania: ASTM International. pp. 12–32. 1996.

Gilbon, D., A. Soniak, S. Doriot, and J.P. Mardon. "Irradiation Creep and Growth Behavior, and Microstructural Evaluation of Advanced Zr-Base Alloys." Zirconium in the Nuclear Industry: Twelfth International Symposium. G.P. Sabol and G.D. Moan, eds. ASTM STP 1354. West Conshohocken, Pennsylvania: ASTM International. pp. 51–73. 2000.

Goll, W., H. Spilker, and E.H. Toscano. "Short-Time Creep and Rupture Tests on High Burnup Fuel Rod Cladding." *Journal of Nuclear Materials*. Vol. 289. pp. 247–253. 2001.

Gray, W.J. "Inventories of Iodine-129 and Cs-137 in the Gaps and Grain Boundaries of LWR Spent Fuels." Proceedings of the Materials Research Society Conference. Symposium Proceedings 556. Pittsburgh, Pennsylvania: Materials Research Society. pp. 487–494. 1999.

———. "Spent Fuel Dissolution Rates as a Function of Burnup and Water Chemistry." PNNL–11895. Richland, Washington: Pacific Northwest National Laboratory. 1998.

Gray, W.J. and C.N. Wilson. "Spent Fuel Dissolution Studies FY 1991 to 1994." PNL–10540. Richland, Washington: Pacific Northwest National Laboratory. 1995.

Gray, W.J., D.M. Strachan, and C.N. Wilson. "Gap and Grain Boundary Inventories of CS, Tc, and Sr in Spent LWR Fuel." Proceedings of the Materials Research Society Conference. Symposium Proceedings 257. Pittsburgh, Pennsylvania: Materials Research Society. pp. 353–360. 1992.

Greene, C., C.S. Brossia, D.S. Dunn, and G.A. Cragolino. "Environmental and Electrochemical Factors on the Localized Corrosion of Zircaloy-4." Proceedings of the CORROSION 2000 Conference. Paper No. 210. Houston, Texas: NACE International. 2000.

Guenther, R.J., D.E. Blahnik, and N.J. Wildung. "Radiochemical Analyses of Several Spent Fuel Testing Materials." PNL–10113. Richland, Washington: Pacific Northwest National Laboratory. 1994.

Gruss, K., C.L. Brown, and M.W. Hodges. "U.S. Nuclear Regulatory Commission Acceptance Criteria and Cladding Considerations for the Dry Storage of Spent Fuel." TOPFUEL Conference. Wurtzburg, Germany. 2003.

Hardie, D. and M.W. Shanahan. "Stress Reorientation of Hydrides in Zirconium–5% Niobium." *Journal of Nuclear Materials*. Vol. 55. pp. 1–3. 1975.

Hayes, S.J., M.G. Bale, P.J. Henningson, J.K. McCoy, M.K. Punatar, and D.A. Wesley. "Fuel Rod Analysis for Dry Storage of Spent Nuclear Fuel." DPC-NE-2-14. Rev. 0. Charlotte, North Carolina: Duke Power Company. 2001.

Hillner, E., D.G. Franklin, and J.D. Smee. "The Corrosion of Zircaloy-Clad Fuel Assemblies in a Geological Repository Environment." WAPD-3173. West Mifflin, Pennsylvania: Bettis Atomic Power Laboratory. 1994.

International Atomic Energy Agency. "Durability of Spent Nuclear Fuels and Facility Components in Wet Storage." IAEA-TECDOC-1012. Vienna, Austria: International Atomic Energy Agency. 1998.

Jégou, C., S. Peugeot, J.F. Lucchini, C. Corbel, V. Broudic, and J.M. Bart. "Effect of Spent Fuel Burnup and Composition on Alteration of U(Pu)O₂ Matrix." Proceedings of the Materials Research Society Conference. Symposium Proceedings 663. Pittsburgh, Pennsylvania: Materials Research Society. pp. 399-408. 2001.

Johnson, L.H. and D.F. McGinnes. "Partitioning of Radionuclides in Swiss Power Reactor Fuels." NAGRA Technical Report 02-07. Wettingen, Switzerland: National Cooperative for Disposal of Radioactive Waste. 2002.

Johnson, L.H. and J.C. Tait. "Release of Segregated Nuclides From Spent Fuel." SKB Technical Report 97-18. Stockholm, Sweden: Swedish Nuclear Fuel and Waste Management Company. 1997.

Johnson, A.B., Jr. and E.R. Gilbert. "Technical Basis for Storage of Zircaloy-Clad Fuel in Inert Gases." PNL-4835. Richland, Washington. Pacific Northwest Laboratory. 1983.

Kai, J.J., C.H. Tsai, J.J. Shiao, W.F. Hsieh, C.S. Tu, Y.S. Lee, L.F. Lin, and K.Y. Huang. "Effects of Irradiation on the Microstructural Evolution and Corrosion Resistance of Zirconium Alloys." Fifth International Symposium on Environmental Degradation of Materials in Nuclear Power Systems—Water Reactors. La Grange Park, Illinois: American Nuclear Society. pp. 190-198. 1992.

Kearns, J.J. "Terminal Solubility and Partitioning of Hydrogen in the Alpha Phase of Zirconium, Zircaloy-2 and Zircaloy-4." *Journal of Nuclear Materials*. Vol. 22. pp. 292-303. 1967.

Kim, Y.S. and S.S. Kim. "The Cause for Accelerated Corrosion of Zircaloy-4 Cladding at High Burnup." Proceedings of the 2000 International Topical Meeting on Light Water Reactor Fuel Performance, Park City, Utah, April 10-13, 2000. Published on CD-ROM. La Grange Park, Illinois: American Nuclear Society. 2000.

Kim, Y.S., K.S. Rheem, and D.K. Min. "Phenomenological Study of In-Reactor Corrosion of Zircaloy-4 in Pressurized Water Reactors." Zirconium in the Nuclear Industry: Tenth International Symposium. A.M. Garde and E.R. Bradley, eds. ASTM STP 1245. West Conshohocken, Pennsylvania: ASTM International. pp. 745-759. 1994.

Kleykamp, H. "The Chemical State of the Fission Products in Oxide Fuels." *Journal of Nuclear Materials*. Vol. 131. pp. 221-246. 1985.

Knaab, H. and K. Knecht. "Pool-Site Inspection and Examination Techniques Applied by Kraftwerk Union AG Fuel Service." Proceedings of the 26th Conference on Remote Systems Technology. La Grange Park, Illinois: American Nuclear Society. 1978.

Knittel, D.R. and A. Bronson. "Pitting Corrosion on Zirconium—A Review." *Corrosion*. Vol. 40. pp. 9–13. 1984.

Koo, Y.-H., B.-H. Lee, J.-S. Cheon, and D.-S. Sohn. "Pore Pressure and Swelling in the Rim Region of LWR High Burnup UO₂ Fuel." *Journal of Nuclear Materials*. Vol. 295. pp. 213–220. 2001.

Kreyns, P.H., W.F. Bourgeois, C.J. White, P.L. Charpentier, B.F. Kammenzind, and D.G. Franklin. "Embrittlement of Reactor Core Materials." Zirconium in the Nuclear Industry: Eleventh International Symposium. E.R. Bradley and G.P. Sabol, eds. ASTM STP 1298. West Conshohocken, Pennsylvania: ASTM International. pp. 758–782. 1996.

Kreyns, P.H., G.L. Spahr, and J.E. McCauley. "An Analysis of Iodine Stress Corrosion Cracking of Zircaloy-4 Tubing." *Journal of Nuclear Materials*. Vol. 61. pp. 203–212. 1976.

Lanning, D.D. and C.E. Beyer. "Estimated Maximum Cladding Stresses for Bounding PWR Fuel Rods During Short Term Operations for Dry Cask Storage." Richland, Washington: Pacific Northwest National Laboratory. ML040290474. January 2004.

Lassmann, K., C.T. Walker, J. van de Laar, and F. Lindstrom. "Modeling the High Burnup UO₂ Structure in LWR Fuel." *Journal of Nuclear Materials*. Vol. 226. pp. 1–8. 1995.

Levy, I.S., B.A. Chin, E.P. Simonen, C.E. Beyer, E.R. Gilbert, and A.B. Johnson, Jr. "Recommended Temperature Limits for Dry Storage of Spent Light Water Reactor Zircaloy-Clad Fuel Rods in Inert Gas." PNL-6189. Richland, Washington: Pacific Northwest Laboratory. 1987.

Limon, R., C. Cappelaere, and T. Bredel. "A Formulation of the Spent Fuel Cladding Creep Behavior for Long Term Storage." Proceedings of the 2000 International Topical Meeting on Light Water Reactor Fuel Performance, Park City, Utah, April 10–13, 2000. Published on CD-ROM. La Grange Park, Illinois : American Nuclear Society. 2000.

Lippins, M., D. Boulanger, and L. Mertens. "Industry Challenges and Expectations with Respect to Fission Gas Release." Proceedings of the Fission Gas Behavior in Water Reactor Fuels, Cadarache, France, September 26–29, 2000. Paris, France: Nuclear Energy Agency. pp. 31–45. 2000.

Loida, A., B. Kienzler, and H. Geckeis. "Corrosion Behavior of Pre-Oxidized High Burnup Spent Fuel in Salt Brine." Scientific Basis for Nuclear Waste Management XXVII. Symposium Proceedings 807. V.M. Oversby and L.O. Werme, eds. Warrendale, Pennsylvania: Materials Research Society. pp. 53–58. 2004.

———. "Mobilization/Retention of Radionuclides During Corrosion of High Burnup Spent Fuel and Backfill Materials in Salt Brines." *Scientific Basis for Nuclear Waste Management XXVI. Symposium Proceedings 757*. R.J. Finch and D.B. Bullen, eds. Warrendale, Pennsylvania: Materials Research Society. pp. 433–439. 2003.

Loida, A., B. Grambow, and H. Geckeis. "Congruent and Incongruent Radionuclide Release During Matrix Dissolution of Partly Oxidized High Burnup Spent Fuel." *Proceedings of the Material Research Society. Symposium Proceedings 663*. Warrendale, Pennsylvania: Materials Research Society. pp. 417–426. 2001.

———. "Anoxic Corrosion of Various High Burnup Spent Fuel Samples." *Journal of Nuclear Materials*. Vol. 238. pp. 11–22. 1996.

Louthan, M.R. and R.P. Marshall. "Control of Hydride Reorientation in Zircaloy." *Journal of Nuclear Materials*. Vol. 9. pp. 170–184. 1963.

Macdonald, D.D. and G. Cragolino. "Corrosion and Erosion Corrosion of Seam Cycle Materials." *Handbook on Water Technology for Thermal Power Systems*. P. Cohen, ed. New York: American Society of Mechanical Engineers. pp. 659–1,034. 1989.

MacEwen, S.R., J. Faber, Jr., and A.P.L. Turner. "The Use of Time-of-Flight Neutron Diffraction to Study Grain Interaction Stresses." *Acta Metallurgica*. Vol. 71. p. 657. 1983.

Manaktala, H.K. "Characteristics of Spent Nuclear Fuel and Cladding Relevant to High-Level Waste Source Term." CNWRA 93-006. San Antonio, Texas: CNWRA. 1993.

Mankowski, G., Y. Roques, G. Chatainier, and F. Dabosi. "Stress Corrosion Cracking of Zircaloy-4 in Neutral Aqueous Chloride Solution." *British Corrosion Journal*. Vol. 19. pp. 17–22. 1984.

Manzel, R. and M. Coquerelle. "Fission Gas Release and Pellet Structure at Extended Burnup." *Proceedings of the 1997 International Topical Meeting on LWR Performance, Portland, Oregon, March 2–6, 1997*. La Grange Park, Illinois: American Nuclear Society. pp. 463–470. 1997.

Manzel, R. and C.T. Walker. "High Burnup Fuel Microstructure and its Effect on Fuel Rod Performance." *Proceedings of the 2000 International Topical Meeting on Light Water Reactor Fuel Performance, Park City, Utah, April 10–13, 2000*. Published on CD-ROM. La Grange Park, Illinois: American Nuclear Society. 2000.

Mardon, J.P., D. Charquet, and J. Senevat. "Influence of Composition and Fabrication Process on Out-of-Pile and In-Pile Properties of M5 Alloy." *Zirconium in the Nuclear Industry: Twelfth International Symposium*. G.P. Sabol and G.T. Moan, eds. ASTM STP 1354. West Conshohocken, Pennsylvania: ASTM International. pp. 505–524. 2000.

Mardon, J.P., G. Garner, P. Beslu, D. Charquet, and J. Senevat. "Update on the Development of Advanced Zirconium Alloys for PWR Fuel Rod Claddings." *Proceedings of the 1997 International Topical Meeting on LWR Fuel Performance, Portland, Oregon, March 2–6, 1997*. La Grange Park, Illinois: American Nuclear Society. pp. 405–412. 1997.

Marshall, R.P. "Control of Hydride Orientation in Zircaloy by Fabrication Practice." *Journal of Nuclear Materials*. Vol. 24. pp. 49–59. 1967a.

———. "Influence of Fabrication History on Stress-Oriented Hydrides in Zircaloy." *Journal of Nuclear Materials*. Vol. 24. pp. 34–48. 1967b.

Marshall, R.P. and M.R. Louthan. "Tensile Properties of Zircaloy with Oriented Hydrides." *Transactions of ASM*. Vol. 63. pp. 693–700. 1963.

Matsuo, Y. "Thermal Creep of Zircaloy-4 Cladding Under Internal Pressure." *Journal of Nuclear Science and Technology*. Vol. 24. pp. 111–119. 1987.

Mayazumi, M. and T. Onchi. "Creep Deformation of Unirradiated Zircaloy Nuclear Fuel Cladding Tube Under Dry Storage Conditions." *Journal of Nuclear Materials*. Vol. 171. pp. 383–388. 1990.

Meyer, R.O. "NRC Activities Related to High Burnup, New Cladding Types, and Mixed-Oxide Fuel." Proceedings of the 2000 International Topical Meeting on Light Water Reactor Fuel Performance, Park City, Utah, April 10–13, 2000. Published on CD-ROM. La Grange Park, Illinois: American Nuclear Society. 2000.

Meyer, R.E. "The Electrochemistry of the Dissolution of Zirconium in Aqueous Solutions of Hydrofluoric Acid." *Journal of the Electrochemical Society*. Vol. 111. pp. 147–155. 1964.
McCoy, J.K. "Fuel and Cladding Oxidation Under Expected Repository Conditions." High-Level Radioactive Waste Management: Proceedings of the Seventh Annual International Conference, Las Vegas, Nevada, April 29–May 3, 1996. La Grange Park, Illinois: American Nuclear Society. pp. 396–398. 1996.

McCoy, J.K. and T.W. Doering. "Prediction of Cladding Life Waste Package Environments." Proceedings of the Fifth Annual International Conference on High-Level Radioactive Waste Management, Las Vegas, Nevada, May 22–26, 1994. La Grange Park, Illinois: American Nuclear Society. Vol. 2. pp. 565–572. 1994.

Miller, A.K., M. Brooks, T.Y. Cheung, and A. Tasooji. "Estimate of Zircaloy Integrity During Dry Storage of Spent Nuclear Fuel." EPRI NP-6387. Palo Alto, California: Electric Power Research Institute. 1989.

Mogensen, M., J.H. Pearce, and C.T. Walker. "Behavior of Fission Gas in the Rim Region of High Burn-up UO₂ Fuel Pellets with Particular Reference to Results from an XRF Investigation." *Journal of Nuclear Materials*. Vol. 264. pp. 99–112. 1999.

Mohanty, S., T.J. McCartin, and D.W. Esh. "Total-System Performance Assessment (TPA) Version 4.0 Code: Module Descriptions and User's Guide." San Antonio, Texas: CNWRA. 2000.

Mohanty, S., R. Codell, J.M. Menchaca, R. Janetzke, M. Smith, P. LaPlante, M. Rahimi, and A. Lozano. "System-Level Performance Assessment of the Proposed Repository at Yucca Mountain Using the TPA Version 4.1 Code." CNWRA 2002-05. Rev. 2. San Antonio, Texas: CNWRA. 2004.

Neal, W.L., S.A. Rawson, and W.M. Murphy. "Radionuclide Release Behavior of Light Water Reactor Spent Fuel Under Hydrothermal Conditions." Proceedings of the Materials Research Society Conference. Symposium Proceedings 112. Pittsburgh, Pennsylvania: Materials Research Society. pp. 505–515. 1988.

Northwood, D.O. and U. Kosasih. "Hydrides and Delayed Hydrogen Cracking in Zirconium and its Alloys." *International Metals Review*. Vol. 28, No. 2. pp. 92–121. 1983.

NRC. "Risk Insights Baseline Report." ML040560162. Washington, DC: NRC. 2004. .
<www.nrc.gov/reading-rm/adams.html>

———. NUREG–1762, "Integrated Issue Resolution Status Report." Washington, DC: NRC. 2002.

Oversby, V.M. "Uranium Dioxide, SIMFUEL, and Spent Nuclear Fuel Dissolution Rates—A Review of Published Data. TR–99-02. Stockholm, Sweden: Swedish Nuclear Fuel and Waste Management Company. 1999.

Pan, Y.-M., C.S. Brossia, G.A. Cragnolino, V. Jain, O. Pensado, and N. Sridhar. "Effect of In-Package Chemistry on the Degradation of Vitrified High-Level Radioactive Waste and Spent Nuclear Fuel Cladding." CNWRA 2002-01. San Antonio, Texas: CNWRA. 2001.

Peehs, M. and J. Fleisch. "LWR Spent Fuel Storage Behavior." *Journal of Nuclear Materials*. Vol. 137. pp. 190–202. 1986.

Peehs, M., G. Kaspar, and E. Steinberg. "Experimentally Based Spent Fuel Dry Storage Performance Criteria." Proceedings of the Third International Spent Fuel Technology Symposium/Workshop. USDOE–CONF–860417/UC–85. Vol. 1. pp. S–316 through S–331. 1985.

Pescatore, C., M.G. Cowgill, and T.M. Sullivan. "Zircaloy Cladding Performance Under Spent Fuel Disposal Conditions." BNL52235. Upton, New York: Brookhaven National Laboratory. 1989.

Piron, J.P., M. Pelletier, and J. Pavegeau. "Helium Behavior in Spent UO₂ and MOX Fuels." Proceedings of the Fission Gas Behavior in Water Reactor Fuels, Cadarache, France, September 26–29, 2000. Paris, France: Nuclear Energy Agency. pp. 311–320. 2000.

Poinssot, C., P. Lovera, and M.-H. Faure. "Assessment of Evolution with Time of the Instant Release Fraction of Spent Nuclear Fuel in Geological Disposal Conditions." Proceedings of the Material Research Society Conference. Symposium Proceedings 713. Pittsburgh, Pennsylvania: Materials Research Society. pp. 615–623. 2002.

Poinssot, C., P. Toulhoat, J.P. Grouiller, J. Pavageau, J.P. Piron, M. Pelletier, P. Dehaut, C. Cappelaere, R. Limon, L. Desgranges, C. Jégou, C. Corbel, S. Maillard, M.H., Faure, J.C. Cicariello, and M. Masson. "Synthesis on the Long-Term Behavior of the Spent Nuclear Fuel, Volumes 1 and 2." CEA–R–5958(E). Saclay, France: Commissariat A L'Energie Atomique. 2001.

Pourbaix, M. *Atlas of Electrochemical Equilibria in Aqueous Solutions*. Houston, Texas: NACE International. 1974.

Prussin, S.G., D.R. Olander, W.K. Lau, and L. Hansson. "Release of Fission Products (Xe, I, Te, Cs, Mo, and Tc) from Polycrystalline UO_2 ." *Journal of Nuclear Materials*. Vol. 154. pp. 25–37. 1988.

Puls, M.P. "The Influence of Hydride Size and Matrix Strength on Fracture Initiation at Hydrides in Zirconium Alloys." *Metallurgical Transactions*. Vol. 19A. pp. 1,507–1,522. 1988.

Raj, R. and M.F. Ashby. "Intergranular Fracture at Elevated Temperature." *Acta Metallurgica*. Vol. 25. pp. 653–666. 1975.

Ramsdell, Jr., J.V., C.E. Beyer, D.D. Lanning, U.P. Jenquin, R.A. Schwarz, D.L. Strenge, P.M. Daling, and R.T. Dahowski. NUREG/CR-6703, PNNL-13257, "Environmental Effects of Extending Fuel Burnup Above 60 GWd/MTU." Washington, DC: NRC. January 2001.

Roberts, J.T.A. *Structural Materials in Nuclear Power Systems*. New York, New York: Plenum Press. 1981.

Röllin, S., K. Spahiu, and U.-B. Eklund. "Determination of Dissolution Rates of Spent Fuel in Carbonate Solutions Under Different Redox Conditions with a Flow-Through Experiment." *Journal of Nuclear Materials*. Vol. 297. pp. 231–243. 2001.

Rothman, A.J. "Potential Corrosion and Degradation Mechanisms of Zircaloy Cladding on Spent Nuclear in a Tuff Repository." UCID-20172. Livermore, California: Lawrence Livermore National Laboratory. 1984.

Sabol, G.P., R.J. Comstock, G. Schoenberger, H. Kunishi, and D.L. Nuhfer. "In-Reactor Fuel Cladding Corrosion Performance at Higher Burnups and Higher Coolant Temperatures." Proceedings of the 1997 International Topical Meeting on LWR Fuel Performance, Portland, Oregon, March 2–6, 1997. La Grange Park, Illinois: American Nuclear Society. pp. 397–404. 1997.

Sanders, C.E. and I.C. Gauld. NUREG/CR-6798, ORNL/TM-2001/259, "Isotopic Analysis of High-Burnup PWR Spent Fuel Samples From the Takahama-3 Reactor." Washington, DC: NRC. January 2003.

Sawatzky, A. and C.E. Ellis. "Understanding Hydrogen in Zirconium." Zirconium in the Nuclear Industry: Twelfth International Symposium. G.P. Sabol and G.D. Moan, eds. ASTM STP 1354. West Conshohocken, Pennsylvania: ASTM International. pp. 32–48. 2000.

Schwartz, M.W. and M.C. Witte. "Spent Fuel Cladding Integrity During Dry Storage." UCID-21181. Livermore, California: Lawrence Livermore National Laboratory. 1987.

Shi, S.-Q., and M.P. Puls. "Dependence of the Threshold Stress Intensity Factor on Hydrogen Concentrations During Delayed Hydride Cracking in Zirconium Alloys." *Journal of Nuclear Materials*. Vol. 218. pp. 20–26. 1994.

Siegmann, E. "Cladding Credit in TSPA-VA." Workshop on Significant Issues and Available Data Waste Form Degradation and Radionuclide Mobilization Expert Elicitation Project, San Francisco, California. Las Vegas, Nevada: Duke Engineering and Services, Inc. 1997a.

———. "Cladding Credit in TSPA-VA." Workshop on Alternative Models and Interpretations Form Degradation and Radionuclide Mobilization Expert Elicitation Project, San Francisco, California. Las Vegas, Nevada: Duke Engineering and Services, Inc. 1997b.

Siegmann, E. and P. Macheret. "Evaluating Cladding Creep During Dry Storage and Repository Emplacement." Scientific Basis for Nuclear Waste Management XXV. Symposium Proceedings 713. B.P. McGrail and G.A. Cragolino, eds. Warrendale, Pennsylvania: Materials Research Society. pp. 681–688. 2002.

Siegmann, E., J.K. McCoy, and R. Howard. "Cladding Evaluation in the Yucca Mountain Repository Performance Assessment." Scientific Basis for Nuclear Waste Management XXVIII. Symposium Proceedings 608. R.W. Smith and D.W. Shoesmith, eds. Warrendale, Pennsylvania: Materials Research Society. pp. 3–9. 2000.

Simpson, L.A. and C.D. Cann. "Fracture Toughness of Zirconium Hydride and its Influence on the Crack Resistance of Zirconium Alloys." *Journal of Nuclear Materials*. Vol. 87. pp. 303–316. 1979.

Speidel, M.O. "Stress Corrosion Cracking of Zirconium Alloys." *ARPA Handbook of Stress Corrosion Cracking and Corrosion Fatigue (Draft)*. M.O. Speidel and R.W. Staehle, eds. 1976. Stout, R.B. and H.R. Leider. "Waste Form Characteristics Report Revision 1." UCRL-ID-108314. Version 1.3. San Francisco, California: Lawrence Livermore National Laboratory. 1998.

Stroes-Gascoyne, S., L.H. Johnson, and D.M. Sellinger. "The Relationship Between Gap Inventories of Stable Xenon, ^{137}Cs , and ^{129}I in Used CANDU Fuel." *Nuclear Technology*. Vol. 77. pp. 320–330. 1997a.

Stroes-Gascoyne, S., L.H. Johnson, J.C. Tait, J.L. McConnell, and R.J. Poth. "Leaching of Used CANDU Fuel: Results from a 19-Year Leach Test Under Oxidizing Conditions." Proceedings of the Materials Research Society Conference. Symposium Proceedings 465. Pittsburgh, Pennsylvania: Materials Research Society. p. 511. 1997b.

Stroes-Gascoyne, S. "Measurements of Instant-Release Terms of Cs-137, Sr-90, Tc-99, I-129 and C-14 in Used CANDU Fuels." *Journal of Nuclear Materials*. Vol. 238. pp. 264–277. 1996.

Stroes-Gascoyne, S., J.C. Tait, R.J. Porth, J.L. McConnell, and W.J. Lincoln. "Release of C-14 from the Gap and Grain Boundary Regions of Used CANDU Fuels to Aqueous Solutions." *Waste Management*. Vol. 12, No. 5. pp. 385–392. 1994.

Stroes-Gascoyne, S., J.C. Tait, N.C. Garisto, R.J. Porth, J.P.M. Ross, G.A. Glowka, and T.R. Barnsdale. "Instant-Release of C-14, Tc-99, Sr-90, and Cs-137 from Used CANDU Fuel at 25 °C in Distilled Deionized Water." Proceedings of the Materials Research Society Conference. Symposium Proceedings 257. Pittsburgh, Pennsylvania: Materials Research Society. pp. 373–380. 1992.

Suzuki, M. and S. Kawasaki. "Oxidation of Zircaloy Cladding in Air." *Journal of Nuclear Materials*. Vol. 140. pp. 32-43. 1986.

Tait, J.C. and J.L. Luht. "Dissolution Rates of Uranium from Unirradiated UO₂ and Uranium and Radionuclides from Used CANDU Fuel Using the Single-Pass Flow-Through Apparatus." Report No. 06819-REP-01200-0006 R00. Toronto, Canada: Atomic Energy of Canada, Ltd. 1997.

Tait, J.C., R.J. Cornett, L.A. Chant, J. Jirovec, J. McConnell, and D.L. Wilkin. "Determination of Cl Impurities and ³⁶Cl Instant Release From Used CANDU Fuels." Proceedings of the Materials Research Society Conference. Symposium Proceedings 465. Pittsburgh, Pennsylvania: Materials Research Society. pp. 503-510. 1997.

Tasooji, A., R.E. Einziger, and A.K. Miller. "Modeling of Zircaloy Stress-Corrosion Cracking: Texture Effects and Dry Storage Spent Fuel Behavior. Zirconium in the Nuclear Industry: Sixth International Symposium. D.G. Franklin and R.B. Adamson, eds. ASTM STP 824. West Conshohocken, Pennsylvania: ASTM International. pp. 595-626. 1984.

Thomas, G.R. "Updated Model for Predicting Spent Fuel Cladding Integrity During Dry Storage." UCRL-ID-134217. Livermore, California: Lawrence Livermore National Laboratory. 1999.

Thurber, W.C. and S. Marschke. "Fuel Rod Cladding as a Barrier to Radionuclide Release in a High-Level Waste Repository." Proceedings of the Eighth International Conference on High-Level Radioactive Waste Management, Las Vegas, Nevada, May 11-14, 1998. La Grange, Illinois: American Nuclear Society. pp. 471-473. 1998.

Tsai, H. "Cladding Behavior During Dry Cask Handling and Storage." Proceedings of the Nuclear Safety Research Conference, Washington, DC, October 21, 2003. Published on CD ROM: Fuels and Cladding Materials. Washington, DC: NRC. 2003.

Une, K., K. Nogita, S. Kashibe, T. Toyonaga, and M. Amaya. "Effect of Irradiation-Induced Microstructural Evolution on the High Burnup Fuel Behavior." Proceedings of the 1997 International Topical Meeting on LWR Performance, Portland, Oregon, March 2-6, 1997. La Grange Park, Illinois: American Nuclear Society. pp. 478-489. 1997.

Van Konynenburg, R.A., C.F. Smith, H.W. Culham, and H.D. Smith. "Carbon-14 in Waste Packages for Spent Fuel in a Tuff Repository." Proceedings of the Materials Research Society Conference. Symposium Proceedings 84. Pittsburgh, Pennsylvania: Materials Research Society. pp. 185-196. 1987.

Van der Sande, J.B. and A.L. Bement. "An Investigation of Second Phase Particles in Zircaloy-4 Alloy." *Journal of Nuclear Materials*. Vol. 52. pp. 115-118. 1974.

Van Swam, L.F., G.M. Bain, W.C. Dey, D.D. Davis, and H. Heckermann. "BWR and PWR Fuel Performance at High Burnup." Proceedings of the 1997 International Topical Meeting on LWR Performance, Portland, Oregon, March 2-6, 1997. La Grange Park, Illinois: American Nuclear Society. pp. 3-1. 1997a.

- Van Swam, L.F., A.A. Strasser, J.D. Cook, and J.M. Burger. "Behavior of Zircaloy-4 and Zirconium Liner Zircaloy-4 Cladding at High Burnup." Proceedings of the 1997 International Topical Meeting on LWR Fuel Performance, Portland, Oregon, March 2-6, 1997. La Grange Park, Illinois: American Nuclear Society. pp. 421-431. 1997b.
- Walker, C.T. "Assessment of the Radial Extent and Completion of Recrystallisation in High Burn-up UO_2 Nuclear Fuel by EPMA." *Journal of Nuclear Materials*. Vol. 275. pp. 56-62. 1999.
- Wilson, C.N. "Summary of Results From the Series 2 and Series 3 NNWSI Bare Fuel Dissolution Tests." Proceedings of the Materials Research Society Conference. Symposium Proceedings 112. Pittsburgh, Pennsylvania: Materials Research Society. pp. 473-483. 1988.
- Wilson, C.N. and H.F. Shaw. "Experimental Study of the Dissolution of Spent Fuel at 85 °C in Natural Groundwater." Proceedings of the Materials Research Society Conference. Symposium Proceedings 84. Pittsburgh, Pennsylvania: Materials Research Society. pp. 123-130. 1987.
- Yang, R., O. Ozer, and H.S. Rosenbaum. "Current Challenges and Expectations of High Performance Fuel for the Millennium." Proceedings of the 2000 International Topical Meeting on Light Water Reactor Fuel Performance, Park City, Utah, April 10-13, 2000. Published on CD-ROM. La Grange Park, Illinois: American Nuclear Society. 2000.
- Yau, T.-L. "Stress Corrosion Cracking of Zirconium Alloys." *Stress Corrosion Cracking—Materials Performance and Evaluation*. R.H. Jones, ed. Materials Park, Ohio: ASM International. pp. 299-311. 1992.
- . "The Corrosion Properties of Zirconium Alloys in Chloride Solutions." Proceedings of the CORROSION '83 Conference. Paper No. 26. Houston, Texas: NACE International. 1983.
- Yau, T.-L. and M. Maguire. "Electrochemical Properties of Zirconium in Oxidizing Hydrochloric Acid Solutions." *Corrosion*. Vol. 40. pp. 289-296. 1984.
- Yau, T.-L. and R.T. Webster. "Corrosion of Zirconium and Hafnium." *Metals Handbook: Vol. 13—Corrosion Materials*. Materials Park, Ohio: ASM International. pp. 707-721. 1987.
- Young, L. *Anodic Oxide Films*. New York City, New York: Academic Press. p. 257. 1961.

APPENDIX A

ORIGEN-ARP Input Listing Sample

```
'This SCALE input file was generated by
'OrigenArp Version 2.00 2-12-2002
=arp
15x15
5
3
722.2222
722.2222
722.2222
30
30
30
1
1
1
0.7135
ft33f001
end
#origens
0$$ a4 33 all 71 e t
15x15 library, interpolated to 5.000000 wt% -- ft33f001
3$$ 33 a3 1 27 a16 2 a33 18 e t
35$$ 0 t
56$$ 10 10 a10 0 a13 16 a15 3 a18 1 e
57** 0 a3 1e-05 0.3333333 e t
Cycle 1 -65gwdhighbudecay
1 MTU
58** 30 30 30 30 30 30 30 30 30 30
60** 72.22222 144.4444 216.6667 288.8889 361.1111 433.3333 505.5556
577.7778 650 722.2222
66$$ a1 2 a5 2 a9 2 e
73$$ 922340 922350 922360 922380 80000 240000 250000 260000 270000
280000 400000 410000 500000 60000 170000 70000
74** 445 50000 230 949325 136000 5920 330 12940 70 9870 221440 700 3510
195 10 60
75$$ 2 2 2 2 4 4 4 4 4 4 4 4 4 4 4 4
t
54$$ a8 1 a11 0 e
56$$ a2 9 a6 3 a10 10 a15 3 a17 4 e
57** 0 a3 1e-05 e t
Decay - 65gwdhighbudecay
1 MTU
60** 0.01 0.03 0.1 0.3 1 3 10 30 38.0117
61** f0.05
65$$
'Gram-Atoms Grams Curies Watts-All Watts-Gamma
3z 1 0 0 3z 3z 3z 6z
3z 1 0 0 3z 3z 3z 6z
3z 1 0 0 3z 3z 3z 6z
t
15x15 library, interpolated to 5.000000 wt% -- ft33f001
3$$ 33 a3 2 27 a33 18 e t
35$$ 0 t
56$$ 10 10 a10 9 a15 3 a18 1 e
```

```

57** 0 a3 1e-05 0.3333333 e t
Cycle 2 -65gwdhighbudecay
1 MTU
58** 30 30 30 30 30 30 30 30 30 30
60** 72.22222 144.4444 216.6667 288.8889 361.1111 433.3333 505.5556
577.7778 650 722.2222
66$$ a1 2 a5 2 a9 2 e t
54$$ a8 1 a11 0 e
56$$ a2 9 a6 3 a10 10 a15 3 a17 4 e
57** 0 a3 1e-05 e t
Decay - 65gwdhighbudecay
1 MTU
60** 0.01 0.03 0.1 0.3 1 3 10 30 38.0117
61** f0.05
65$$
'Gram-Atoms Grams Curies Watts-All Watts-Gamma
3z 1 0 0 3z 3z 3z 6z
3z 1 0 0 3z 3z 3z 6z
3z 1 0 0 3z 3z 3z 6z
t
15x15 library, interpolated to 5.000000 wt% -- ft33f001
3$$ 33 a3 3 27 a33 18 e t
35$$ 0 t
56$$ 10 10 a10 9 a15 3 a18 1 e
57** 0 a3 1e-05 0.3333333 e t
Cycle 3 -65gwdhighbudecay
1 MTU
58** 30 30 30 30 30 30 30 30 30 30
60** 72.22222 144.4444 216.6667 288.8889 361.1111 433.3333 505.5556
577.7778 650 722.2222
66$$ a1 2 a5 2 a9 2 e t
54$$ a8 1 a11 0 e
56$$ a2 10 a6 1 a10 10 a14 5 a15 3 a17 2 e
57** 0 a3 1e-05 e t
Cycle 3 Down - 65gwdhighbudecay
1 MTU
60** 0.3 1 3 10 30 100 300 1000 3000 10000
61** f0.05
65$$
'Gram-Atoms Grams Curies Watts-All Watts-Gamma
3z 3z 1 0 1 1 0 1 3z 6z
3z 3z 1 0 1 1 0 1 3z 6z
3z 3z 1 0 1 1 0 1 3z 6z
81$$ 2 0 26 1 a7 200 e
82$$ 2 2 2 2 2 2 2 2 2 2 e
83**
1.E+7 8.E+6 6.5E+6 5.E+6 4.E+6 3.E+6
2.5E+6 2.E+6 1.66E+6 1.33E+6 1.E+6 8.E+5
6.E+5 4.E+5 3.E+5 2.E+5 1.E+5 5.E+4
1.E+4 e
84**
2.E+7 6.434E+6 3.E+6 1.85E+6 1.4E+6
9.E+5 4.E+5 1.E+5 1.7E+4 3.E+3 5.5E+2
1.E+2 3.E+1 1.E+1 3.04999E+0 1.77E+0
1.29999E+0 1.12999E+0 1.E+0 8.E-1 4.E-1
3.25E-1 2.25E-1 9.999985E-2 5.E-2 3.E-2
9.999998E-3 1.E-5 e
t
Cycle 3 Down - 65gwdhighbudecay Time Step 1
Cycle 3 Down - 65gwdhighbudecay Time Step 2
Cycle 3 Down - 65gwdhighbudecay Time Step 3
Cycle 3 Down - 65gwdhighbudecay Time Step 4

```

```

Cycle 3 Down - 65gwdhighbuddecay Time Step 5
Cycle 3 Down - 65gwdhighbuddecay Time Step 6
Cycle 3 Down - 65gwdhighbuddecay Time Step 7
Cycle 3 Down - 65gwdhighbuddecay Time Step 8
Cycle 3 Down - 65gwdhighbuddecay Time Step 9
Cycle 3 Down - 65gwdhighbuddecay Time Step 10
56$$ 0 0 a10 1 e t
56$$ 0 0 a10 2 e t
56$$ 0 0 a10 3 e t
56$$ 0 0 a10 4 e t
56$$ 0 0 a10 5 e t
56$$ 0 0 a10 6 e t
56$$ 0 0 a10 7 e t
56$$ 0 0 a10 8 e t
56$$ 0 0 a10 9 e t
56$$ 0 0 a10 10 e t
56$$ f0 t
end
=opus
TYPARAMS=NUCLIDES
UNITS=CURIES
LIBTYPE=ALL
TIME=YEARS
NPOSITION=1 2 3 4 5 6 7 8 9 10 end
end
=opus
TYPARAMS=NUCLIDES
UNITS=WATTS
LIBTYPE=ALL
TIME=YEARS
NPOSITION=1 2 3 4 5 6 7 8 9 10 end
end
=opus
TYPARAMS=NUCLIDES
UNITS=CURIES
SYMNUC=Am-241 Cs-135 I-129 Np-237 Pu-239 Pu-240 Sr-90 Tc-99 end
NRANK=8
LIBTYPE=ALL
TIME=YEARS
NPOSITION=1 2 3 4 5 6 7 8 9 10 end
end
=opus
TYPARAMS=NUCLIDES
UNITS=WATTS
SYMNUC=Am-241 Am-243 Cs-135 I-129 Np-237 Pu-239 Pu-240 Tc-99 end
NRANK=8
LIBTYPE=ALL
TIME=YEARS
NPOSITION=1 2 3 4 5 6 7 8 9 10 end
end
=opus
TYPARAMS=NUCLIDES
UNITS=CURIES
SYMNUC=C-14 Cl-36 Cs-135 I-129 Tc-99 end
NRANK=5
LIBTYPE=ALL
TIME=YEARS
NPOSITION=1 2 3 4 5 6 7 8 9 10 end
end
=opus
TYPARAMS=NUCLIDES
UNITS=CURIES

```

```
SYMNUC=Ac-227 Ag-108M Am-241 Am-242M Am-243 C-14 Cl-36 Cm-243 Cm-244
Cm-245 Cm-246 Cs-135 Cs-137 I-129 Mo-93 Nb-94 Ni-59 Ni-63 Np-237 Pa-231
Pb-210 Pd-107 Pu-238 Pu-239 Pu-240 Pu-241 Pu-242 Ra-226 Se-79 Sm-151
Sn-121M Sn-126 Sr-90 Tc-99 Th-229 Th-230 U-232 U-233 U-234 U-235 U-236
U-238 Zr-93 end
NRANK=43
LIBTYPE=ALL
TIME=YEARS
NPOSITION=1 2 3 4 5 6 7 8 9 10 end
end
#shell
copy ft71f001 C:\scale5\OrigenArp\65withCandCl.f71
del ft71f001
end
```

